EIR-Bericht Nr. 444

EIR-Bericht Nr.

Eidg. Institut für Reaktorforschung Würenlingen
Schweiz

Fast Reactor Experiments with Thorium at the PROTEUS Facility

R. Chawla, K. Gmür, M. Jermann,
R. Richmond, U. Schmocker

Würenlingen, November 1981

EIR Report No. 444

FAST REACTOR EXPERIMENTS WITH THORIUM AT THE PROTEUS FACILITY

R. Chawla, K. Gmür, M. Jermann, R. Richmond, U. Schmocker*

E I R

Würenlingen, November 1981

* Present address: ASK, CH-5303 Würenlingen

CONTENTS

Abstract

The largescale utilization of thorium is usually linked to its introduction in fast breeder reactors and/or advanced converters. While the basic nuclear data used in physics calculations for fast reactors operating on the ^{239}Pu-^{238}U cycle have been repeatedly checked and improved over the years, relatively large uncertainties have continued to exist for the cross-section data necessary for analysing Th-containing fast reactor systems. This has been mainly due to the sparseness of clean, integral experiments with thorium - a gap which the programme of integral measurements described in this report seeks, at least in part, to fill.

The present experiments were carried out in the zero-energy reactor facility, PROTEUS, at EIR. This is essentially a coupled system, consisting of a central test zone driven critical by annular thermal driver zones. Six different configurations for the central fast test zone were considered in the current programme, the principal fuel/blanket materials used being in the form of rods of 15 % PuO_2/UO_2, depleted UO_2, ThO_2 and Th-metal. The first test lattice (Core 11) corresponded to a normal GCFR core and enabled checks to be made for infinite-dilution reaction rates for ^{232}Th and ^{233}U in a standard fast reactor spectrum. The second test lattice (Core 12) had one third of the PuO_2/UO_2 fuel rods of Core 11 replaced by ThO_2 rods, simulating a relatively homogeneous introduction of thorium into a fast reactor core. Core 13 was a heterogeneous configuration with a central ThO_2 blanket zone surrounded by an annular PuO_2/UO_2 zone. The fourth test lattice was again a heterogeneous configuration but with an axial ThO_2 blanket. Cores 15 and 16, the last two test zones, were similar to Cores 13 and 14, respectively, but with Th-metal replacing ThO_2.

For each experimental configuration, measurements were made of the principal reaction rate ratios at the centre, as well as of reaction rate distributions across the test zone. Wherever possible, both absolute and thermal-comparison techniques were applied for reaction rate ratio measurements, thereby providing some check on the different systematic errors. Neutron spectrum measurements, using spherical proton-recoil counters, were carried out in Cores 12, 14 and 16. The measured neutron energy range was ∿10 keV-2.3 MeV.

Calculations for the various test lattices were carried out using two different data libraries and processing codes. These were: (i) the U.K. adjusted data set, FGL5, and its associated cell code, MURALB, and (ii) the U.S. code, GGC-4, with a data library based on ENDF/B-4 cross-sections. Transport-theory analyses for the experimental configurations of Cores 11, 12, 13 and 15 were carried out using a 1-D, cylindrical-geometry model for the PROTEUS reactor. For analysis of the axial-blanket experiments (Cores 14 and 16), a 2-D diffusion-theory model was employed for the whole reactor. Separate calculations were carried out for evaluating the neutron spectrum measurements, the axial-blanket experiments being analysed in collaboration with ORNL using a 2-D transport-theory model (25).

In Cores 11 and 12, physics parameters at the centre were mainly determined by the test lattice itself and only marginally influenced by the outer reactor zones. These experimental configurations could thus be regarded as benchmarks for the basic nuclear data. In both lattices, the agreement between experiment and ENDF/B-4 based calculations was better than [illegible] (25). This was surprising in view of the normally assumed large (≳ 10-20 %) uncertainties for [illegible] capture cross-sections and at first seemed to contradict the results of recent

differential measurements which suggested that the ENDF/B-4 data was too high (7). Certain revisions of the latter measurements have, however, now been published, the originally reported results for ^{232}Th capture being increased on average by ~11 %, i.e. brought back to values reasonably consistent with ENDF/B-4 (45).

The performance of the MURALB/FGL5 calculational route for predicting σ_c(Th232)/σ_f(Pu239) was similar to that of the GGC-4 (ENDF/B-4) route for Core 11. In Core 1 , however, where the ^{232}Th cross-sections were no longer infinitely dilute, the GGC-4 calculation of resonance self-shielding effects seemed to perform significantly better. Both calculational routes yielded σ_f(Th232)/σ_f(Pu239) values ~12 % lower than measurements in Cores 11 and 12, suggesting that the ^{232}Th fission cross-sections in current use are too low. This should, however, have relatively minor effect on neutron balances for ^{232}Th-containing fast reactors. Calculational results for σ_f(U233)/σ_f(Pu239) agreed within ~1 % with experiment, indicating the adequacy of infinite-dilution ^{233}U fission cross-sections. Results for additionally measured reaction rate ratios, e.g. ^{238}U capture and fission, relative to ^{239}Pu fission, showed the same trends as reported for earlier PROTEUS-GCFR cores (29, 37).

In the internal ThO_2 and Th-metal blanket configurations of Cores 13 and 15, there was a strong coupling between the blanket and the outer PuO_2/UO_2 zone. Calculational procedures had to be carefully checked for the effects of the approximations applied. As such, these two configurations may be regarded as providing benchmark tests for data and methods in the analysis of heterogeneous Th-containing fast reactors. Central reaction rate ratio results in Cores 13 and 15 confirmed the earlier observation that the GGC-4 calculation of resonance

self-shielding effects for ^{232}Th capture appears significantly better than that of the MURALB/FGL5 route. As in Cores 11 and 12, σ_f(Th232)/σ_f(Pu239) was underpredicted. The underprediction in Core 15, however, was much less than in the other lattices, suggesting that the neutron flux in the MeV region was being overpredicted in the Th-metal blanket - a conclusion reinforced by results for σ_f(U238)/σ_f(Pu239).

Radial distributions of reaction rates through the internal blankets and into the surrounding PuO_2/UO_2 lattice provided further experimental checks in Cores 13 and 15. Two different transport-theory models were used for the whole-reactor calculations. Comparison of calculation and experiment for the traverses for ^{232}Th capture and ^{232}Th fission led to conclusions consistent with those drawn from the central reaction rate ratio measurements. Overall, the results for Cores 13 and 15 indicated that the breeding characteristics of heterogeneous Th-containing fast reactor cores appear to be predictable to accuracies comparable to those for ^{238}U-containing systems.

Analysis of the axial Th-blanket configurations of Cores 14 and 16 was very much more sensitive to the influence of the PROTEUS thermal driver regions than was the case for the internal blanket experiments of Cores 13 and 15. This was due to the larger size of the fertile zone, combined with the fact that core neutrons were incident on the blanket from one side only. Comparisons of measurement and calculation for blanket-centre reaction rate ratios, as well as for axial reaction rate traverses, were rather unsatisfactory. The shortcomings were shown to be [illegible] by the inadequate number of neutron energy groups that could be used at the time of the 3-D whole-reactor calculation.

Neutron spectrum measurements in the axial Th-blankets of Cores 14 and 16 provided [illegible] comparisons between

of the data and methods than did the integral reaction rates. The ORNL analysis of these experiments (2), for example, permitted a testing of ENDF/B-5 cross-sections, and it was demonstrated how the new (n,n') data for ^{232}Th improved the agreement between measured and calculated spectra above 500 keV but worsened it below 200 keV. The neutron-spectrum results, however, could provide little evidence regarding the ^{232}Th capture and fission data per se and were clearly complementary to the reaction rate measurements.

Zusammenfassung

Die Verwendung von Thorium als Kernbrennstoff wird vor allem im Zusammenhang mit seinem Einsatz in fortgeschrittenen, hochkonvertierenden Reaktoren und/oder Schnellen Brütern diskutiert. Während die nuklearen Basisdaten für den ^{239}Pu-^{238}U Brennstoffzyklus seit Jahren immer wieder überprüft und verbessert werden, mussten bei der Berechnung thoriumhaltiger Schneller Brutreaktoren relativ grosse Unsicherheiten in den nuklearen Wirkungsquerschnittsdaten in Kauf genommen werden. Dies war hauptsächlich auf den Mangel an integralen Benchmarkexperimenten zurückzuführen. In der vorliegenden Arbeit werden kritische Experimente mit thoriumhaltigen Gitteranordnungen im Nullleistungsreaktor PROTEUS beschrieben, welche helfen sollen, die Unsicherheiten in den nuklearen Wirkungsquerschnittsdaten des ^{233}U-^{232}Th-Brennstoffzyklus wenigstens teilweise zu verringern.

Der Nullleistungsreaktor PROTEUS am EIR besteht aus einer selbst unterkritischen schnellen Zone, welche mit zwei ringförmigen thermischen Treibern umgeben ist, um die Kritikalität des Gesamtsystems zu erreichen. In der vorliegenden Arbeit werden Untersuchungen an sechs verschiedenen Testzonenanordnungen beschrieben. Als Brennstoffmaterial für die Spalt- und Brutzonen der Testgitter wurden Stäbe aus 15 % PuO_2/UO_2, abgereichertem UO_2, ThO_2, resp. Th-Metall eingesetzt. Das erste der untersuchten Testgitter (Core 11) entsprach einem normalen GCFR-Kern mit 15 % PuO_2/UO_2 Stäben. In diesem Testgitter konnten die ungestörten (für unendliche Verdünnung) ^{232}Th- und ^{233}U-Reaktionsraten in einem reinen GCFR-Spektrum gemessen werden. Für die Experimente im zweiten Gitter (Core 12) wurde ein Drittel der PuO_2/UO_2-Stäbe durch ThO_2-Stäbe ersetzt, wodurch eine relativ homogene Verteilung von ThO_2 in einem schnellen Gitter simuliert werden konnte. Vier weitere untersuchte Cores bestanden aus

heterogenen Gitteranordnungen. Core 13 und 15 enthielten beide eine zentrale Blanketzone aus ThO_2, resp. Th-Metall, welche von einer PuO_2/UO_2-Zone umgeben war. In Core 14 und Core 16 wurden axiale Blanketzonen aus ThO_2, resp. Th-Metall eingebaut.

Im Zentrum jeder Testzonenanordnung wurde die wichtigsten charakteristischen Reaktionsratenverhältnisse, sowie radiale und axiale Reaktionsratentraversen durch Spalt- und Blanketzone gemessen. Wenn immer möglich wurden sowohl absolute, wie auch relative (zu den thermischen) Reaktionsratenverhältnisse bestimmt. Dadurch konnten systematische Fehler besser erkannt werden. Neutronenspektrumsmessungen im Energiebereich von ~10 keV bis 2.3 MeV wurden mit kugelförmigen Rückstossprotonenzählern in den Cores 12, 14 und 16 durchgeführt.

Zur Berechnung der einzelnen Testgitteranordnungen wurden zwei verschiedene nukleare Datenbibliotheken und Zellrechnungsprogramme verwendet: (1) den adjustierten englischen Datensatz FGL5 zusammen mit dem Zellcode MURALB und 2) den amerikanischen Code GGC-4 unter Verwendung der auf ENDF/B 4 basierenden Feingruppendaten. Für die Berechnungen von Cor 11, 12, 13 und 15 wurde die Transportgleichung für ein eindimensionales, zylindersymmetrisches Ganzreaktormodell gelöst. Bei der Analyse der Anordnungen mit axialen Blanketzonen (Cores 14 und 16) wurde ein zweidimensionales Diffusionsmodell verwendet. Für die Analysen der Neutronenspektrumsmessungen waren spezielle Rechnungen notwendig. Die berechneten Spektren für die Cores 14 und 16 wurden - in Zusammenarbeit mit dem CNL - aus zweidimensionalen Transportrechnungen gewonnen, 25).

Die reaktorphysikalischen Parameter im Zentrum von Core 11 und 12 sind hauptsächlich durch die Eigenschaften der zentralen Testzone bestimmt; den Einfluss der äussere Reaktorzone (Treiber, Reflektor) ist unbedeutend. Diese beiden Gitteranordnungen können deshalb als Benchmarkkonfigurationen zur

Ueberprüfung der nuklearen Daten betrachtet werden. Eine wichtige Grösse ist das Reaktionsratenverhältnis σ_c(Th232)/σ_f(Pu239), da dieses die Brutrate bestimmt. Für beide Gitteranordnungen ist die Uebereinstimmung zwischen gemessenem und aufgrund von ENDF/B-4 Daten berechnetem Verhältnis besser als ∿2 %. Dieses Ergebnis ist überraschend, wenn man die relativ grosse Unsicherheit (± 10-20 %) in den nuklearen ^{232}Th-Einfangsquerschnitten berücksichtigt. Zudem schienen unsere Resultate neueren differentiellen Messungen zu widersprechen (7). Die Ergebnisse der differentiellen Messungen wurden jedoch kürzlich um 11 % nach oben korrigiert (45) und sind somit in recht guter Uebereinstimmung mit den ursprünglichen ENDF/B-4 Daten für den ^{232}Th-Einfangsquerschnitt.

Rechnungen mit MURALB/FGL5 und GGC-4/ENDF/B-4 ergaben für Core 11 sehr ähnliche Reaktionsratenverhältnisse für σ_c(Th232)/σ_f(Pu239). Grössere Abweichungen wurden allerdings für die Ergebnisse in Core 12 beobachtet, wo die Resonanzselbstabschirmung für ^{232}Th eine wichtige Rolle spielt. Es zeigte sich, dass dieser Effekt in GGC-4/ENDF/B-4 deutlich besser berücksichtigt wird als in MURALB/FGL5. Beide Rechenverfahren ergeben für Core 11 und 12 um rund 12 % tiefere σ_f(Th232)/σ_f(Pu239)-Verhältnisse als die entsprechenden Messungen. Die ^{232}Th-Spaltquerschnitte in der ENDF/B-4 Datenbibliothek liegen wahrscheinlich zu tief. Dies hat allerdings nur einen unbedeutenden Einfluss auf die Neutronenbilanz im Schnellen Brüter mit Thorium. Die berechneten σ_f(U233)/σ_f(Pu239)-Verhältnisse stimmen bis auf etwa 1 % mit den gemessenen Werten überein. Die ^{233}U-Spaltquerschnitte für mündliche Veröffentlichung scheinen daher in der ENDF/B-4 Datenbibliothek korrekt zu sein. Die Ergebnisse für zusätzliche Th-spezifische Reaktionsratenverhältnisse wie z.B. σ_c(U238)/σ_f(Pu239) liegen im Rahmen früherer PROTEUS-Untersuchungen (29, 37).

Die internen ThO_2- resp. Th-Metall-Brutzonen von Core 13 resp. Core 15 zeigten eine starke neutronische Kopplung mit der umgebenden PuO_2/UO_2-Zone. In den Rechnungen mussten deshalb die benützten Näherungsmethoden genau überprüft werden. Diese beiden Gitteranordnungen können als Benchmarkprobleme sowohl zur Ueberprüfung der nuklearen Grunddaten als auch der Rechenmethoden betrachtet werden. Die Ergebnisse für die im Zentrum der Testzone gemessenen und berechneten Reaktionsratenverhältnisse bestätigten die frühere Feststellung, dass mit GGC-4/ENDF/B-4 der Resonanzselbstabschirmungseffekt für ^{232}Th-Einfang besser erfasst werden kann als mit MURALB/FGL5. Wie in Core 11 und 12 wurde σ_f(Th232)/σ_f(Pu239) auch in den internen Blanketzonen durch die Rechnung unterschätzt. Die Unterschätzung ist in Core 15 allerdings deutlich geringer als in den anderen Gitteranordnungen. Dies deutet darauf hin, dass im Th-Metallblanket der Neutronenfluss im MeV-Bereich überschätzt wird - eine Folgerung, die durch die σ_f(U238)/σ_f(Pu23)-Ergebnisse unterstützt wird.

Radiale Reaktionsratentraversen durch die zentrale Brutzone und die umgebende PuO_2/UO_2-Zone erlaubten eine zusätzliche Ueberprüfung der verwendeten Daten und Rechenmethoden. Zur rechnerischen Analyse wurden zwei verschiedene 1D-Transportmodelle benützt. Die Vergleiche zwischen berechneten und gemessenen ^{232}Th-Einfangs- und ^{232}Th-Spaltratentraversen bestätigen die bereits aufgrund der Ergebnisse für die zentralen Reaktionsratenverhältnisse gemachten Aussagen über die nuklearen Basisdaten und Rechenmethoden. Zusammenfassend darf aufgrund der Ergebnisse für Core 13 und 15 festgestellt werden, dass die Eigenschaften heterogener Gitteranordnungen für schnelle Brutreaktoren mit zentralen, thoriumhaltigen Blanketzonen mit vernünftiger Genauigkeit berechnet werden können - vergleichbar mit entsprechenden Anordnungen mit zentralen ^{238}U-Blanketzonen.

Die Ergebnisse für Core 14 und 16 zeigten eine viel stärkere Beeinflussung der axialen Thoriumzonen durch Neutronen aus den thermischen Treiberzonen des PROTEUS-Reaktors als in den zentralen Blankets von Core 13 und 15. Die Gründe liegen einerseits in den relativ grossen axialen Blanketzonen, andererseits in der Tatsache, dass Neutronen aus der Kernzone nur von einer Seite in die Blanketzone eindringen. Die Vergleiche zwischen gemessenen und berechneten Resultaten sind recht unbefriedigend und zwar sowohl für die im Blanketzentrum gemessenen Reaktionsratenverhältnisse wie auch für die axialen Reaktionsratentraversen. Es wurde festgestellt, dass insbesondere die ungenügende Energieauflösung (10 Gruppen) in den zweidimensionalen Ganzreaktorrechnungen grosse Abweichungen zwischen den gemessenen und berechneten Resultaten verursacht.

Die Neutronenspektrumsmessungen in den axialen Thoriumzonen von Core 14 und 16 lieferten in einigen Aspekten eine umfassendere Ueberprüfung der nuklearen Daten und der Rechenmethoden als dies allein mit den integralen Reaktionsratenmessungen möglich war. Die ORNL-Analysen der Spektrumsmessungen (25) erlaubten zudem die Ueberprüfung der ENDF/B-5 Th-Querschnittsdaten. Dabei wurde u.a. festgestellt, dass die neuen ^{232}Th (n,n')-Querschnittsdaten die Uebereinstimmung zwischen berechnetem und gemessenem Neutronenspektrum im Energiebereich oberhalb 500 keV klar verbessern, unterhalb 200 keV aber schlechtere Ergebnisse liefern als die ^{232}Th(n,n')-Daten aus der ENDF/B-4 Bibliothek. Die Neutronenspektrumsmessungen geben andererseits nur wenig Informationen über die ^{232}Th-Einfangs- und Spaltquerschnitte; diese müssen aus Reaktionsratenmessungen gewonnen werden. Neutronenspektrums- und Reaktionsratenmessungen konnten aber gemeinsam wichtige, sich ergänzende Informationen liefern.

LIST OF FIGURES

LIST OF FIGURES (contd.)

LIST OF FIGURES (cont'd.)

LIST OF TABLES

1. INTRODUCTION

The worldwide occurrence of thorium is estimated as 1-3 times that of uranium (1-3). Since thorium is purely a fertile material and must first be converted to fissile ^{233}U, its largescale utilization as a nuclear fuel is usually linked to its introduction in fast breeder reactors and/or advanced converters. Reactor strategies which seek to optimise usage of the total available thorium and uranium reserves, are usually based on a symbiosis between fast and thermal reactor systems, e.g. FBR/HTR (4).

In recent years, there was increased interest in applying the ^{233}U-^{232}Th fuel cycle to fast reactors following the suggestion that it might offer superior proliferation resistance to that of the ^{239}Pu-^{238}U cycle. The NFCE study (1), however, has concluded that the use of denatured ^{233}U-^{238}U fuel would not necessarily alter proliferation risks in a significant manner. The longterm utilization of thorium as a basic energy resource thus remains the more important argument for development of the thorium fuel cycle for fast reactor applications.

1.1 Physical Characteristics of the Thorium Cycle in Fast Reactors

It is useful to first compare the material properties of thorium and uranium in both the oxide and metal form (3). While ThO_2 has a slightly lower density than UO_2, its significantly higher melting point and thermal conductivity permit higher power densities to be tolerated. More important, perhaps, are the differences in material properties between the metals. Not only is the phase-transition temperature of

Th-metal about twice as high as that of U-metal, its irradiation behaviour characteristics are also much more satisfactory. The breeding gains achievable with thorium and uranium metals are, due to harder neutron spectra, considerably higher than with the corresponding oxides. That Th-metal may prove to have adequate material properties for use in fast reactors, and U-metal not, is thus clearly an advantageous feature of the thorium fuel cycle.

There are, however, from the reactor physics standpoint, certain disadvantages of using ^{233}U-^{232}Th as a fast reactor fuel. The η-factor for ^{233}U is significantly lower in a fast reactor than that of ^{239}Pu. Further, the fast fission effect is much lower in ^{232}Th than in ^{238}U. Both these factors result in lower breeding gains for the thorium cycle. The fact that the fissile inventory of a ^{233}U-fuelled system is usually lower than for a ^{239}Pu-fuelled system provides only a slight compensating effect on the fuel doubling time. As indicated earlier, however, the use of Th-metal, rather than of ThO_2, could yield net breeding characteristics for a ^{233}U-Th system which are quite comparable to those of a ^{239}Pu-fuelled system using UO_2 as the fertile material (5).

An advantage of using ^{232}Th instead of ^{238}U in a fast reactor is that the sodium void coefficient is significantly improved, while the Doppler coefficient remains sufficiently negative. Since the sodium void effect is widely accepted as an important safety feature for a fast reactor, this has provided additional incentive for the introduction of thorium-containing systems.

The reprocessing of ^{233}U-Th fuels (which is still to be established as commercially viable) is complicated by the occurrence of ^{232}U and its daughters, the decay of which

results in the emission of high-energy γ-rays. In a fast reactor the production of ^{232}U is enhanced through the high-threshold $^{232}Th(n,2n)$ reaction, and the effect is particularly pronounced for thorium present in the core.

1.2 Thorium in Symbiotic Strategies

The use of ^{233}U-Th fuel in homogeneous fast reactor cores does not, overall, provide an attractive alternative to ^{239}Pu-^{238}U. It is of greater interest to consider the introduction of thorium in separate radial, axial and internal blanket zones in a fast reactor - while retaining ^{239}Pu as the principal fissile nuclide. It has been shown that for such heterogeneous configurations the blanket region related, as well as the global, breeding ratios for both ThO_2 and Th-metal are quite comparable to those for UO_2 (3).

There are several other advantages of using PuO_2-UO_2 as the core material and introducing thorium only in separate blanket zones. Thus, the benefits of the high fast fission effect in ^{238}U in the core are retained. Secondly, ^{232}U production due to the $^{232}Th(n,2n)$ reaction is much lower with thorium present only in the blanket. Finally, with no ^{233}U being bred in the core, the shutdown control problem associated with ^{233}Pa decay ($T_{1/2}$=27.0 days) is very much reduced.

Considering that ^{233}U is a slightly less favourable fuel in a fast reactor core than ^{239}Pu, there would be no particular incentive to recycle the ^{233}U bred in the thorium blanket zones back into a fast reactor. A preferred option would be implementation of the thorium cycle in symbiotic strategies employing both fast and thermal reactor systems.

This follows from the fact that ^{233}U, with its higher thermal η-value, is a better thermal reactor fuel than both ^{235}U and ^{239}Pu. Operation of the ^{233}U-^{232}Th cycle in thermal reactors such as the HTR and CANDU can, in fact, result in finite breeding gains. An attractive strategy would thus be to operate FBRs with thorium blanket zones and PuO_2/UO_2 cores, and to use the blanket-produced ^{233}U for fueling advanced thermal converters which could then operate in an almost self-sufficient manner on the thorium cycle.

1.3 The Need for Integral Experiments

In order to be able to assess the performance of thorium-containing fast reactors with an accuracy comparable to that currently achievable for ^{239}Pu-^{238}U FBRs, it is necessary to provide a sufficiently broad range of integral experiments for checking the basic nuclear data. Thus, while the basic data used in calculations for the ^{239}Pu-^{238}U cycle have been repeatedly checked and improved over the years, relatively large uncertainties continue to exist for the cross-section data necessary for analysing thorium-containing fast reactor systems. For a ^{233}U-^{232}Th fuelled LMFBR, for example, uncertainties of $\pm$ 10-20 % have been estimated for ^{232}Th capture, $\pm$ 5-10 % for ^{232}Th fission, and $\pm$ 10-15 % for inelastic scatter (6). The corresponding figures quoted for ^{233}U capture and fission are $\pm$ 20-30 % and $\pm$ 3-5 %, respectively.

Recent differential measurements for ^{232}Th yielded values of the capture cross-section (7) and the total cross-section (8) which differ very significantly from those in the U.S. ENDF/B-IV library.* A review of the available integral measurements for thorium in fast systems, on the other hand,

---

* see Abstract, p. vi, for latest situation

suggested that ENDF/B-IV performs surprisingly well (9). The authors of this review did, however, comment on the sparseness of good, analysable integral experiments. A need has thus existed for providing further experimental checks.

The programme of integral measurements for thorium described in this report seeks to satisfy the above need, at least in part. It should thus help in checking the validity of any conclusions that are drawn from calculational studies for the thorium fuel cycle in fast reactors (1). Apart from the determination of integral parameters in well-defined fast neutron spectra, a major point of emphasis in the current programme has been the measurement, and comparison with calculation, of important reaction rate distributions in the vicinity of core/blanket interfaces. These measurements should thus be of particular relevance for checking design calculations for fast reactor systems with heterogeneous blanket zones of ThO_2 and/or Th-metal.

Detailed descriptions of the various core configurations considered, the measurement and calculational methods employed, as well as of the results obtained, are given in the following chapters.

2. EXPERIMENTAL CONFIGURATIONS

2.1 The PROTEUS Reactor

All the experiments for the current thorium programme were carried out in the zero-energy reactor facility, PROTEUS, at [illegible]. A cutaway view of the reactor, essentially a coupled thermal/fast system, is shown in Fig. 1. Figs. 2 and 3 give horizontal and vertical sectional views.

A central fast test zone (5, in Fig. 1) was driven critical by annular thermal driver zones (2 and 3). A reduction by a factor of ~10 was thereby achieved for the Pu-inventory of the fast test lattice, relative to that which would have been necessary for a critical single-zone reactor of the same composition. The central test zone (5) had a diameter of 0.50 m and contained over 2000 fuel rods of 1.40 m nominal length arranged in a lattice of 10 mm hexagonal pitch.

The thermal driver consisted of a D_2O - (3) and a graphite-moderated zone (2). Both these zones contained 5 % enriched UO_2 fuel. A natural-uranium metal buffer zone (4) was located between the D_2O-driver and the fast test lattice, and this served to capture the thermal neutrons coming from the driver and convert them, in part, into fast fission neutrons. A partial compensation of leakage losses from the fast zone was thereby achieved. An optimal zone layout thus enabled the central neutron spectrum in the test zone to closely approximate that of a gas-cooled fast power reactor - an important criterion for carrying out integral measurements relevant to this type of reactor.

A central test column (6, in Fig. 1) could be moved in and out of the test zone. Apart from being used for the introduction of measurement probes, such as foils and neutron spectrometers,

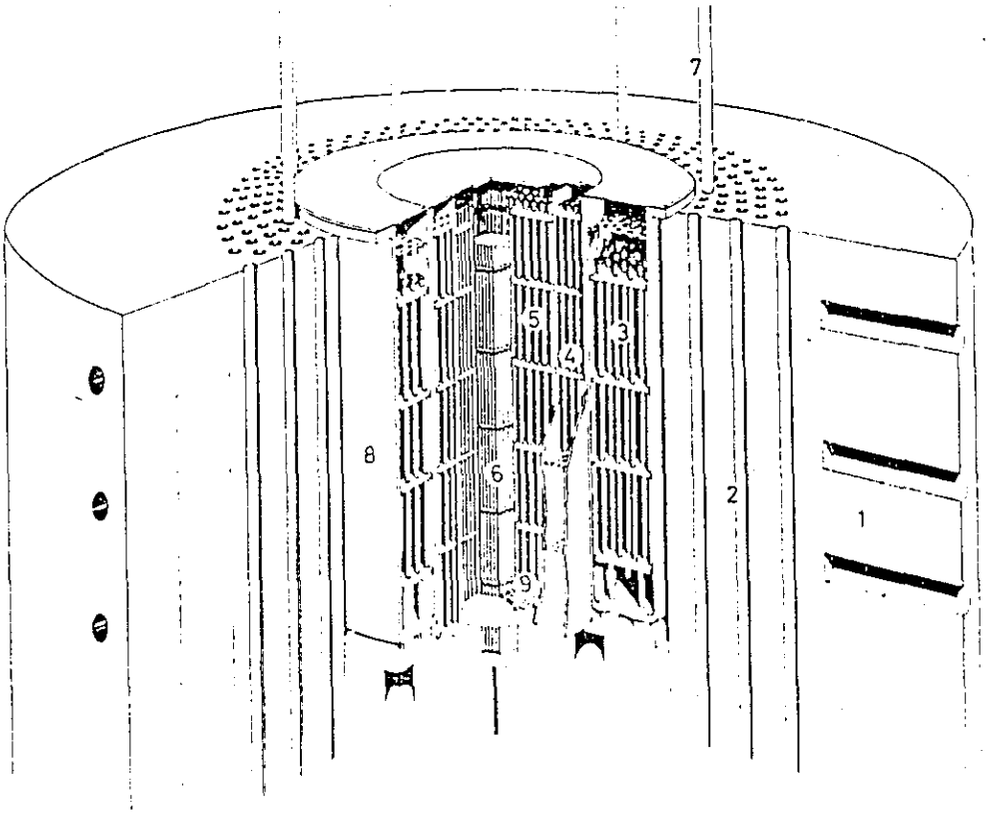

1 GRAPHITE REFLECTOR
2 GRAPHITE DRIVER
3 D_2O-DRIVER
4 BUFFER
5 FAST ZONE
6 TEST COLUMN
7 CONTROL ROD
8 MODERATOR TANK
9 REMOVABLE GRID PLATE

Fig. 1 Cutaway [illegible] PROTEUS Reactor

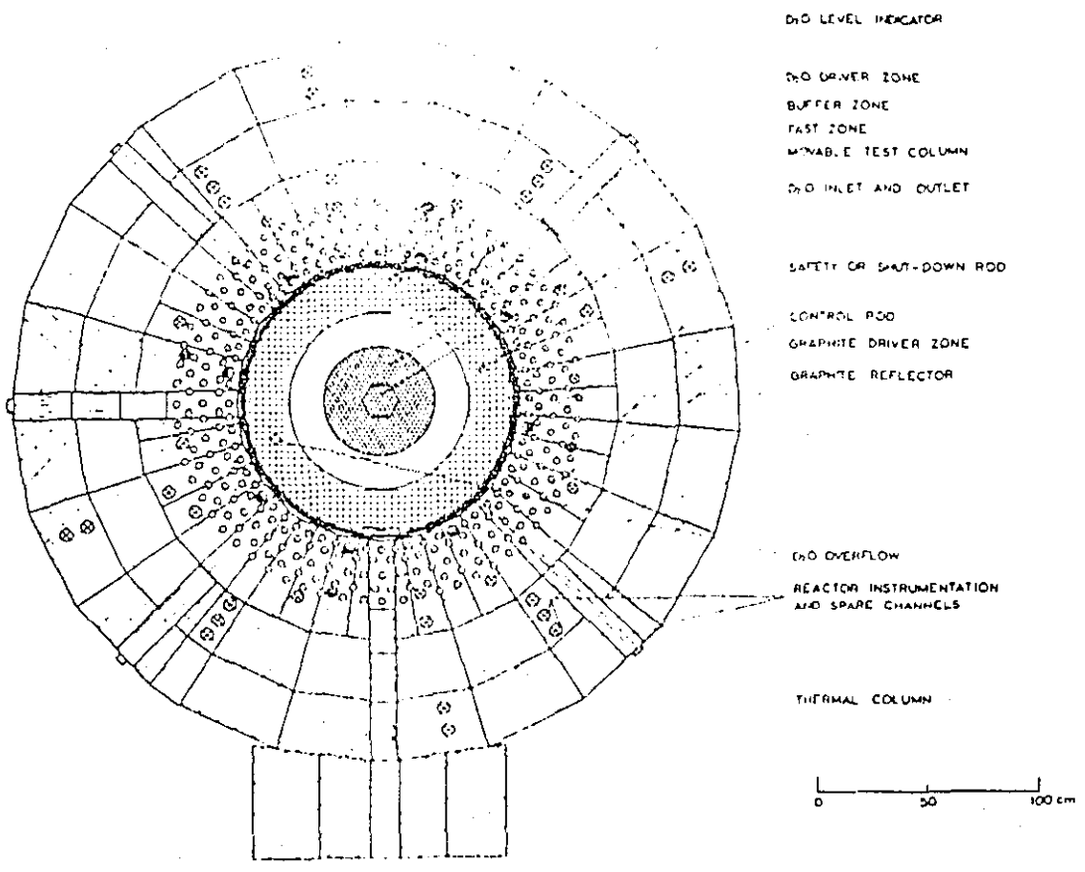

Fig. 2 Horizontal Sectional View of the PROTEUS Reactor

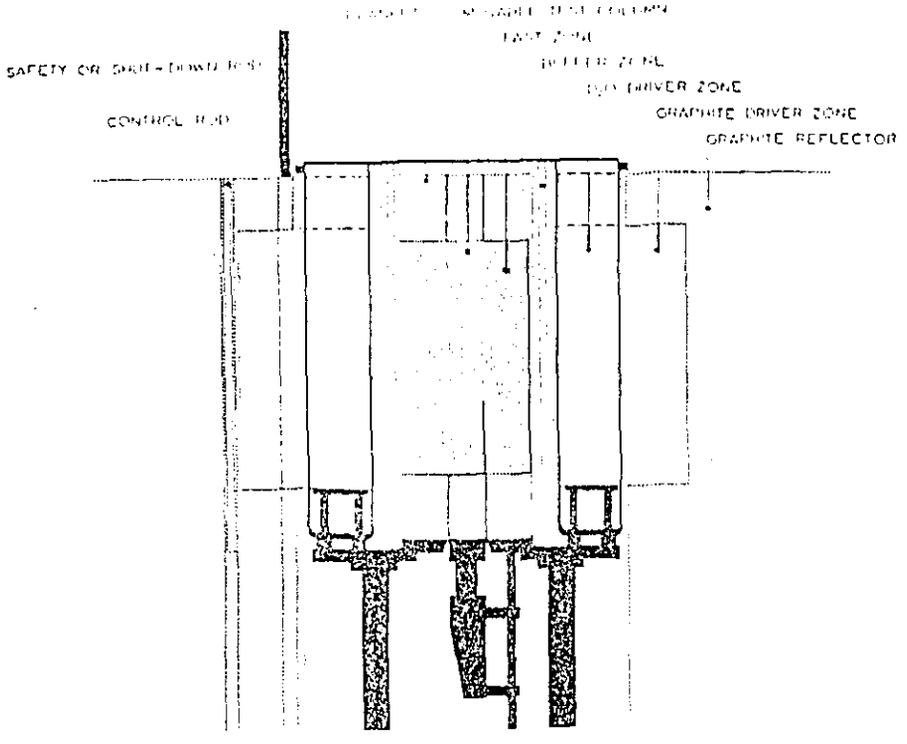

Fig. 3 Vertical Sectional View of the PROTEUS Reactor

the column also provided some flexibility in the experimental programme in that it was an easily replaceable central region of the test lattice.

2.2 Core Configurations for the Thorium Programme

Experiments were carried out in six different core configurations (Table 1). There were four principal materials used for the test zones in the various configurations, viz. PuO_2/UO_2 fuel, depleted UO_2, ThO_2 and Th-metal. Details of the form in which these materials were used are given in Table 2.

2.2.1 Core 11, Standard PuO_2/UO_2 Lattice

The test lattice in this case corresponded to that of a normal GCFR core. All the fuel rods in the test zone were of the same composition, and consisted of a central 0.67 m length of 15 % PuO_2/UO_2 fuel (12 cigars) with depleted UO_2 blanket material (6 cigars at each end) making up the total length of 1.40 m. The core layout was essentially as shown in Fig. 4 for Core 12, except that all the rod positions shown in the test zone were occupied by PuO_2/UO_2 rods of the above type. The lattice was thus constructed on a hexagonal pitch of 10 mm. Measurements for Core 11 were carried out in the centre of, as well as radially across, the test lattice.

2.2.2 Core 12, Mixed PuO_2/UO_2-ThO_2 Lattice

In this Core, one third of the fuel rods of Core 11 were replaced by ThO_2 rods. Fig. 4 shows a horizontal section

Table 1 Core Configurations for the PROTEUS Thorium Programme

CORE 11	NORMAL PuO_2/UO_2 LATTICE	TEST OF INFINITELY DILUTE XSECS FOR TH232 AND U233
CORE 12	MIXED ThO_2-PuO_2/UO_2 LATTICE	TEST OF XSECS FOR TH232 AND U233 IN SOFTER SPECTRUM AND CHECK OF SHIELDING FACTORS FOR TH232
CORE 13	HETEROGENEOUS CONFIGURATION WITH A CENTRAL RADIAL ThO_2 ZONE	TEST OF XSECS AND CALCULATION METHODS
CORE 14	HETEROGENEOUS SYSTEM WITH AN UPPER AXIAL ThO_2 BLANKET	
CORE 15	AS CORE 13, BUT THORIUM METAL REPLACING OXIDE	
CORE 16	AS CORE 14, BUT THORIUM METAL REPLACING OXIDE	

Table 2 Description of the Fuel and Blanket Materials

a) PuO_2/UO_2 Cigars

Fuel Material		PuO_2/UO_2 Pellets
Pu/(Pu+U)	(w %)	14.96
$^{240}Pu/Pu$	(w %)	17.69
$^{241}Pu/Pu$	(w %)	2.15
$^{235}U/U$	(w %)	0.42
Density	(g/cm^3)	10.6
Pellet Diameter	(mm)	6.7
Pellet Length	(mm)	6.9
Cigar Can Material		Al
Wall Thickness	(mm)	0.085
Fuel Length in Cigar	(mm)	55.4

b) Depleted UO_2 Cigars

Blanket Material		UO_2 Pellets
$^{235}U/U$	(w %)	0.42
Density	(g/cm^3)	10.5
Pellet Diameter	(mm)	6.7
Pellet Length	(mm)	7.1
Cigar Can Material		Al
Wall Thickness	(mm)	0.085
Fuel Length in Cigar	(mm)	55.4

(Table 2 cont'd)

c) ThO_2 Cigars

Blanket Material		Sintered ThO_2 particles of density 9.9 g/cm^3 and mean diameter 406 µm
Cigar Can Material		18/8 Steel
Inner Diameter	(mm)	6.9
Outer Diameter	(mm)	7.0
Cigar Length	(m)	0.334
Filling Factor for ThO_2 Particles in the Cigar	(vol %)	61.4
ThO_2 Density in the Cigar	(g/cm^3)	6.08

The above types of fuel and blanket cigars were filled into hollow 18/8 steel tubes of

Inner Diameter	(mm)	7.4
Outer Diameter	(mm)	8.2
Nominal Length	(m)	1.40

d) Th Metal Rods

Blanket Material		Thorium Metal
Density	(g/cm^3)	11.3
Diameter	(mm)	19.0
Length	(m)	0.356

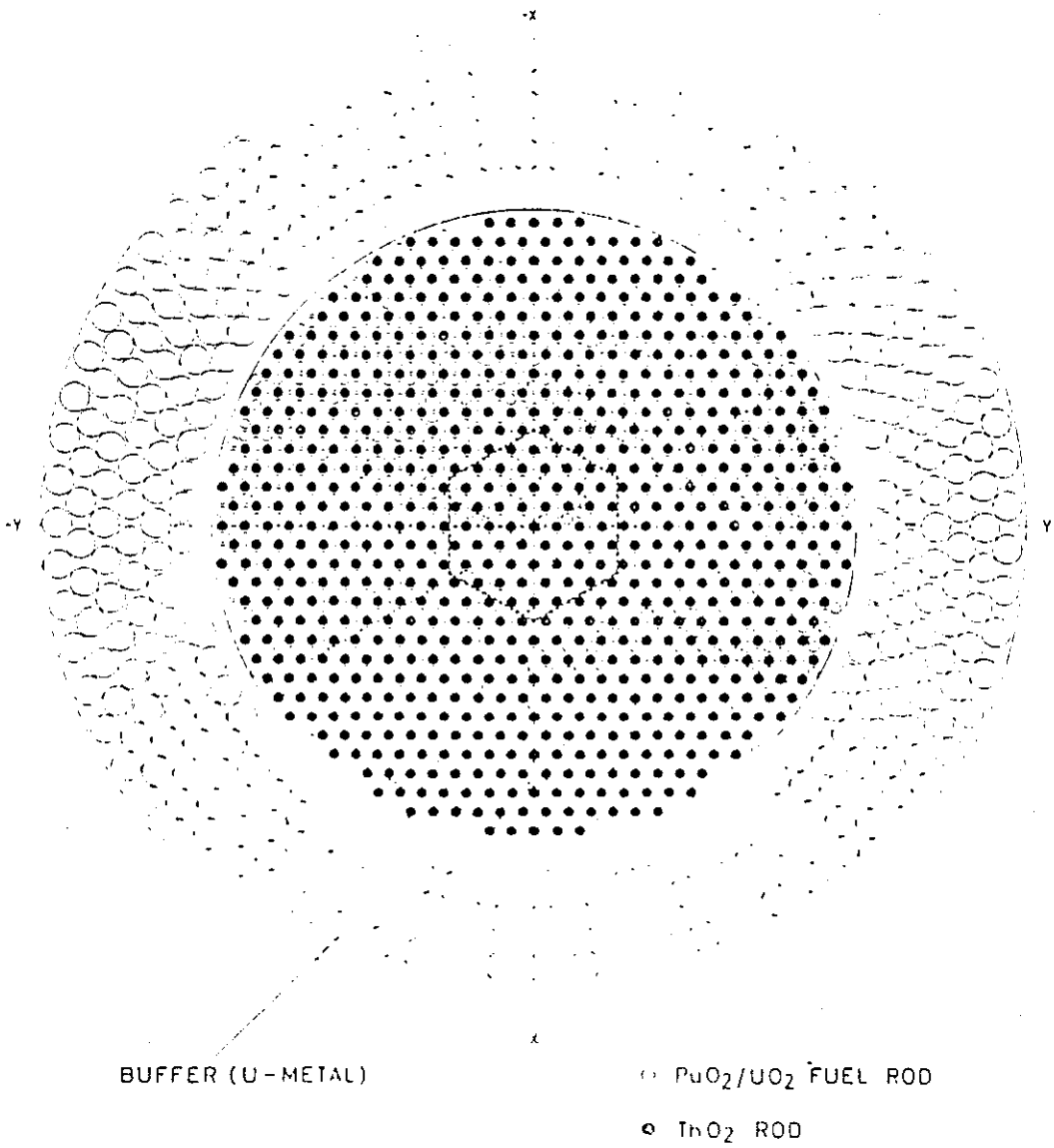

Fig. 4 Horizontal Sectional View for Core 12

across the [illegible] It is seen that a relatively [illegible] linearly into the PuO_2/U[illegible]

The PuO_2/U[illegible] fuel [illegible] was built up somewhat differently from [illegible] each consisted of 18 PuO_2/U[illegible] [illegible] PuO_2 cigars

at the ends, i.e. a PuO_2/UO_2 length of ∿ 1.00 m and UO_2 lengths of ∿ 0.17 m at the ends. The ThO_2 rods consisted of three 0.33 m long ThO_2 cigars (Table 2), bounded at both ends by the same length of depleted UO_2 as in the case of the PuO_2/UO_2 rods. Thus, in effect, the mixed PuO_2/UO_2-ThO_2 test lattice of Core 12 was of height ∿ 1.00 m and diameter 0.50 m, with upper and lower UO_2 blanket zones of 0.17 m thickness. Measurements (reaction rates and neutron spectrum) were carried out in the centre of the test zone only.

2.2.3 Core 13, Lattice with Internal ThO_2 Blanket

This was the first of four core configurations for the investigation of heterogeneous thorium blanket zones. A ThO_2 zone of diameter 0.137 m was introduced into the centre of the standard PuO_2/UO_2 lattice, 169 ThO_2 rods of the type used in Core 12 being used for creating this zone. Fig. 5 gives the horizontal sectional view for Core 13 and shows the internal ThO_2 blanket surrounded by the annular PuO_2/UO_2 zone ∿ 0.17 m thick. The PuO_2/UO_2 rods used in Core 13 were of the same type as those in Core 12.

Apart from measurements made in the centre of the ThO_2 zone, reaction rate distributions were measured across the blanket/core interface since these provided a sensitive test for the calculation of the breeding ratio in a heterogeneous core. The measurement positions used for determining the reaction rate traverses in Core 13 are indicated in Fig. 5.

2.2.4 Core 14, Lattice with Axial ThO_2 Blanket

The layout for Core 14 is shown schematically in Fig. 6. Also indicated in the figure is the composition of each fuel

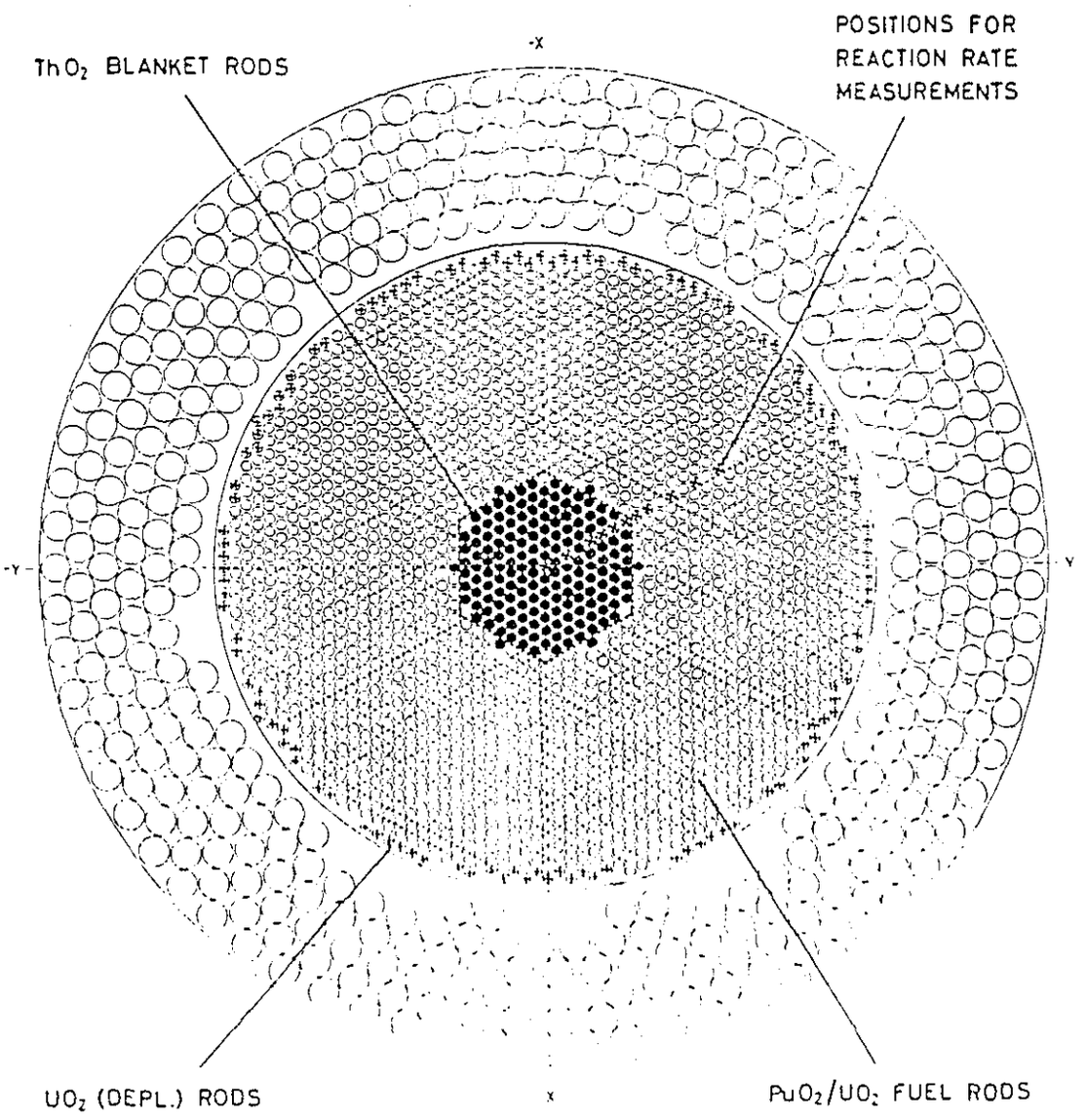

Fig. 5 Horizontal Sectional View for Core 13

rod in the test lattice [illegible], with 3 depleted UO_2 [illegible] above (Table 2). As in the previous cores, the test-lattice rods were located on a hexagonal pitch of 10 mm.

In order to obtain clean, well-defined boundary conditions for the whole-reactor calculations, the axial ThO_2 blanket was covered with a steel shielding block 0.60 m thick. Further, a boron plastic layer was introduced as shown (Fig. 6) for

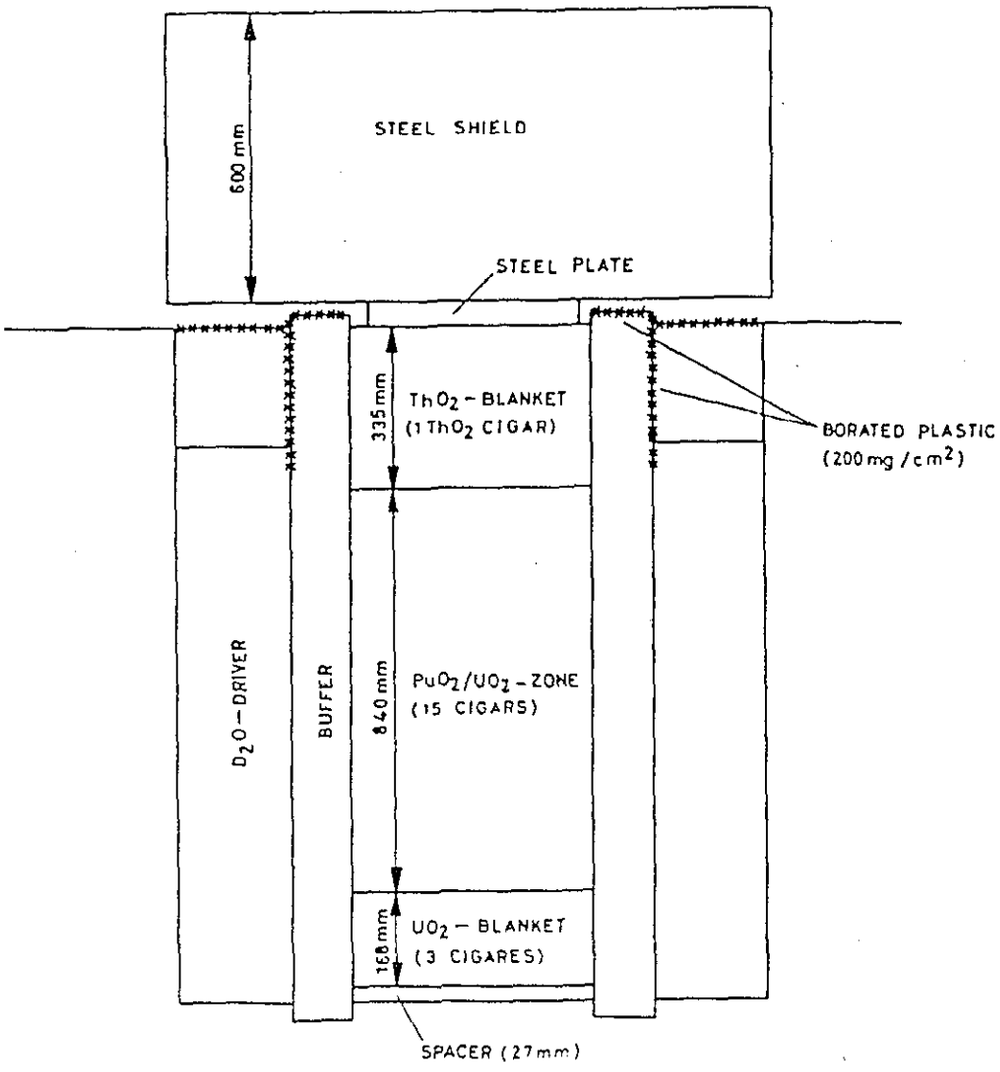

Fig. 6 Reactor Layout for Core 14

reducing the influence of thermal-driver neutrons on measurements made in the ThO_2 blanket.

Axial reaction rate traverses across the core/blanket interface were of principal interest in the Core 14 measurements, and these were determined along the central axis. The neutron spectrum at the centre of the ThO_2 blanket was also determined. Experimental details for the various measurements are given in Chapter 3.

2.2.5 Core 15, Lattice with Internal Th-Metal Blanket

The layout for this Core was similar to that for Core 13, with the difference that the central blanket zone was one of Th-metal instead of ThO_2. Fig. 7 shows the horizontal sectional view for Core 15 and also indicates the measurement positions used for obtaining radial reaction rate traverses across the blanket/core regions.

The Th-metal rods used for constructing the internal blanket were of diameter 19 mm and were located on a hexagonal pitch of 21 mm (Fig. 7). The closer packing achieved for the rods, as well as the fact that they were of solid Th-metal (while the ThO_2 rods consisted of sintered particles in steel cigars, Table 2) meant that the cell-averaged thorium density for the Th-metal zone was nearly a factor of 4 higher than for the ThO_2 zone. Thus, in a certain sense, the measurements carried out in Core 15 provided a more stringent test for ^{232}Th data than did the corresponding measurements in Core 13.

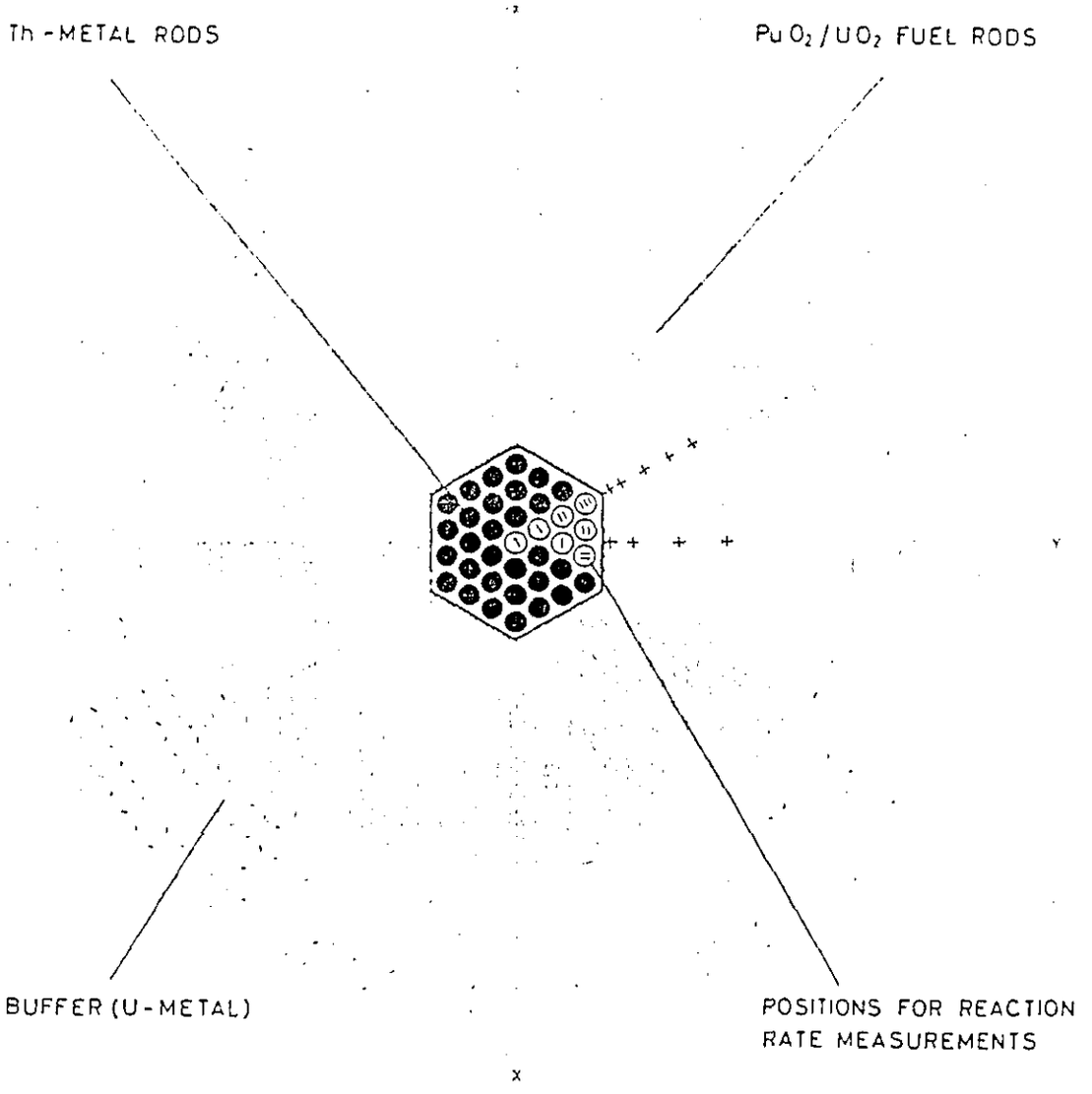

Fig. 7 Horizontal Sectional View for Core 15

2.2.6 Core 16, Lattice with Axial Th-Metal Blanket

The layout for Core 16 was similar to that for Core 14 (Fig. 6), with Th-metal replacing ThO_2 for the axial blanket zone. As for Core 15, the 19 mm-diameter Th-metal rods were arranged on a hexagonal lattice pitch of 21 mm. The programme of measurements for Core 16 was similar to

that for Core 14, with reaction rate traverses being determined along the central axis and the neutron spectrum being measured at the centre of the Th-metal blanket.

3. EXPERIMENTAL METHODS

3.1 Reaction Rate Measurements

3.1.1 Measuring Equipment

(a) Activation Foils and Deposits

Metallic foils, 0.01 mm - 0.20 mm thick, or deposits of $\sim$ 1 mg/cm^2 thickness, were used for the various activation measurements. They were introduced into the desired measurement positions in the reactor and, after irradiation, counted on an appropriate γ-counting system.

In the case of ^{239}Pu, ^{235}U and ^{233}U, the foils were Al-alloyed and Ni-plated, the amount of fissile material contained in each type of foil being $\sim$ 4 mg/cm^2.

(b) Fission Track Detectors

Each sample consisted of a fissile or fissionable deposit of 10-100 µg/cm^2 thickness, together with a MAKROFOL-plastic cover foil. After an irradiation, the plastic foils were etched and a staining procedure carried out to facilitate automatic counting of the fission tracks using a Quantimet automatic image analyser (10).

(c) Fission Chambers

Back-to-back gas-filled fission chambers were used for the direct counting of fission events occuring in two different deposits of fissile and/or fissionable material. Four activation foils were usually mounted in between the two chamber deposits to enable normalisation of reaction rates with respect to foils at other locations in the reactor.

Certain checks on systematic errors were carried out using

a specially constructed fission chamber. This could be operated either in the usual mode, i.e. as a gas-filled ionisation chamber counting in 2π-geometry (11), or as a low-geometry counter using a Si surface-barrier detector.

(d) Counting Systems

The principal γ-counting equipment consisted of a twin Ge(Li) detector system having a relative efficiency (with respect to a standard NaI system) of ∿ 25 %. This was coupled to an automatic sample changer which could carry upto a maximum of 60 samples. A PDP-11/40 computer enabled on-line analysis of the obtained count rates.

The counting of fission-product γ-rays from fission activation foils, as also the counting of certain low induced-activity samples, was carried out using a twin NaI scintillation detector system. This was coupled to a 12-location automatic sample changer and to counting electronics which included amplification stabilizers.

Certain special measurements requiring the counting of low-energy γ-rays or X-rays involved the use of a Hyperpure Ge detector system (12).

A standard low-geometry α-counting system with a Si surface-barrier detector was used for both absolute and relative calibration of α-emitting deposits.

3.1.2 Measurement Techniques

Each type of reaction rate ratio measurement was, as far as possible, carried out using more than one experimental technique. This enabled some check to be provided on the

different systematic errors (Section 3.1.5 (d)). The two broad categories of measurement techniques employed are discussed below.

(a) Absolute Techniques

A given reaction rate becomes expressible in absolute terms when one knows the number of atoms of the nuclide in the foil or deposit, as also the net, effective counting efficiency of the detector system employed.

In the case of the metal foils (depleted uranium, thorium, etc.), the number of atoms of, say, ^{238}U or ^{232}Th, was obtained from the weight of the foil. Thin deposits (^{239}Pu, ^{237}Np, ^{232}Th, etc.) were calibrated using the low-geometry α-counter. It was not possible to determine the amount of fissile material in the Al-alloyed fission foils with adequate accuracy but these were, in any case, used for relative measurements only.

For neutron capture rate measurements in ^{238}U and ^{232}Th, the effective efficiency of the Ge(Li) detector system employed for counting the activated foils was determined through the use of appropriate α-calibrated deposits, viz. ^{243}Am-^{239}Np and ^{237}Np-^{233}Pa, respectively (13-15). The γ-rays counted were the 278 keV ^{239}Np line for ^{238}U capture and the 312 keV ^{233}Pa line for ^{232}Th capture.

For measurement of the $^{232}Th(n,2n)$ reaction rate, the 25.6 keV ^{231}Th γ-ray was counted using the HPGe detector system, the detector efficiency being determined via an α-calibrated ^{235}U-^{231}Th deposit. Since the $^{232}Th(n,2n)$ measurement was made relative to the ^{232}Th capture rate in a single, irradiated Th-metal foil ($\sim$ 0.01 mm thick), there was no need, in this particular case, to determine the

number of ^{232}Th atoms in the counted sample (12).

Absolute fission rates were obtained from fission chamber count-rates using α-calibrated deposits. The validity of assuming a 2π-geometry in the counting of the fission products was confirmed through measurements made using the special low-geometry fission chamber (Section 3.1.1 (c)).

(b) Thermal Comparison Techniques

The measurements involved simultaneous irradiation of foils and fission chambers located in both the test lattice and in the PROTEUS thermal column (10). A given reaction rate ratio in the core was thus obtained relative to its known value in a standard thermal spectrum. The absolute calibration of foils, deposits and counting-system efficiencies was unnecessary. Clearly, the thermal-comparison approach could not be applied to the measurement of threshold reactions such as ^{232}Th and ^{238}U fission.

3.1.3 Typical Experimental Procedures

(a) Reaction Rate Ratios at Core Centre

One may consider here, as a typical experiment, the measurement of the ^{232}Th capture and fission rates relative to ^{239}Pu fission.

Th-metal foils and Al-alloyed ^{239}Pu fission foils were introduced into a fuel rod at the centre of the test lattice, the foil diameter in each case being identical to that of the fuel pellets. A fission chamber, containing ^{232}Th and ^{239}Pu fission deposits, as also Th and Pu foils, was located in a 60mm-diameter cavity 0.20 m above the core centre.

A second fission chamber, containing ^{239}Pu fission deposits and Th-metal foils, was located in the PROTEUS thermal column.

The experimental parameters obtained from such an irradiation were:

for ^{232}Th capture - absolute value at core centre

ratio between values at core centre and in the thermal column

for ^{239}Pu fission - absolute value in the core cavity

ratio between values at core centre and in the cavity

ratio between values in the cavity and in the thermal column

for ^{232}Th fission - absolute value in the core cavity

ratio between values at core centre and in the cavity

The final results deducible from the above parameters are seen to be: (i) the ratio of ^{232}Th capture to ^{239}Pu fission at core centre (both absolute and thermal-comparison values), and (ii) the core-centre fission ratio for $^{232}Th/^{239}Pu$ (absolute value only).

(b) Reaction Rate Traverses

Distributions across core and blanket regions were measured for each of the principal reaction rates. This was achieved by the relative counting of a number of foils (of the appropriate type) which had been irradiated simultaneously at different locations.

3.1.4 Special Measurements

(a) Infinite-Dilution Reaction Rates

In measuring an infinite-dilution reaction rate (i.e. reaction rate in a material which does not normally occur at the location at which the measurement is being made), care was taken to ensure that the foils were adequately thin. This was particularly important in measuring the ^{232}Th capture rate in the PuO_2/UO_2 fuel and the ^{238}U capture rate in the various Th blanket zones. Resonance capture cross-sections for both nuclides are of the order of 100-1000 b at lower energies and, with a significant neutron flux fraction at these energies, foil self-shielding effects can be quite important. It was estimated that foil thickness would have to be in the range 0.01-0.001 mm for the resonance self-shielding correction to be < 1 % at a typical location.

Th-metal foils of thickness 0.01-0.02 mm were used to investigate self-shielding effects for ^{232}Th capture in the PuO_2/UO_2 fuel zone. Fig. 8 shows the results obtained from measurements with foil packets of various thickness. The bend in the curve at a thickness of ~ 0.2 mm indicates that, broadly speaking, one may consider two different types of neutron capture events as occuring in a given foil. These would correspond to a high and a low resonance cross-section value and thus result in self-shielding effects of different magnitudes.

^{238}U capture measurements were particularly difficult in the axial Th blanket zones because of the very small relative low-energy component in the neutron flux (Section 3.3). Self-shielding effects for the foil thickness that was available (0.1 mm) were estimated as being too high for meaningful measurements, and depleted U deposits of

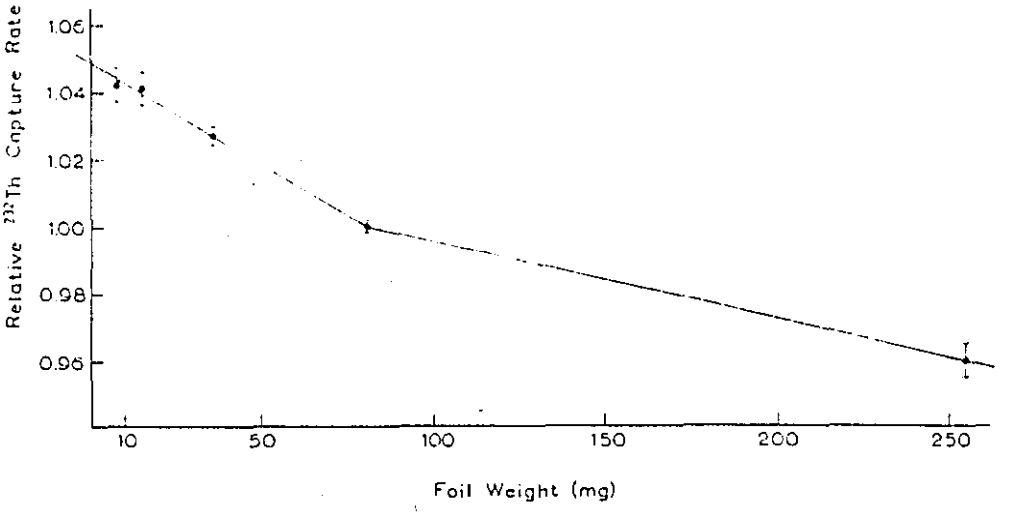

Fig. 8 Relative ^{232}Th Capture Rates Measured in the PuO_2/UO_2 Test Zone using Th-Metal Foils of Various Thickness (The correction for a 0.2 mm foil - ∿85 mg weight - was ∿ 5.0±0.5 %)

∿ 1 mg/cm^2 thickness were therefore used instead. The ^{239}Np activity induced in the deposits was, however, rather low, resulting in significant statistical errors. Subsidiary measurements did indicate that if a 0.1 mm U-metal foil had been used for the capture measurements, instead of a deposit, the self-shielding correction at the centre of the Th-metal axial blanket would have been as high as ∿ 50 %. Foil self-shielding effects for ^{238}U capture in the central Th blanket zones were very much smaller.

In the measurement of ^{233}U and ^{239}Pu fission rates in the Th zones, as also that of ^{233}U fission in the PuO_2/UO_2 fuel, foil self-shielding effects were smaller than the experimental errors from other sources.

(b) Fission Ratio Measurements in Different Neutron Spectra

The measurement of fission ratios, in most cases, entailed the fission-product γ-counting of irradiated, Al-alloyed foils. This counting was carried out on the NaI detector system (Section 3.1.1 (d)), employing a γ-energy threshold of ∿ 600 keV. Since, for a given fissile or fissionable nuclide, the fission-product yields depend on the neutron spectrum, it was important that the correlation of foil count-rates with actual fission rates be carried out through fission-chamber measurements at appropriate locations in the test lattice. This was quite straightforward for core-centre measurements, with the fission-chamber cavity located ∿ 0.20 m above the centre (Section 3.1.3 (a)).

For the axial-blanket measurements, with relatively large spatial variations occurring in the neutron spectrum, it was necessary to conduct separate fission-chamber/foil irradiations to investigate the appropriate correlations. The results showed that at the centre of the axial-blanket zones, for example, corrections for the different fission-product yields were only ∿ 1-2 % for ^{239}Pu and ^{233}U but upto ∿ 6 % for the fissionable nuclides, viz. ^{232}Th and ^{238}U.

The use of fission track recorders provided an independent check on fission ratio results obtained from the foil/chamber measurements. There was no systematic error associated with neutron-spectrum variations in this case. The method was, however, considerably more painstaking with several repeated irradiations necessary to achieve high statistical accuracies (better than, say ± 0.3 %).

In certain instances where activation foils were not available, e.g. for ^{237}Np, fission ratios were determined via track recorders alone.

3.1.5 Experimental Errors

(a) Foil Effects

Perturbations caused by the mounting of activation foils in the test lattice were estimated through measurements using different foil thicknesses, geometries and, where applicable, nuclide compositions.

Except in the case of infinite-dilution reaction rate measurements (Section 3.1.4 (a)), the effect of mounting a foil of finite thickness at a given location in the test lattice was not generally measurable within statistical errors. This may be attributed to the relatively hard neutron spectra involved, as also the absence of significant heterogeneities within a given test zone.

Effects due to extraneous materials in the foils (e.g. Al, isotopic impurities, etc.) were, where significant, accurately corrected for. This was done either experimentally (e.g. in estimating ^{235}U contributions in ^{238}U fission measurements) or on the basis of calculations (e.g. for higher Pu-isotope contributions in ^{239}Pu fission measurements). It should be mentioned that any finite errors due to foil composition effects tended to cancel out in the case of fission activation foils, since these were used only for relative measurements between two or more locations in the test lattice.

Typical foil-associated uncertainties of the various types were well within $\pm$ 1 %.

(b) Fission Chamber Effects

Perturbations caused by the introduction of a fission chamber in the test lattice, as well as in the PROTEUS thermal

column, were checked by comparing the relative activities of foil pairs as measured with and without the chamber. These checks confirmed that (i) the presence of a chamber in the lattice (∿ 0.20 m above the centre) had no measurable influence on core-centre measured reaction rate ratios and (ii) ratios measured in a chamber mounted in the thermal column were identical to those in graphite without the chamber present.

Reaction rate ratio measurements in the immediate vicinity of the fission chamber in the test lattice did indicate local spectrum perturbations. These were, however, of little consequence in establishing the correlation between fission-foil γ-activities and actual fission events in the core - effectively the only purpose for which the lattice chamber was employed (Section 3.1.4 (b)).

As discussed above, no corrections needed to be applied to account for the presence of a fission chamber either in the core cavity or in the thermal column. The associated uncertainties were negligibly small.

(c) Counting Errors

The statistical accuracies achieved in counting (foils, chambers, track detectors, etc.) were generally in the range ± 0.1-1.0 %. At remote locations in the axial blankets, however, the statistical errors were considerably higher (upto ∿± 10 %).

The systematic error associated with fission-related counting (e.g., pulse pile-up effects for the chambers, background corrections for the foils and track detectors, track overlap for the track detectors, etc.) was generally of the order of ± 1 %. In relative measurements the applied

corrections tended to cancel out, reducing the uncertainty even further.

Foil self-absorption effects in the γ-counting for ^{232}Th and ^{238}U capture measurements were of the order of 5 % in each case (for 0.1-0.2 mm thick metal foils). The associated error was negligible with the thermal-comparison technique since similar foils were used in both lattice and thermal-column irradiations. For the absolute measurements, with the correction being applied in the counting of the lattice foil alone, the associated error was $\sim \pm$ 0.5 %.

In the case of the ^{232}Th(n,2n) measurements, self-absorption effects (even for the 0.01 mm foil thickness used) were as high as ∿ 30 % for the 25.6 keV ^{231}Th γ-ray. The associated uncertainty here was ∿ ± 1.5 % (12).

(d) Other Systematic Errors

As mentioned earlier, a check on systematic errors was provided by the application of more than one experimental technique wherever possible. The various sources of error for absolute measurements of core-centre reaction rate ratios have been discussed elsewhere (13-15) and amounted, in the present experiments, to ± 1-2 %. For the thermal-comparison technique, the principal systematic error is the uncertainty in the thermal cross-section values, once again in the range ± 1-2 %.

The experimental results quoted in Section 5 for σ_c(Th232)/σ_f(Pu239), σ_c(U238)/σ_f(Pu239) and σ_f(U233)/σ_f(Pu239) represent average values obtained applying both absolute and thermal-comparison techniques. In each case, the agreement between the individual measurements was within the systematic errors refered to above.

3.2 Neutron Spectrum Measurements

The neutron spectrum measurements were carried out using spherical proton-recoil proportional counters of the SP2 type (Fig. 9) (16), manufactured by A.E.E., Winfrith (U.K.). The measured energy range covered the interval from ∿ 10 keV to 2.3 MeV. Below 50 keV, the measurements were made applying an electronic neutron-gamma discrimination technique. In the higher neutron energy range, wall-effect reduction was achieved by using increased gas pressures (upto ∿ 10 atm) and gas mixtures containing argon (because of its high stopping power for protons). Table 3 gives the specifications for the various counters used.

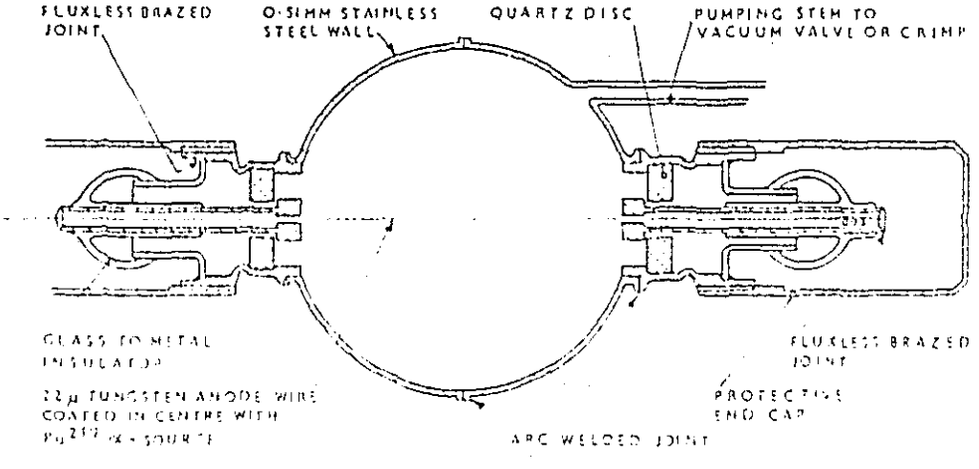

Fig. 9 The SP2 Counter (16)

Table 3 Specifications for the SP2 Counters Used

Counter	Radius (mm)	Gas pressure (atm)		Energy range[a] (MeV)	High voltage (V)
		H_2	CH_2		
W73C-22A	20.02	0.484	0.026	0.035-0.18	1200
W73C-23A	20.03	0.446	0.026	0.035-0.18	1200
W73C-21A	20.01	0.917	0.052	0.045-0.28	1500
69-42-808	19.93	1.123	-	0.045-0.28	1500
W71E-24	19.99	1.019	-	0.145-0.28	1500
W71E-23	19.99	2.728	0.189	0.09 -0.65	2100
W71E-26	20.00	2.936	0.203	0.09 -0.65	2100
W71E-22	19.98	9.694	-	0.15 -1.10	3600
W73C-24	20.05	3.787	1.515[b]	0.28 -1.60	2300
W73J-21	20.04	4.866	4.806[b]	0.6 -2.3	2800
W73J-22	20.04	5.093	4.775[b]	0.6 -2.3	2800

[a]Available energy range without electronic n-γ discrimination

[b]Argon gas pressure

The neutron spectra were derived from the measured proton-recoil spectra using the unfolding code, SPEC4 (17). Systematic errors in the present measurements were generally between ± 4 and ± 10 %, depending on the neutron energy range and the specific counter used. The errors at energies where the neutron-gamma discrimination technique had to be applied were of the order of ± 15 %. The resolution of the measured spectra (which depends, in part, on the count rates obtained) was typically in the range 10-15 %.

A detailed description of the experimental procedures applied for neutron spectrum measurements in PROTEUS has been given separately in an earlier report (18).

For measurement of the neutron spectrum at the centre of the mixed PuO_2/UO_2-ThO_2 lattice (Core 12), the proton-recoil counter was introduced into the test zone along with its preamplifier via a 50 mm diameter hole extending through the axial blanket and the top half of the core. The preamplifier was specially miniaturised (Fig. 10) to minimise spectrum distortion effects. Introduction of the counter-preamplifier assembly for the axial blanket measurements in Cores 14 and 16 was carried out via a hole extending through the top steel shield to the blanket centre (Fig. 11).

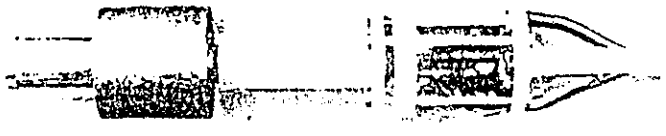

Fig. 10 The SP2 Counter-Preamplifier Assembly

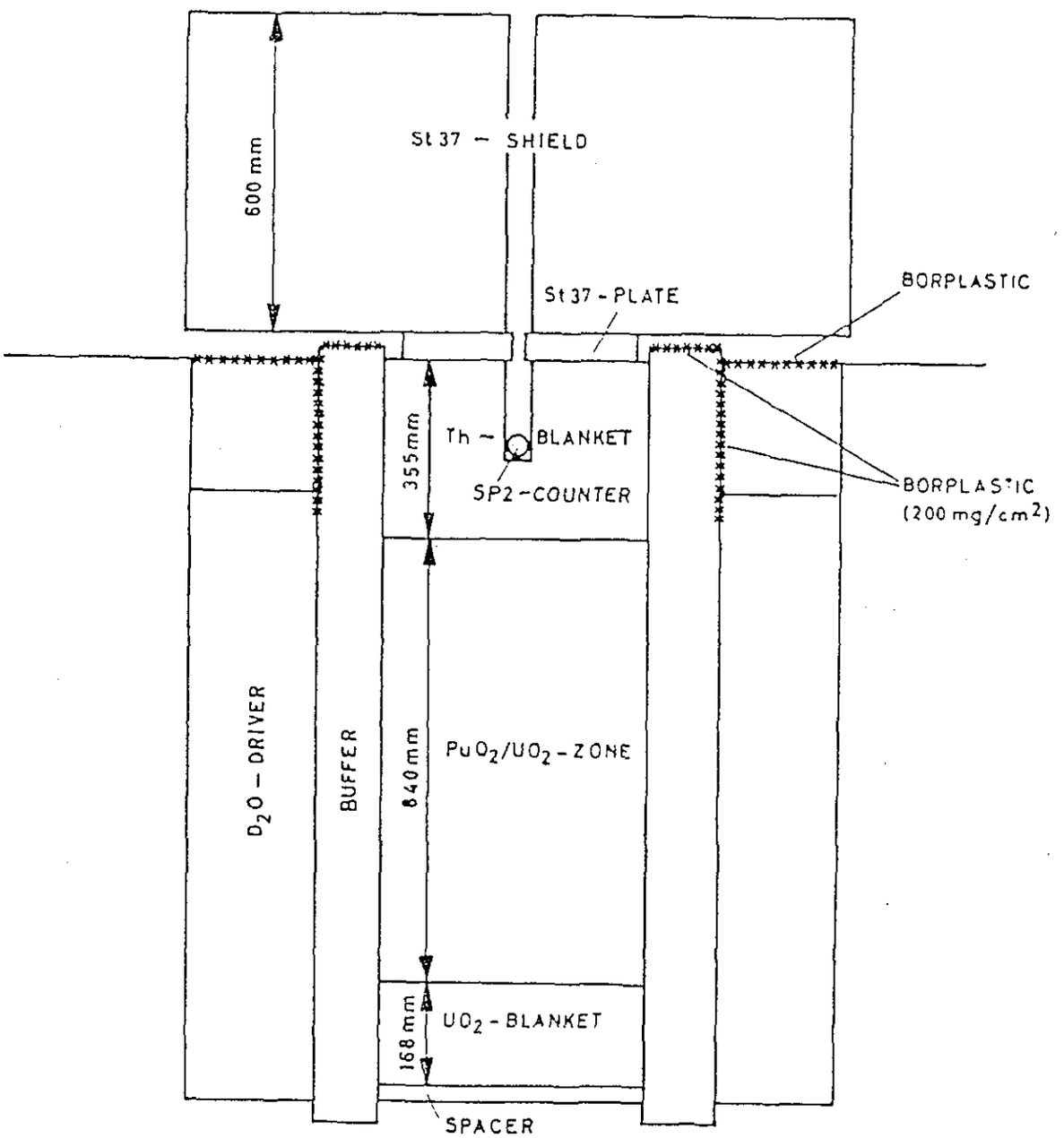

Fig. 11 Positioning of the SP2 Counter for the Axial Th-Blanket Measurements

4. CALCULATIONAL MODELS AND NUCLEAR DATA

For analysis of the PROTEUS thorium-programme experiments, appropriate macroscopic cross-section sets had to be prepared for the central PuO_2/UO_2-fuelled zone as well as for the internal and axial blanket zones. Data for the other regions of the PROTEUS reactor (i.e., buffer, driver, reflector and interface zones) were the same for each core configuration and could be used in the form already available from previous studies (10,19). One may thus limit the discussion here to broad-group cross-section preparation for the central PuO_2/UO_2 and thorium containing zones.

4.1 Data Sources for Lattice Calculations

Two different data libraries and processing codes have been used currently. The first route employed was the U.K. 2240 fine-group adjusted data library, FGL5, and its associated cell code, MURALB (20). (For some nuclides, FGL5 contains only a coarser representation with shielding factors and cross-sections in a 37 broad-group structure). Secondly, use was made of the U.S. code, GGC-4 (21), which includes a data library with resonance parameters and 99-group cross-sections derived from ENDF/B-4 point data using the SUPERTOG code.

For the current work on thorium systems it is important to note that, in FGL5, ^{232}Th and ^{233}U are broad-group nuclides whose cross-sections and shielding factors were, in fact, taken over from the 50-group LIB-IV library (22) which is itself derived from ENDF/B-4 via the MINX code (see Fig. 12). Fig. 13 shows, for example, ^{232}Th capture cross-sections in the 37- and 99-group representations of the FGL5 and GGC-4 data sets. It is only in the 10-300 eV ^{232}Th resonance region that the two representations are seen to appear markedly different as a consequence of the different group structures.

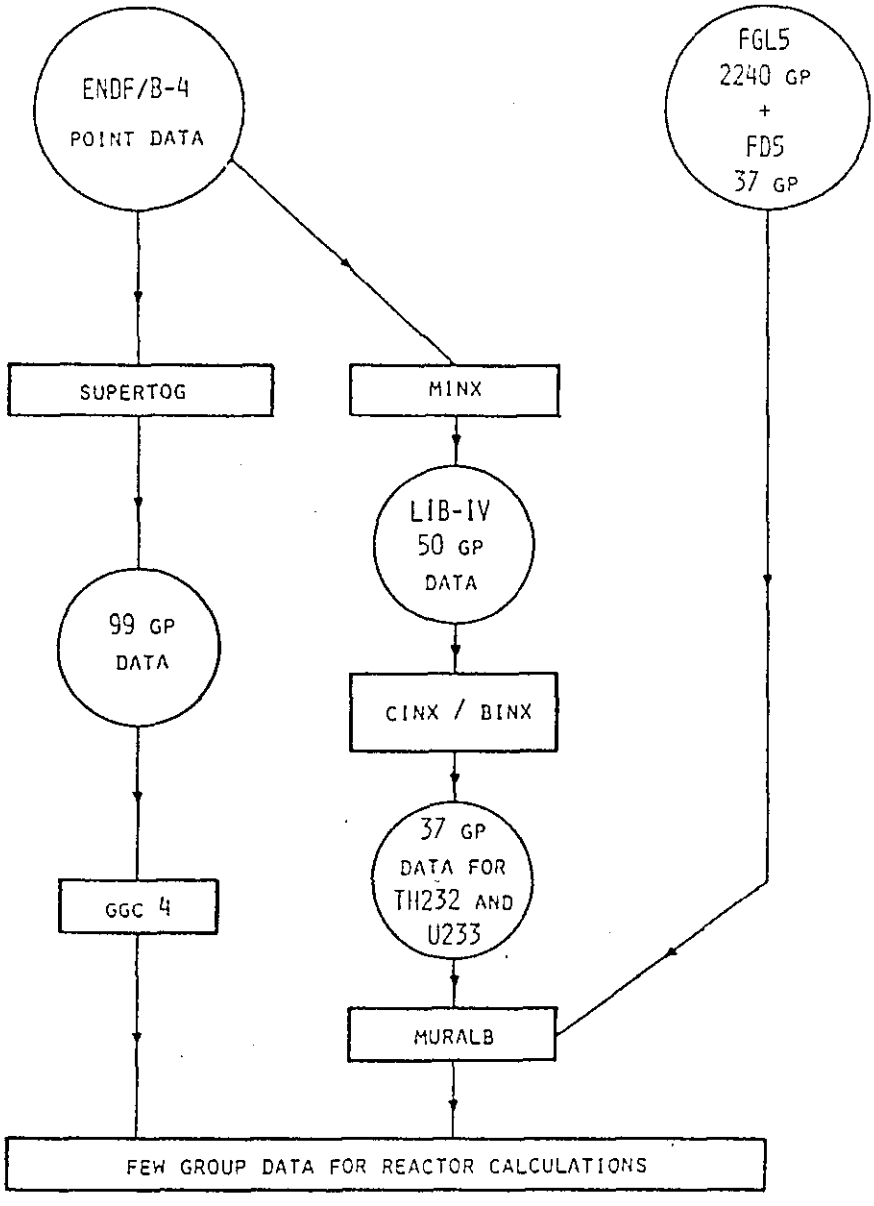

Fig. 12 Cross-section Preparation for Analysis of the Thorium Experiments

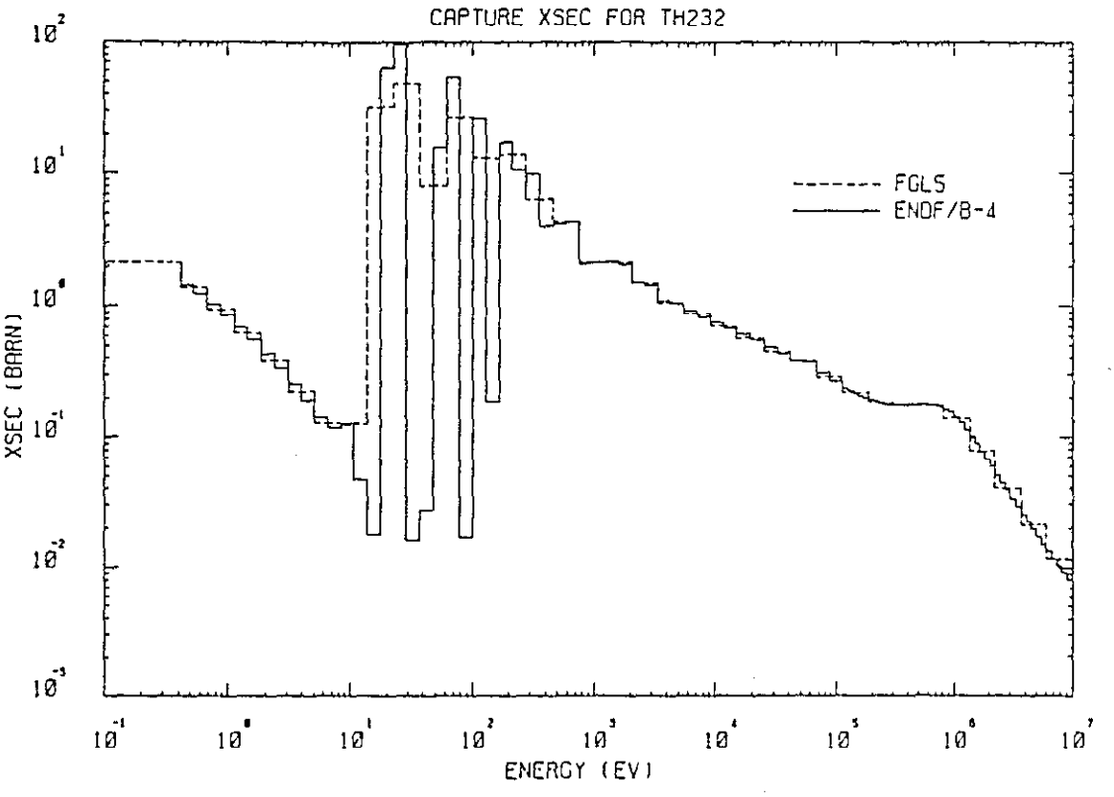

Fig. 13 Comparison of FGL5 and GGC-4 Cross-sections for $^{232}Th(n,\gamma)$

Calculations for some of the present experiments (in particular the axial-blanket cores) have also been carried out at the Oak Ridge National Laboratory, the ORNL AMPX-II scheme (23) having been used in these for preparation of the broad-group zone cross-sections. Initial studies on the effects of using the recently evaluated ENDF/B-5 ^{232}Th cross-sections are also included in the work done at Oak Ridge. The results and implications of the various ORNL studies are, for the main part, reported separately (24, 25). Some excerpts from Ref. 25, relevant to the discussion of the axial-blanket spectrum measurements are, however, given in Sections 4.4.2, 5.4.2 and 5.4.3.

4.2 The 1-D PROTEUS Model

Analyses for the experimental configurations of Cores 11,12,13 and 15 (Chapter 2) were carried out using a one-dimensional, cylindrical-geometry model for the PROTEUS reactor. Table 4 indicates the radial zoning used. The finite axial dimensions for each zone were taken into account through an appropriate value of the axial buckling. All calculations were carried out in 28 energy groups, spanning the neutron energy range from ~16.5 MeV down to thermal. Table 5 gives the energy boundaries of the 28-group structure used.

Three separate codes, which are currently incorporated into the RSYST calculational scheme at EIR (26), were available for carrying out the 1-D calculations, viz. SN-1D, SURCU and DIFF-1D. SN-1D is a slightly modified version of the ANISN code (27), while SURCU has been developed at EIR (28) and DIFF-1D at IKE (Institut für Kernenergetik), Stuttgart (26). SN-1D alone was used in most cases, except in that of Core 15 for which all three codes were applied in a comparative study.

As already mentioned, the data for Zones 4-15 of Table 4 remained unaltered in the various calculations. The 28-group cross-sections for these zones were taken over from earlier PROTEUS-GCFR studies (10,29). Table 6 gives the cell-averaged number densities for the various nuclides in Zones 2-15.

The FGL5-based broad-group cross-sections for Zone 1 (and Zone 2) of the Core 11 configuration were obtained from a heterogeneous MURALB cell calculation (B^2_{crit}=12.6 m^{-2}). Table 7 indicates the geometry for the PuO_2/UO_2 cell, as also the nuclide densities in the individual regions. Critical, heterogeneous cell calculations with the GGC-4 code, i.e. using ENDF/B-4 cross-sections, were carried out in similar fashion. For the whole-reactor calculation with the SN-1D code, the approximations used for

Table 4 Cylindrical 1-D Model for PROTEUS

Zone No.	Outer Radius (cm)	Material	B_z^2 (m^{-2})
1+	6.826*	PuO_2/UO_2 (Core 11) ThO_2 (Core 13) Th-Metal (Core 15)	5.06
2+	23.790	PuO_2/UO_2	5.06
3**+	24.475	UO_2 (depl.)	5.06
4	26.343	Steel + Air	0
5	36.311	U-Buffer	4.33
6	38.300	Air	0
7	38.800	Al	0
8	40.018	D_2O-Refl.+Al	7.00
9	57.022	D_2O-Driver	7.00
10	61.300	D_2O-Refl.+Al	7.00
11	61.800	Al	0
12	62.828	Air	0
13	68.759	Dilute C-Refl.	5.06
14	79.223***	C-Driver	5.06
15	161.800	C-Reflector	5.06

* for Core 15: $\bar{r}$ = 6.707 cm

** only in Core 13; in Core 11 and Core 15 PuO_2/UO_2 instead of UO_2 (depl.)

*** critical C-driver radius for Core 11; for Core 13 and Core 15 the value was 81.20 cm

\+ In Core 13 Zones 1-3 were filled with PuO_2/UO_2 and ThO_2 rods in the ratio 2:1 (mixed PuO_2/UO_2-ThO_2 lattice)

Table 5 Energy Boundaries for the 10-,28- and 37-Group Cross-section Sets

Gp.No. 10-Gp.Set	Gp.No. 28-Gp.Set	Gp.No. 37-Gp.Set	Lower Energy Boundary
			16.487 MeV
		1	10.000 ↓
		2	6.0653
	1	3	3.6788
	2	4	2.2313
1	3	5	1.3533
	4	6	820.85 keV
	5	7	497.86 ↓
2	6	8	301.97
	7	9	183.15
	8	10	111.09
3	9	11	67.379
	10	12	40.865
	11	13	24.786
4	12	14	15.034
	13	15	9.1183
		16	5.5304
	14	17	3.3543
		18	2.0345
5	15	19	1.2340
		20	748.45 eV
	16	21	453.96 ↓
		22	275.33
	17	23	167.00
		24	101.29
6	18	25	61.435
		26	37.262
	19	27	22.600
		28	13.708
	20	29	8.3141
7	21	30	5.0428
	22	31	3.0586
	23	32	1.8551
8	24	33	1.1252
	25	34	0.68245
	26	35	0.41393
9	27	36	$9.9881.10^{-2}$
10	28	37	$9.5853.10^{-3}$

Table 6 Zone-Averaged Nuclide Densities for the 1D-PROTEUS Model ($\times 10^{30}$ m^{-3})

(a) Zones 2-5

Nuclide	PuO_2/UO_2 (Zone 2)	UO_2(depl.) (Zone 3)	Steel+Air (Zone 4)	U-Buffer (Zone 5)
^{235}U	3.3645E-5*	4.0105E-5	-	2.2025E-4
^{239}Pu	1.1155E-3	-	-	-
^{238}U	7.9524E-3	9.4794E-3	-	3.0349E-2
^{240}Pu	2.4641E-4	-	-	-
O	1.8793E-2	1.9044E-2	4.7512E-6	-
Fe	6.5448E-3	6.6579E-3	4.5347E-2	-
Cr	1.7376E-3	1.8640E-3	-	-
^{241}Pu	2.9745E-5	-	-	-
^{242}Pu	5.4304E-6	-	-	-
Mo	1.2047E-4	1.2054E-4	-	-
Mn	2.4692E-4	2.4708E-4	-	-
Ni	1.0046E-3	1.0053E-3	-	-
Al	1.6642E-3	1.6562E-3	-	8.0616E-3
H	8.6699E-5	-	-	-
N	1.4746E-5	-	1.7660E-5	-
Si	9.4667E-5	9.4726E-5	-	-
^{241}Am	1.1362E-5	-	-	-
C	-	-	4.2288E-4	-

* to be read as 3.3645×10^{-5}

(b) Zones 6-12

Nuclide	Air (Zones 6,12)	Al (Zones 7,11)	D_2O-Refl.+Al (Zones 8,10)	D_2O-Driver (Zone 9)
^{235}U	-	-	-	2.6256E-5
^{238}U	-	-	-	4.9864E-4
O	1.0266E-5		3.2827E-2	3.2789E-2
Fe	-	-	1.0825E-6	1.0825E-6
Al	-	5.8385E-2	7.3590E-4	1.1487E-3
H	-	-	1.1161E-3	1.0794E-3
N	3.81x0E-5	-	-	
D	-	-	6.4538E-2	6.3416E-2

(c) Zones 13-15

Nuclide	D-Refl. (Zone 14)	D-Driver (Zone 15)	C-Refl. (Zone 13)
^{235}U	-	[illegible]	[illegible]
^{238}U	-	[illegible]	-
O	-	[illegible]	-
Al	-	[illegible]	-
H	-	[illegible]	-
[illegible]	[illegible]	[illegible]	[illegible]

Table 7 Geometry and Nuclide Densities for the PuO_2/UO_2 Cell*

Individual-Region Outer Radius (mm)	Nuclide	Density (10^{30} m^{-3})
3.350	^{235}U	8.2633E-5
	^{239}Pu	2.7398E-3
	^{238}U	1.9531E-2
	^{240}Pu	6.0518E-4
	O	4.6146E-2
	^{241}Pu	7.3055E-5
	^{242}Pu	1.3337E-5
	Al	3.9110E-4
	H	2.1293E-4
	^{241}Am	2.7905E-5
3.498	Al	3.5032E-2
4.100	Fe	3.9438E-2
	Cr	1.0470E-2
	Mo	7.2593E-4
	Mn	1.4879E-3
	Ni	6.0539E-3
	Si	5.7046E-4
5.250	O	1.0169E-5
	Al	5.5584E-4
	N	3.7799E-5

* The cell-averaged (homogenised) nuclide densities for the PuO_2/UO_2 cell are given in Table 6(a), first column.

the FGL5-based data were P_0, S_4 while those for the ENDF/B-4 based set were P_1, S_4.

The 28-group cross-sections for the mixed PuO_2/UO_2-ThO_2 lattice of Core 12 (Section 2.2.2) were likewise generated from critical, heterogeneous cell calculations using MURALB and GGC-4. A special collision-probability routine was applied for consideration of the additional heterogeneity of the 2-rod (PuO_2/UO_2, ThO_2) lattice of Core 12 (30). The whole-reactor calculation was, as before, carried out using P_0, S_4 and P_1, S_4 approximations.

For preparation of the 28-group data for Cores 13 and 15, two separate procedures were adopted. In the so-called "Simple Model", the broad-group cross-sections for the fertile and fissile zones (1 and 2, respectively, in Table 4) were obtained from separate cell calculations. The data generated for the PuO_2/UO_2 zone was thus, in this model, identical to that for the Core 11 test zone. The cross-sections for the ThO_2 and Th-metal zones (of Core 13 and 15, respectively) were obtained from zero-buckling cell calculations. Thus, the simple model, while allowing explicit consideration of the rodded structure of the PROTEUS test lattices (cf. Figs. 5 and 7), could not take into account any interaction between the fertile and fissile zones at the cross-section preparation stage. There was, in other words, no spatial dependence of the cross-sections that were generated. Input data for the cell calculations for the ThO_2 and Th-metal lattices are given in Tables 8 and 9.

With the second procedure, the so-called "Detailed Model", an attempt was made to consider the coupling between the fertile and fissile regions of Cores 13 and 15 right from the start, i.e. at the level of cross-section preparation for the individual zones. For the purpose, the thorium zone was divided into 6 regions and the PuO_2/UO_2 zone into another 7. A critical, 13-region MURALB calculation was then carried out in slab

Table 8 Nuclide Densities for the Heterogeneous ThO_2 Cell

Individual-Region Outer Radius (mm)	Nuclide	Density (10^{30} m^{-3})
3.424	^{232}Th	1.3631E-2
	O	2.7266E-2
	N	1.4466E-5
	Fe	9.2135E-4
	Cr	3.1447E-4
	Mo	1.1340E-6
	Mn	2.6877E-5
	Ni	1.3409E-4
	Si	1.3005E-5
4.100	Fe	4.3653E-2
	Cr	1.2243E-2
	Mo	6.6492E-4
	Mn	1.4872E-3
	Ni	6.5613E-3
	Si	6.1922E-4
5.250	O	1.0169E-5
	Al	5.5584E-4
	N	3.7799E-5

Table 9 Nuclide Densities for the Heterogeneous Th-Metal Cell

Individual-Region Outer Radius (mm)	Nuclide	Density (10^{30} m^{-3})	
		Core 15	Core 16
9.500	^{232}Th	2.9332E-2	2.9332E-2
11.026	Al	6.476E-3	7.411E-4
	O	9.401E-6	1.027E-5
	N	3.494E-5	3.816E-5

geometry, cylindrical geometry not having been used due to the exorbitant computing costs that would have been involved. The total thickness taken for the 6 fertile-zone regions was 68.3 mm in the case of Core 13 and 67.1 mm in that of Core 15, i.e. corresponding to the actual zone radius in each case. The thickness assumed for the PuO_2/UO_2 zone was 91.7 mm. The spatial mesh was chosen to be relatively fine at the interface between the fertile and fissile zones so that the sharp variations of cross-sections could be considered in a "reasonable" manner. Reflective boundary conditions were applied on both left and right hand sides in the model. The input data for the 6 regions of the fertile zone (ThO_2, Th-metal) were homogenised nuclide densities deduced from the corresponding heterogeneous cell (Tables 8 and 9, respectively). For the 7 regions of the PuO_2/UO_2 zone, the homogenised nuclide densities of Table 6 were used. The detailed model could, in this manner, generate spatially dependent cross-sections for the fertile and fissile zones. However, it was not possible in this case to consider the pelled structure of the PROTEUS test lattices explicitly.

4.3 The 2-D PROTEUS Model

A two-dimensional model of the PROTEUS reactor was necessary for analysis of the experimental configurations of Cores 14 and 16, i.e. the axial-blanket experiments. Application of a 1-D model in the axial direction would not have been adequate in itself, since there would then be no account taken of the influence of the driver zones. The boron-plastic layer between the axial-blanket and driver zones (Fig. 6) was meant to minimise such an influence. Nevertheless, with the axial blankets being relatively large, "dead" zones from the neutron physics standpoint, the neutron spectra inside them were affected by the driver zones much more than were those inside the internal blankets of Cores 13 and 15.

The calculational approach adopted for the axial-blanket experiments is described here in the context of Core 14. The procedure for Core 16 was very similar and has been detailed elsewhere (31).

Fig. 14 shows the full 2-D model used for the Core 14 analysis. A total of 17 different material zones were considered, with spatially dependent cross-sections being fed in for three of these, viz. the PuO_2/UO_2, ThO_2 and iron-shield zones (1-3, in Fig. 14). The code used for the whole-reactor calculations was DIFF-2D, an RSYST version of 2DB (26). A 10-group structure was employed, the energy boundaries for which are indicated in Table 5. Cross-sections in this broad-group structure were already available for Zones 4-17 (19), core-specific data for Zones 1-3 being generated using two different methods as discussed below.

In the first method ("Simple Model"), 37-group cross-sections for the PuO_2/UO_2 and blanket zones were obtained from independent cell calculations using MURALB, i.e. exactly as in

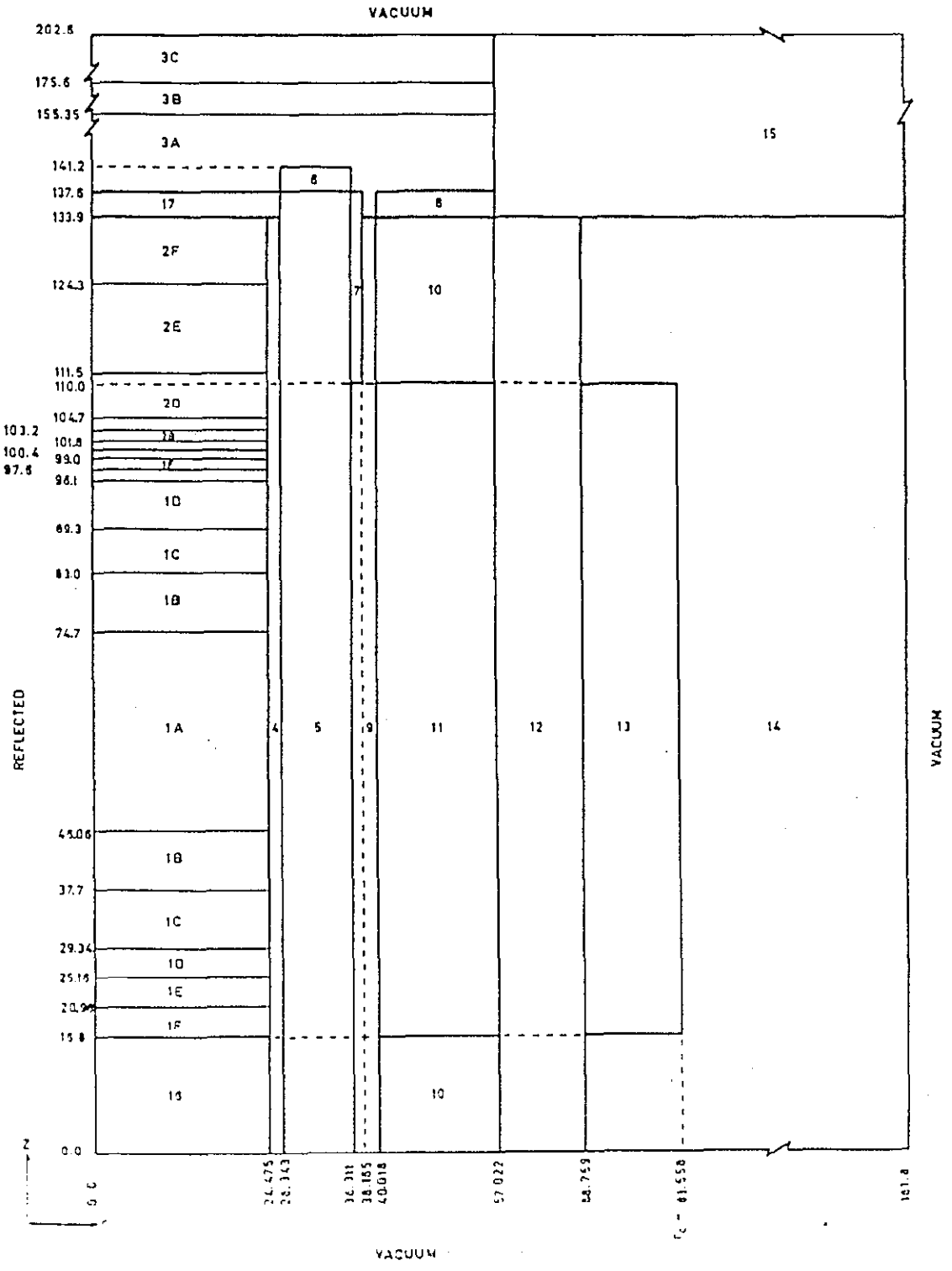

Fig. 14 The 2-D PROTEUS Model for Core 14
(dimensions in cm)

the simple model used for Cores 13 and 15. These macroscopic cross-sections were then used as input to a 1-D calculation with the SN-1D code. Fig. 15 shows the 1-D model used for Core 14, the arrangement of zones being described axially

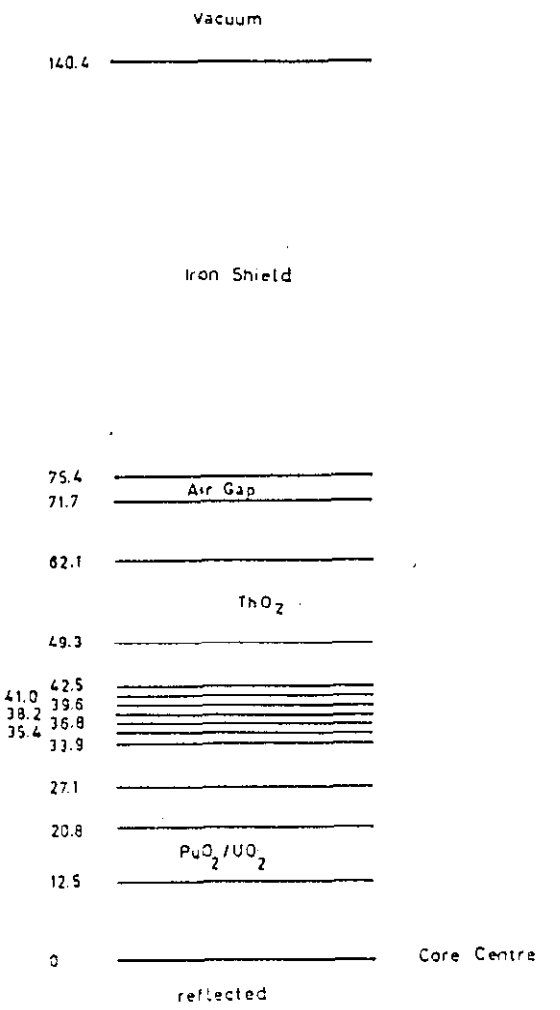

Fig. 15 1-D Model for Core 14 (dimensions in cm)

along the central axis of the reactor. (37-group data for the air-gap and iron-shield zones were generated from microscopic cross-sections obtained in the PuO_2/UO_2 cell calculation.) A single-valued buckling was employed for achieving criticality for the 1-D model, and the space-dependent 37-group fluxes obtained for the critical configuration were used to condense the cross-sections to the 10-group structure used in the 2-D model. In this manner 10-group cross-section sets were obtained for (as indicated in Figs. 14 and 15) 7 different regions in the PuO_2/UO_2 zone, 6 in the blanket and 3 in the iron-shield zone.

As in the analysis of the internal-blanket experiments, a second method ("Detailed Model") was applied so that the interaction between the fertile and fissile zones could be considered at the level of cross-section preparation. This was done by first carrying out a 13-zone, slab-geometry MURALB calculation for the core/blanket portion of the 1-D model of Fig. 15, using reflective boundary conditions at both ends. Space-dependent, 37-group cross-sections obtained for such a critical configuration were then fed as input to the 1-D Model. Finally, as in the simple-model approach, 37-group fluxes from this calculation were used to condense the cross-sections into the desired 10-group structure. The slight disadvantage of the detailed model over the simple one was, as in the Core 13 and 15 analyses, that the rodded structure of the PROTEUS lattices could not be explicitly taken into account.

The various calculations carried out at EIR for Cores 14 and 16 were all based on use of ENDF/B-5 data. As mentioned in Section 4.1, however, certain independent ENDF-based studies for the axial-blanket experiments have been conducted at Oak Ridge [44].

4.4 Neutron Spectrum Calculations

4.4.1 For the Mixed ThO_2-PuO_2/UO_2 Lattice, Core 12

A whole-reactor calculation, for the slightly subcritical configuration in which the spectrum measurement was made (Section 3.2), was first carried out in 28 energy groups using SN-1D. Energy-dependent bucklings, corresponding to the calculated broad-group spectrum at the centre of the test lattice, were then derived and input into a 2240 fine-group MURALB/FGL5 cell calculation. Finally, using the TOFFEE code (32), the calculated fine-group spectrum was homogenised over the heterogeneous cell and smoothed out so as to be consistent with the experimental energy resolution.

The bucklings fed into the MURALB calculation were also used as input into a GGC-4 cell calculation, thereby yielding a 99-group spectrum based on ENDF/B-4 data. An appropriate condensation of the fine-group MURALB spectrum was carried out in the same 99-group structure to enable a direct comparison of FGL5 and ENDF/B-4 based results.

4.4.2 For the Axial Blankets, Cores 14 and 16 (25)

Since a 1-D model of the PROTEUS axial blanket was not adequately representative of the actual geometry and since fine-group 2-D transport calculations of the full geometry were not economically feasible, a compromise approach was used. The procedure, which is outlined in Fig. 16, consisted of performing a broad-group eigenvalue calculation for the full PROTEUS geometry in order to determine the space-dependent fission-rate distribution in the central test regions. The spatial fission rate was then folded with zone-dependent fission-neutron energy distributions to determine a space-energy distributed source which was used to perform a fine-group 2-D neutron transport calculation for the central regions. The axial space

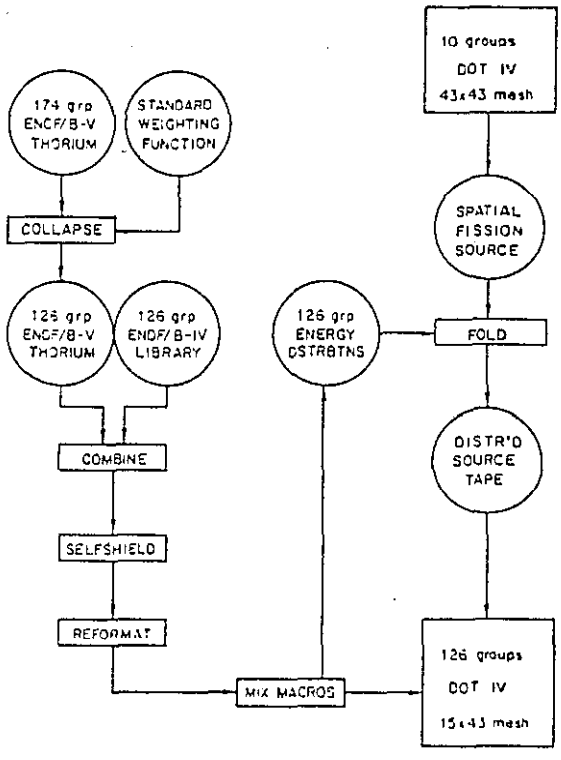

Fig. 16 Cross-section Preparation and Calculational Procedure for the Axial-Blanket Neutron Spectrum Calculations

mesh for the broad-group and fine-group models were identical, while the radial mesh for the fine-group calculation was truncated beyond the uranium buffer region. The DOT-IV discrete-ordinates code (33) was used for both the broad-group and fine-group calculations, which utilized an S_6 angular quadrature and a P_3 cross-section expansion.

Also shown in Fig. 16 is the procedure which was used to prepare the fine-group cross-section data. The analysis used the 129-group CLEAR data library, which contains 75 energy groups within the measured energy range and which is derived from the widely-distributed VITAMIN-C multigroup library (34). In addition to the CLEAR cross-sections which are based on ENDF/B-4 data, a separate data set for ^{233}Th was prepared from ENDF/B-5.

This was done by collapsing a MINX-produced 174-group ^{232}Th data set to the desired 126 groups using a standard "Maxwellian-1/E-fission spectrum" weighting function. All of the cross-section processing utilized the AMPX-II modular code system developed at ORNL (23).

5. RESULTS AND THEIR DISCUSSION

Comparisons of measured and calculated reaction rate ratios, as well as reaction rate distributions, are presented and discussed in Section 5.1 for Cores 11 and 12, in Section 5.2 for Cores 13 and 15, and in Section 5.3 for Cores 14 and 16. Neutron spectrum results for Cores 12, 14 and 16 are discussed separately in Section 5.4.

5.1 Results for Cores 11 and 12

There was no particular difficulty in the analysis and interpretation of results for Cores 11 and 12. In each case, the neutron spectrum at the centre was mainly determined by the test lattice itself and only marginally influenced by the outer buffer, driver and reflector zones. Fig. 17 compares, for example, the calculated neutron spectrum at the centre of Core 11 with that in a single-zone, critical reactor of the same composition as the test lattice. The broad-group fluxes are seen to differ significantly from each other only at the lower neutron energies, where the influence of the thermal-driver zones is clearly noticeable. The fraction of the neutron flux below ~100 eV was, however, only 0.05 % for the PuO_2/UO_2 lattice. As such, the low-energy flux differences appear quite unimportant when considered in terms of fractional differences with respect to the total flux. Fig. 18 displays the neutron spectrum differences in this light.

Reaction rates calculated for the centre of Cores 11 and 12 differed from the corresponding reference values, i.e. values in the corresponding single-zone critical reactor, by less than a few percent in each case (1 % maximum). Discrepancies between measured and calculated test-lattice parameters for these experiments could thus be expected to reflect

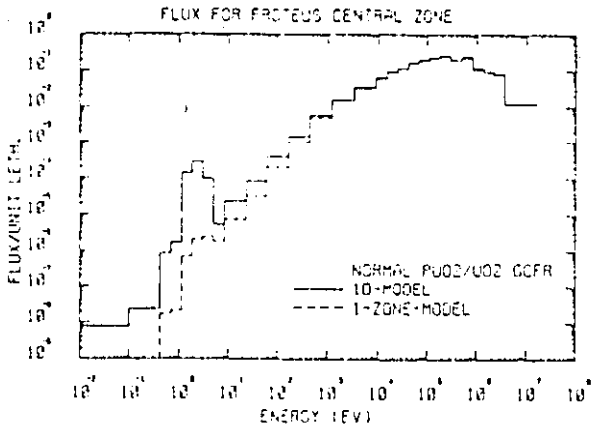

Fig. 17

Comparison of Neutron Spectra in the Centre of Core 11 and in the Reference Single-Zone Reactor

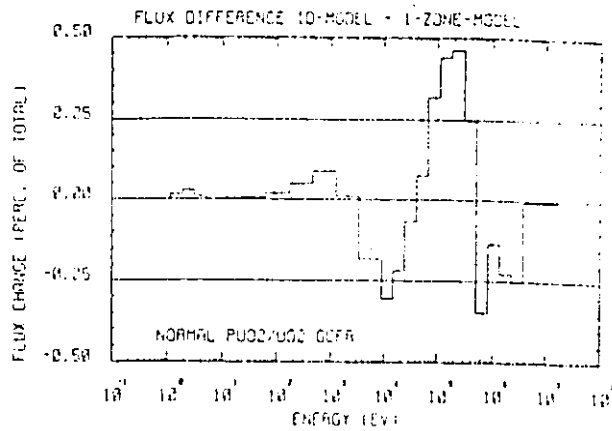

Fig. 18

Differences in the Fig. 17 Spectra relative to Total Flux

uncertainties in the basic nuclear cross-sections, rather than shortcomings in the whole-reactor model used for the calculations. The experimental configurations of Cores 11 and 12, in other words, could be regarded as benchmarks for testing the basic nuclear data.

In order to facilitate the discussion on reaction rate results, Fig. 19 compares the calculated neutron spectra at the centre of Cores 11 and 12. The spectrum in the standard PuO_2/UO_2 GCFR lattice (Core 11) is seen to be significantly harder than that in the mixed PuO_2/UO_2-ThO_2 lattice of Core 12. The median neutron energy values were ∿184 and 147 keV, respectively.

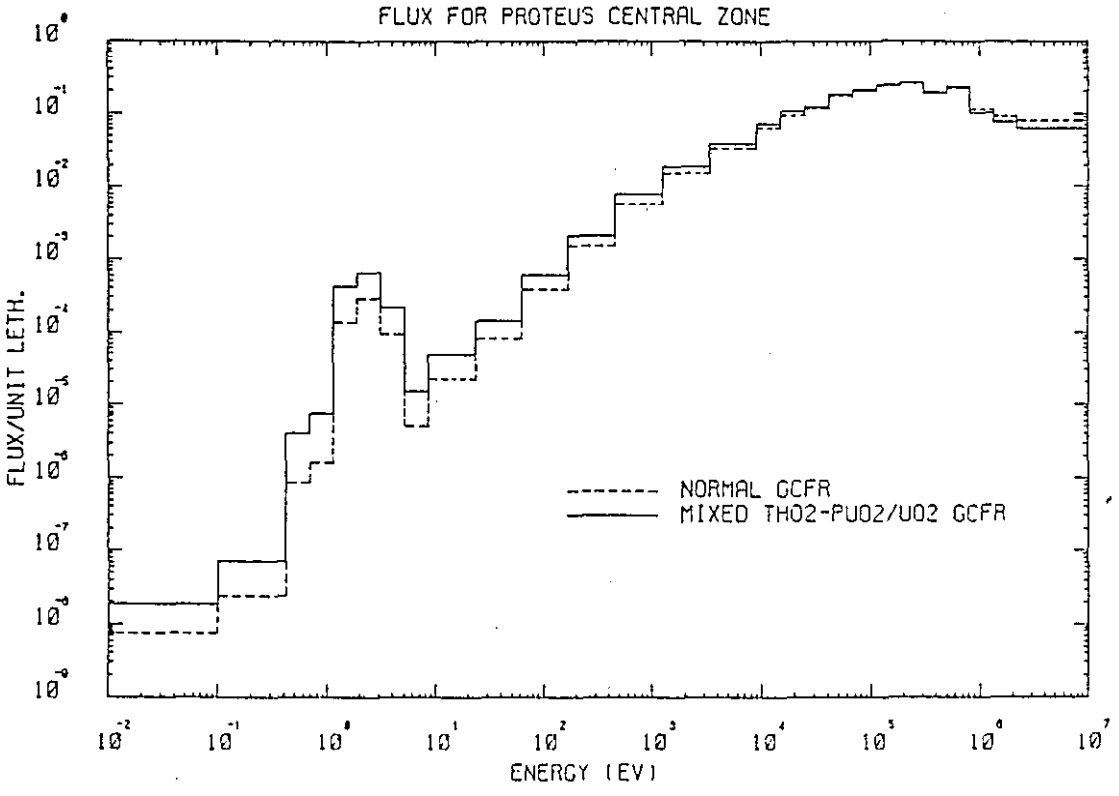

Fig. 19 Calculated Neutron Spectra for Cores 11 and 12

Table 10 gives the comparison of measured and calculated reaction rate ratios (per atom) at the centre of Core 11 and Core 12. In the table, σ_c denotes the effective one-group cross-section for capture, σ_f that for fission and σ_{2n} that for the (n,2n) reaction.

From the present viewpoint of testing ^{232}Th data, the most important reaction rate ratio in Table 10 is σ_c(Th232)/σ_f(Pu239) since it largely determines the ^{233}U breeding capability. The comparison between measured and calculated values of this ratio is seen to be satisfactory in both

Table 10 Comparison of Calculated (C) and Experimental (E) Reaction Rate Ratios at the Centre of CORE 11 and CORE 12

Reaction Rate Ratio	Standard PuO_2/UO_2 Lattice (Core 11)			Mixed ThO_2-PuO_2/UO_2 Lattice (Core 12)		
	Expt. Value	C/E		Expt. Value	C/E	
		FGL5	ENDF/B-4		FGL5	ENDF/B-4
$\frac{\sigma_c(Th232)}{\sigma_f(Pu239)}$	0.2000 ± 1.3 %	0.972	0.980	0.1802 ± 1.7 %	1.041	0.997
$\frac{\sigma_f(Th232)}{\sigma_f(Pu239)}$	$8.061.10^{-3}$ ± 2 %	0.888	0.861	$6.271.10^{-3}$ ± 1.7 %	0.887	0.878
$\frac{\sigma_c(U238)}{\sigma_f(Pu239)}$	0.1327 ± 1.1 %	0.984	1.051	0.1425 ± 1.0 %	0.979	1.044
$\frac{\sigma_f(U238)}{\sigma_f(Pu239)}$	$3.111.10^{-2}$ ± 1.3 %	1.045	0.983	$2.524.10^{-2}$ ± 1.7 %	1.046	0.963
$\frac{\sigma_f(U233)}{\sigma_f(Pu239)}$	1.519 ± 1.3 %	0.990	0.988	-	-	-
$\frac{\sigma_{2n}(Th232)}{\sigma_c(Th232)}$	$6.84.10^{-3}$ ± 2.5 %	1.019	0.869	$5.36.10^{-3}$ ± 5.2 %	1.079	1.011

Cores 11 and 12 - surprisingly so in view of the normally assumed uncertainties in ^{232}Th capture cross-sections (Section 1.3). In order to obtain some insight into the difference between the measured $\sigma_c(Th232)/\sigma_f(Pu239)$ values in Cores 11 and 12, consideration was given to the calculated values of the individual numerator and denominator terms. It was observed that there was relatively little difference between values of the integral ^{239}Pu fission rate in the two lattices. Differences in ^{232}Th capture were found to result from two counteracting effects. The softer neutron spectrum in Core 12 would in itself

have resulted in an increase of ∿14 % in $\sigma_c(^{232}Th)$, but this was counteracted by an even higher decrease (∿20 %) due to resonance self-shielding effects. On comparing the C/E values obtained from the FGL5 and GGC-4 (ENDF/B-4) routes for the two lattices (Table 10), the calculation of self-shielding effects appears to be better by the latter route (see Fig. 20).

The fission rate in ^{232}Th is seen to be consistently under-predicted, suggesting that the basic cross-sections in current use are too low. This will, however, have relatively minor

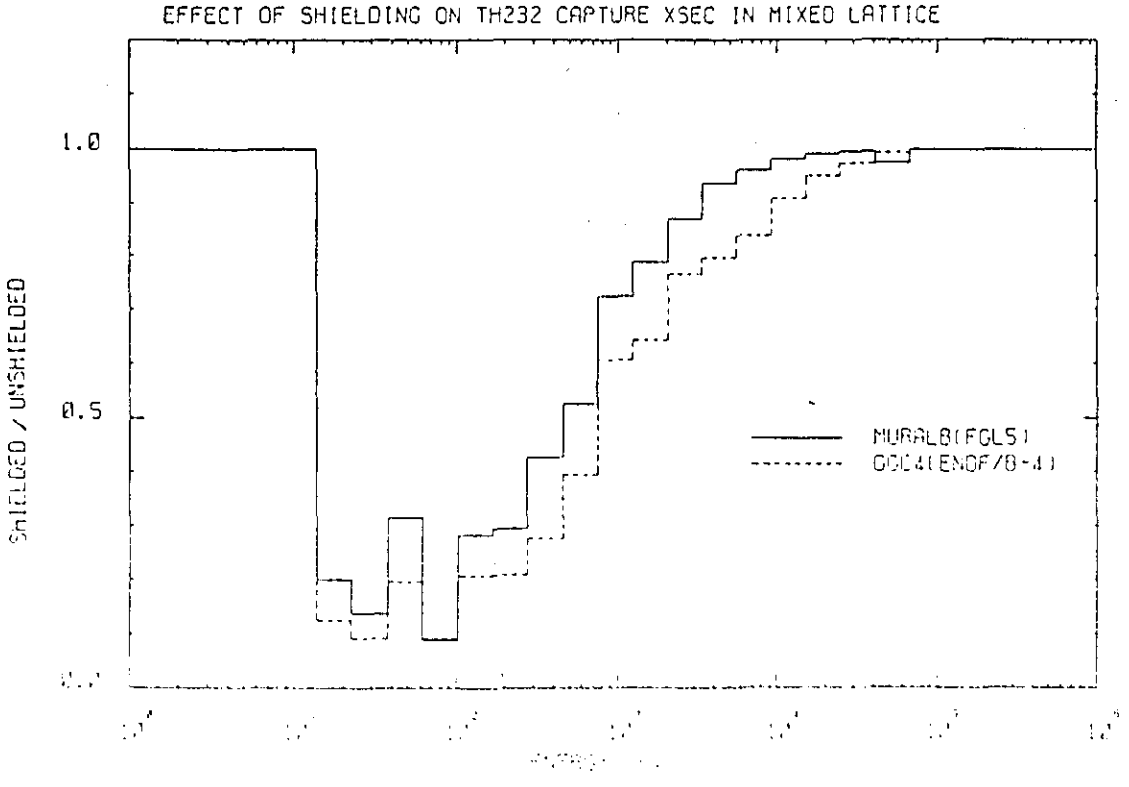

Fig. 20 Self-Shielding Effects for σ_c(Th232) in Core 12

effect on reactor neutron balances because the contribution of ^{232}Th threshold fission is rather small.

The (n,2n) reaction in ^{232}Th, even though less significant than ^{232}Th fission from the neutron-balance viewpoint, is important because it leads to the build-up of ^{233}U whose decay chain produces very hard γ-radiation (Section 1.1). As discussed in Section 3.1.2, the ^{232}Th (n,2n) measurements in most of the current experiments were carried out relative to ^{232}Th capture so as to achieve higher experimental accuracies. The agreement between the measured and calculated ratios in Cores 11 and 12 appears to be quite reasonable from the results of Table 10. This may, however, have been somewhat fortuitous considering the difficulty of accurately predicting such a high (∿6.4 MeV) threshold reaction (35).

Since the present experiments did not contain any ^{233}U in the fuel, it was only for the infinitely dilute fission cross-section of ^{233}U that checks could be made. The results for σ_f(U233)/σ_f(Pu239) in Core 11 appear very good. The additional reaction rates involving ^{238}U capture and fission show the same behaviour as in earlier GCFR cores (29, 36, 37). The ratio of ^{238}U capture to ^{239}Pu fission is overpredicted by ENDF/B-4 based data in GGC-4 and well predicted by the adjusted FGL5 set. ^{238}U fission is overpredicted by ∿5 % by FGL5 and slightly underpredicted by ENDF/B-4.

In summary, on the basis of the integral measurements in the two"data benchmark" configurations of Cores 11 and 12, the ENDF/B-4 based ^{232}Th and ^{233}U cross-sections used in the calculations seem to yield acceptable prediction accuracies. This statement is clearly of importance in the context of ^{232}Th-^{233}U fast-reactor fuel cycle studies of the type reported in (1). In particular, ^{232}Th capture data (infinitely dilute) in ENDF/B-4

appears quite adequate - in contradiction to the results of the recent differential measurements refered to in Section 1.3 (7)*. The present results, in fact, support the broad conclusions drawn in the Argonne survey of earlier integral checks made for ^{232}Th in fast systems (9).

5.2 Results for Cores 13 and 15

With the construction of heterogeneous thorium-containing zones in the centre of the PuO_2/UO_2 standard lattice, Core 13 and Core 15 (homogenised thorium densities of ∿2.2 and 8.4 g/cm^3, respectively, in the central zone) provided, in some sense, more stringent tests for ^{232}Th data than did Cores 11 and 12. The experimental configurations were, as discussed in Section 4.2, amenable to analysis using a 1-D model for the PROTEUS reactor, the values of measured parameters being determined mainly by the properties of the PuO_2/UO_2-fuelled and internal-blanket zones. Due to the strong coupling between the two types of zones, however, calculational procedures for determining the neutron spectra and reaction rate ratios had to be carefully checked for the effects of the approximations applied. As such, the configurations of Cores 13 and 15 may be regarded as providing benchmark tests for data and methods as applied to the analysis of heterogeneous, thorium-containing fast reactors.

As discussed in Section 4.2, two different calculational models were currently used for preparation of 28-group cross-sections for the PuO_2/UO_2 and thorium-containing zones of Cores 13 and 15. In the simple model, separate cell calculations for each type of zone were carried out. In the detailed model, space-dependent cross-sections were generated through a multi-region

---

* see Abstract, p. vi , for latest situation

fine-group calculation which tried to take into account the coupling between fertile and fissile zones. It is in the context of these two calculational models that the results for Cores 13 and 15 are discussed below. It should be stressed, however, that these models do not represent the "best possible", but rather, were meant to point out the sensitivity of calculated results to the approximations used, particularly in the case of reaction rates with large resonance self-shielding effects (viz. ^{238}U capture and ^{232}Th capture). The following nomenclature is used in discussing the calculated results obtained from the two different models:

PHI0: Fluxes SIG0: Broad-Gp. Cross-Sections	Simple Model (constant cross-sections in each zone)
PHI1: Fluxes SIG1: Broad-Gp. Cross-Sections	Detailed Model (space-dependent cross-sections for fissile and fertile zones)

5.2.1 Central Reaction Rate Ratios

Table 11 gives a comparison of measured and calculated reaction rate ratios in the centre of the Core 13 and Core 15 internal blankets, as also in the centre of the standard PuO_2/UO_2 lattice. In order to facilitate intercomparison of the three sets of results, the methodology used for the calculations was similar in each case, viz. the simple model based on FGL5 data. The effects of using ENDF/B-4 data and of applying the detailed model are discussed later in the section.

Once again, the most important central reaction rate ratios was $\sigma_c(Th232)/\sigma_f(Pu239)$ since it determines the ^{233}U breeding characteristics. While being slightly underpredicted in the standard lattice (infinitely dilute check for ^{232}Th data), this ratio is seen to be calculated about 4 % too high in the

Table 11 Comparison of Calculated (C) and Experimental (E) Reaction Rate Ratios (per Atom) in the Centre of the Internal Blankets of CORE 13 and CORE 15 and the Centre of the Standard PuO_2/UO_2 Lattice (CORE 11)

Reaction Rate Ratio	Normal PuO_2/UO_2-Lattice (Core 11)		Heterogeneous Lattice with Central ThO_2Zone (Core 13)		Het.Lattice with Central Th-Metal Zone (Core 15)	
	Experimental Value	C/E*	Experimental Value	C/E*	Experimental Value	C/E**
$\frac{\sigma_c(Th232)}{\sigma_f(Pu239)}$	0.2000 ± 1.3%	0.972	0.1663 ± 1.7%	1.049	0.1499 ± 1.5%	1.030
$\frac{\sigma_f(Th232)}{\sigma_f(Pu239)}$	$8.061.10^{-3}$ ± 2 %	0.888	$5.645.10^{-3}$ ± 2 %	0.888	$4.750.10^{-3}$ ± 2 %	0.959
$\frac{\sigma_c(U238)}{\sigma_f(Pu239)}$	0.1327 ± 1.1%	0.984	0.1773 ± 2 %	1.046	0.1582 ± 2 %	1.014
$\frac{\sigma_f(U238)}{\sigma_f(Pu239)}$	$3.111.10^{-2}$ ± 1.3%	1.045	$2.235.10^{-2}$ ± 2 %	1.026	$1.843.10^{-2}$ ± 2 %	1.167
$\frac{\sigma_f(U233)}{\sigma_f(Pu239)}$	1.519 ± 1.3%	0.990	1.577 ± 1.5%	0.997	1.536 ± 1.5%	1.005
$\frac{\sigma_{2n}(Th232)}{\sigma_c(Th232)}$	$6.84.10^{-3}$ ± 2.5%	1.019	$4.98.10^{-3}$ ± 5.2%	0.968	$5.65.10^{-3}$ ± 2.5%	0.889

* FGL5 Data Set, ANISN Code, Simple Model

** FGL5 Data Set, SURCU Code, Simple Model

internal thorium-containing blanket zones of Cores 13 and 15. This suggests errors in the estimation of resonance self-shielding effects for ^{232}Th capture, as pointed out earlier in the context of the results for Core 12 (Section 5.1). Similar overprediction of the $\sigma_c(Th232)/\sigma_f(Pu239$ ratio in

thorium blankets was also reported for experiments at Argonne (38, 39). However, in view of the large uncertainties of 10-20 % that are normally ascribed to the prediction of ^{232}Th capture in fast systems (Section 1.3), the agreement between calculation and experiment can certainly be regarded as quite satisfactory for both Cores 13 and 15.

The results for σ_c(U238)/σ_f(Pu239) appear to be good for each of the three experimental configurations of Table 11. As discussed later, however, the satisfactory agreement indicated here between calculation and measurement was somewhat fortuitous for the internal thorium-blanket zones and probably resulted from cancelling errors. The preparation of appropriate broad-group cross-sections for ^{238}U capture in the centre of Core 13 and Core 15 (particularly, for the latter) was a rather difficult task, with results being highly sensitive to the calculational model applied.

Regarding the Table 11 results for the threshold fission reactions, σ_f(U238)/σ_f(Pu239) is seen to be significantly overpredicted (as is normally the case with FCL5 data), and σ_f(Th232)/σ_f(Pu239) is consistently underpredicted to an extent which indicates that the ^{232}Th fission cross-sections in current use are too low (Section 5.1). The marked increase in C/E for both these threshold reactions in the Th-metal blanket (Core 15), relative to values in the ThO_2 blanket and the standard lattice, suggests that the neutron flux around 1 MeV is being overpredicted in the metal case. A poorer prediction may be acceptable for ^{232}Th fission than for ^{238}U fission since the absolute magnitude of the former cross-section is much smaller and the contribution to power production correspondingly lower.

The good prediction of the ^{232}Th(n,2n) reaction rate in the standard lattice and in the ThO_2 blanket may be fortuitous

in the light of the large discrepancy in the metal case. As mentioned earlier (Section 5.1), the high threshold for this reaction renders the calculated values extremely sensitive to data and methods. On comparing the experimentally determined ratios for ^{232}Th(n,2n) and ^{232}Th fission in the ThO_2 blanket with those in the Th-metal zone, one notes that the relative attenuation of the two ^{232}Th threshold reactions was of a somewhat dissimilar nature in the two types of blankets. This was shown to be a consequence of the occurrence of considerable structural components and oxygen in the ThO_2 zone (40).

The remaining ratio in Table 11 is σ_f(U233)/σ_f(Pu239), measured here as a spectral index since there was no ^{233}U fuel in the lattices. The experimental values of the ratio are seen to be quite similar in the three Cores, reflecting the qualitative similarity in energy dependence of ^{233}U and ^{239}Pu fission cross-sections. The fact that C/E was close to unity in each case indicates, as noted earlier (Section 5.1), the adequacy of infinitely-dilute ^{233}U fission data in the FGL5 library.

The effects of analysing Cores 13 and 15 by the GGC-4 (ENDF/B-4) route were assessed separately using, once again, the simple model (41). Comparison with the FGL5-based results of Table 11 led to conclusions quite similar to those discussed in the context of the results for Cores 11 and 12 (Section 5.1). The C/E values for σ_c(Th232)/σ_f(Pu239), for example, suggested that self-shielding effects for ^{232}Th capture in the internal blankets were being estimated better by the GGC-4 route than by MURALB/FGL5.

The effects, on the calculated reaction rate ratios in Cores 13 and 15, of using the detailed model instead of the simple model (Section 4.2) are shown in Table 12. The changes are presented effectively in two parts, viz. through the effect

Table 12 Influence of the Different Models for Cross-section Preparation on Central Reaction Rate Ratios (C/E Values) in Cores 13 and 15

Reaction Rate Ratio	Heterogeneous Lattice with Central ThO_2 Zone (Core 13)			Heterogeneous Lattice with Central Th-Metal Zone (Core 15)		
	SIG0×PHI0	SIG1×PHI0	SIG1×PHI1	SIG0×PHI0	SIG1×PHI0	SIG1×PHI1
$\frac{\sigma_c(Th232)}{\sigma_f(Pu239)}$	1.049	1.053	1.057	1.030	1.063	1.063
$\frac{\sigma_f(Th232)}{\sigma_f(Pu239)}$	0.888	0.892	0.902	0.959	0.972	0.985
$\frac{\sigma_c(U238)}{\sigma_f(Pu239)}$	1.046	1.011	0.994	1.014	0.880	0.873
$\frac{\sigma_f(U238)}{\sigma_f(Pu239)}$	1.026	1.029	1.040	1.167	1.163	1.179
$\frac{\sigma_f(U233)}{\sigma_f(Pu239)}$	0.997	1.000	1.001	1.005	1.017	1.013
$\frac{\sigma_{2n}(Th232)}{\sigma_c(Th232)}$	0.915	0.990	1.003	0.889	0.968	0.982

on the broad-group cross-sections (SIG0→SIG1) and, separately, through the effect on the neutron spectrum (PHI0→PHI1). It is seen that, while for the threshold reactions (^{232}Th and ^{238}U fission), the former effect was quite small, the preparation of broad-group cross-sections in the case of reactions with large self-shielding effects was significantly dependent on the model used. This is particularly evident for the case of ^{238}U capture in the centre of the Th-metal zone. As indicated more clearly in Section 5.2.2, neither of the currently used

models proved adequate for treating this particular reaction rate in the Core 15 analysis. Significant improvements in the comparison of calculation and experiment may thus be expected to result in this case from refinement of the methods alone. One might investigate, for example, the effects of anisotropic scattering, neutron streaming and improved leakage models in describing the coupling between the fissile and fertile zones (42).

As mentioned in Section 4.2, three separate codes were available for carrying out 1-D whole-reactor calculations, viz. SN-1D, SURCU and DIFF-1D. A comparison of the results obtained by the three codes (simple model in each case) is shown for the case of Core 15 in Table 13. The differences between the two transport-theory calculations (SURCU and ANISN) are seen to be relatively small. These occurred mainly because of the difficulty in obtaining adequate convergence of the neutron fluxes between ~1-30 eV when using ANISN for the Core 15 analysis (cf. the SURCU, ANISN results for σ_f(U233)/σ_f(Pu239)). The major differences in Table 13, however, are between the diffusion-theory DIFF-1D results and the transport-theory results as a whole. As indicated in Fig. 21, diffusion theory was found to be quite inadequate for satisfactorily predicting flux depression effects in the dense Th-metal zone (Section 5.2.2). Clearly then, it is only results based on transport-theory whole-reactor calculations that should be considered when making comparisons with experiment.

5.2.3 Radial Distributions of Reaction Rates

Radial distributions for the total neutron flux in Core 15 and Core 16 are indicated in Fig. 22. These results, like all other calculated distributions discussed in this section, were obtained from transport-theory whole-reactor calculations

Table 13 Comparison of Central Reaction Rate Ratios (C/E Values) from Different Whole-Reactor Calculations for Core 15*

Reaction Rate Ratio	Diffusion Theory (DIFF-1D)	Transport Theory	
		SURCU	ANISN
$\frac{\sigma_c(Th232)}{\sigma_f(Pu239)}$	1.024	1.030	1.033
$\frac{\sigma_f(Th232)}{\sigma_f(Pu239)}$	1.088	0.959	0.935
$\frac{\sigma_c(U238)}{\sigma_f(Pu239)}$	0.996	1.014	1.022
$\frac{\sigma_f(U238)}{\sigma_f(Pu239)}$	1.315	1.167	1.138
$\frac{\sigma_f(U233)}{\sigma_f(Pu239)}$	0.990	1.005	1.055
$\frac{\sigma_{2n}(Th232)}{\sigma_c(Th232)}$	1.053	0.889	0.861

* FGL5 Data and Simple Model used in each case

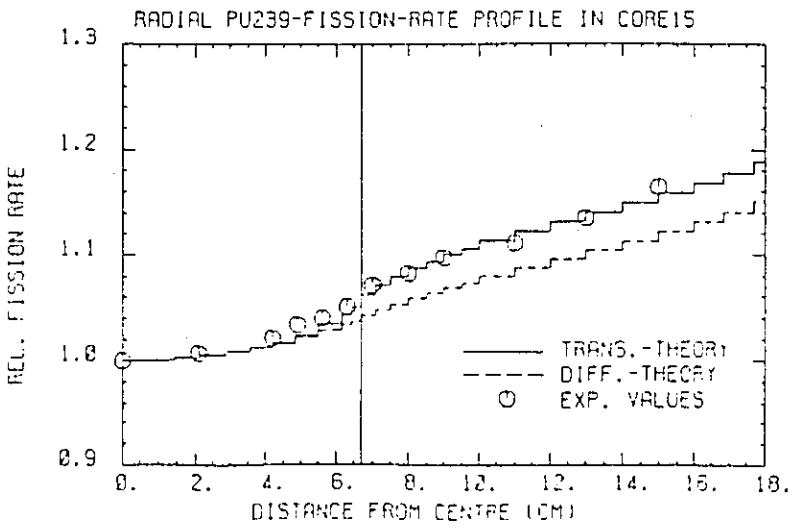

Fig. 21 Radial ^{239}Pu Fission Rate Profile in Core 15

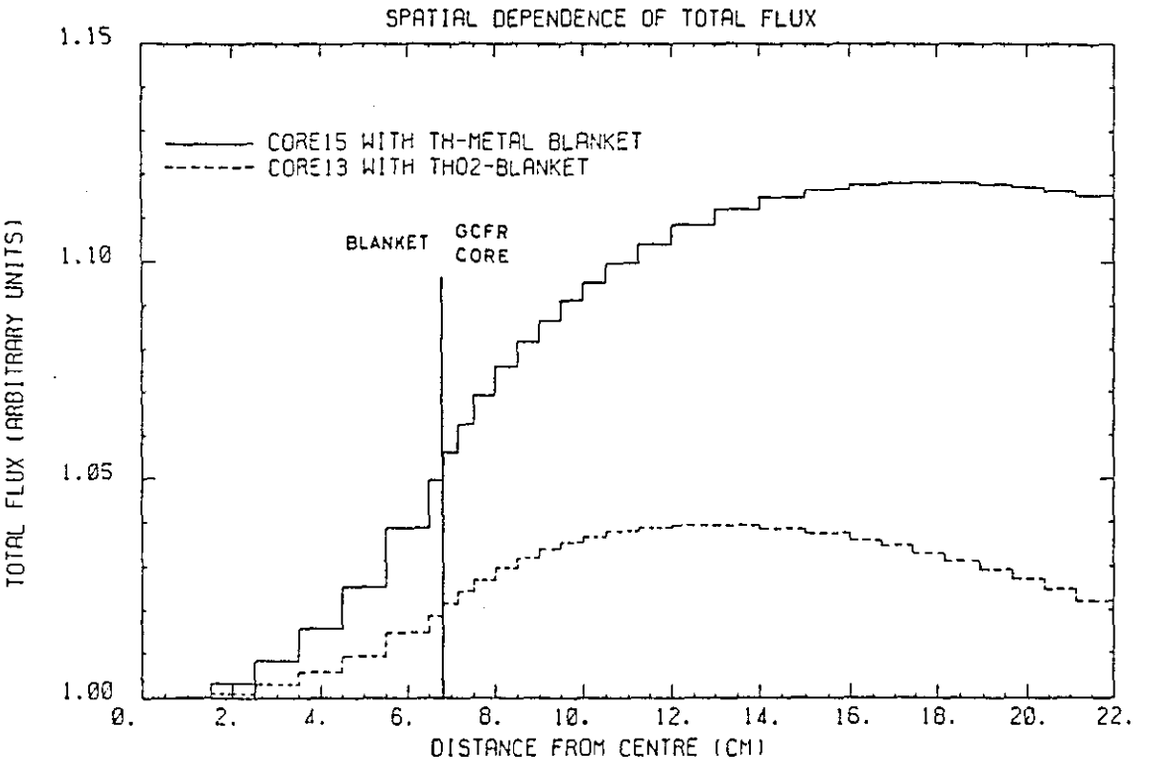

Fig. 22 Radial Distributions for Total Flux in Cores 13 and 15

using FGL5-based cross-sections for the test lattices. It is seen that flux depression effects were considerably greater in the Th-metal blanket than in the ThO_2 zone.

Figs. 23-27 show comparisons between the calculated and experimental results for various reaction rate profiles in Core 13 and Core 15. The influence of the two different models for preparation of broad-group cross-sections is indicated in each case. In Figs. 23 and 24, which give the profiles for ^{232}Th and ^{238}U capture, the effect of going from the simple to the detailed model is shown in two parts (as done in Table 12). Thus, SIG0xPHI0 denotes the calculated distribution obtained with the simple model, SIG1xPHI0 that using cross-sections from the detailed model but fluxes from the simple

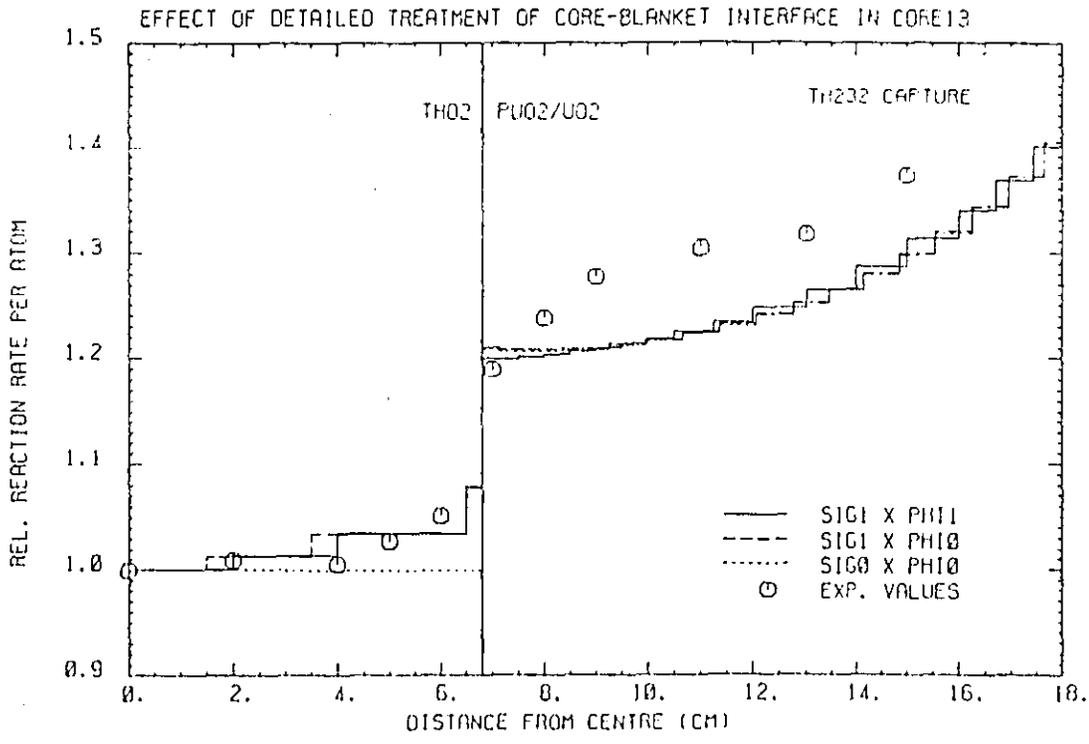

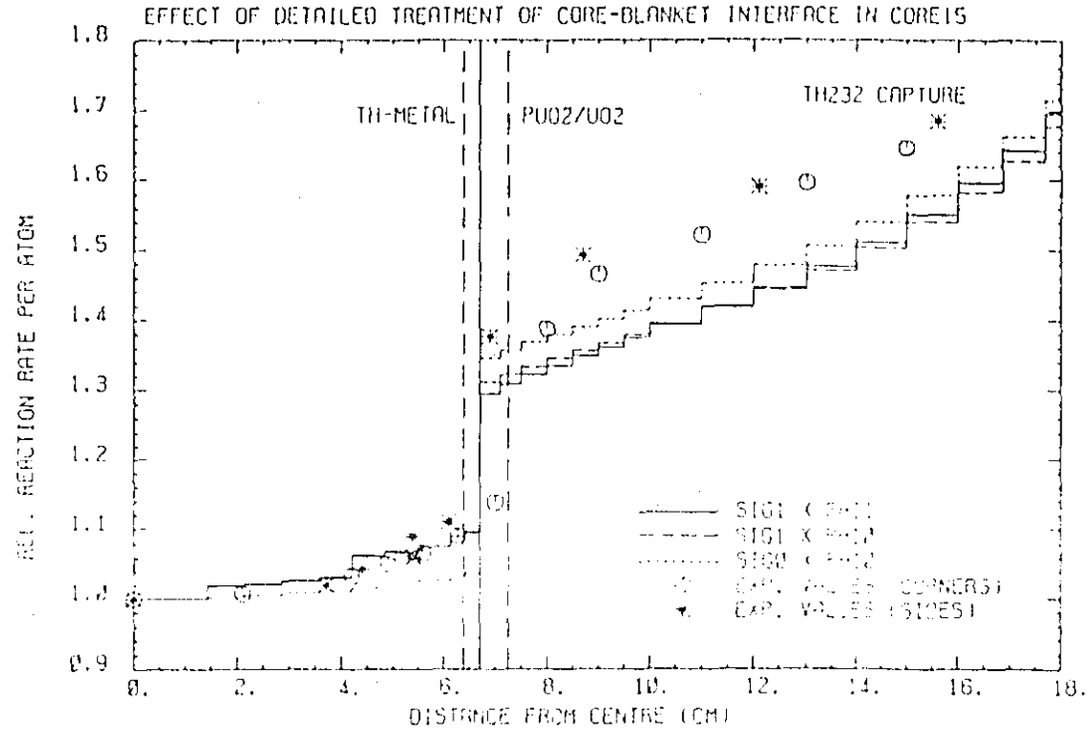

Fig. 23 Radial ^{232}Th Capture Rate Profiles in Cores 13 and 15

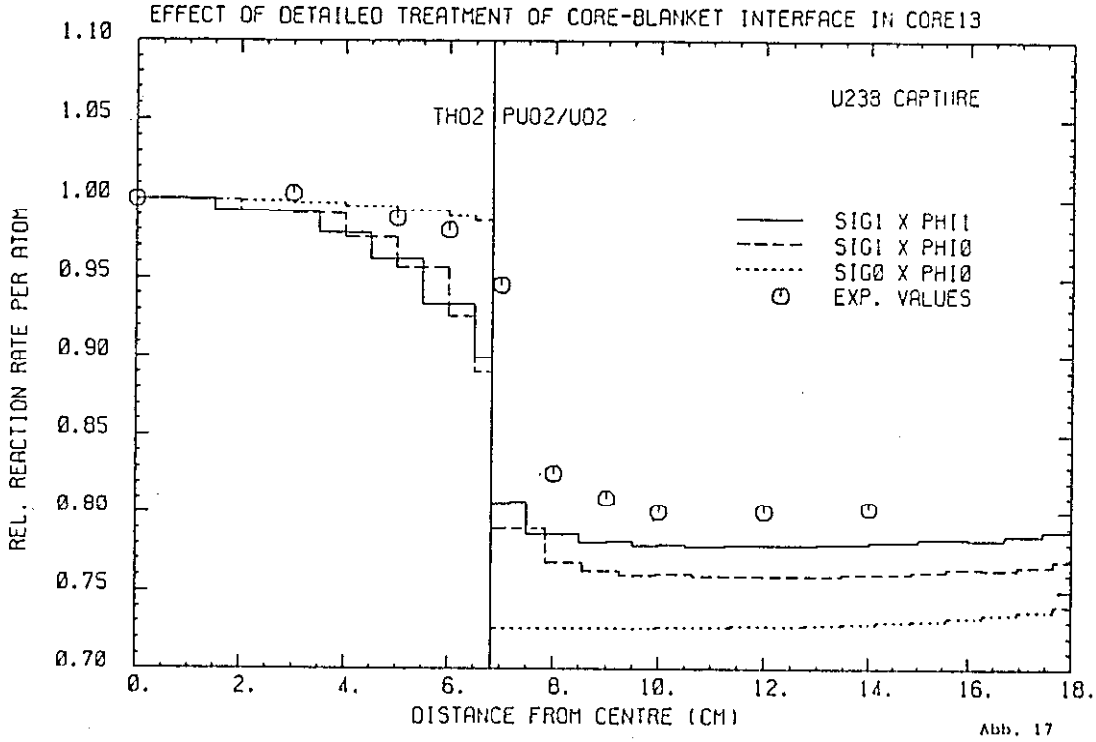

Abb. 17

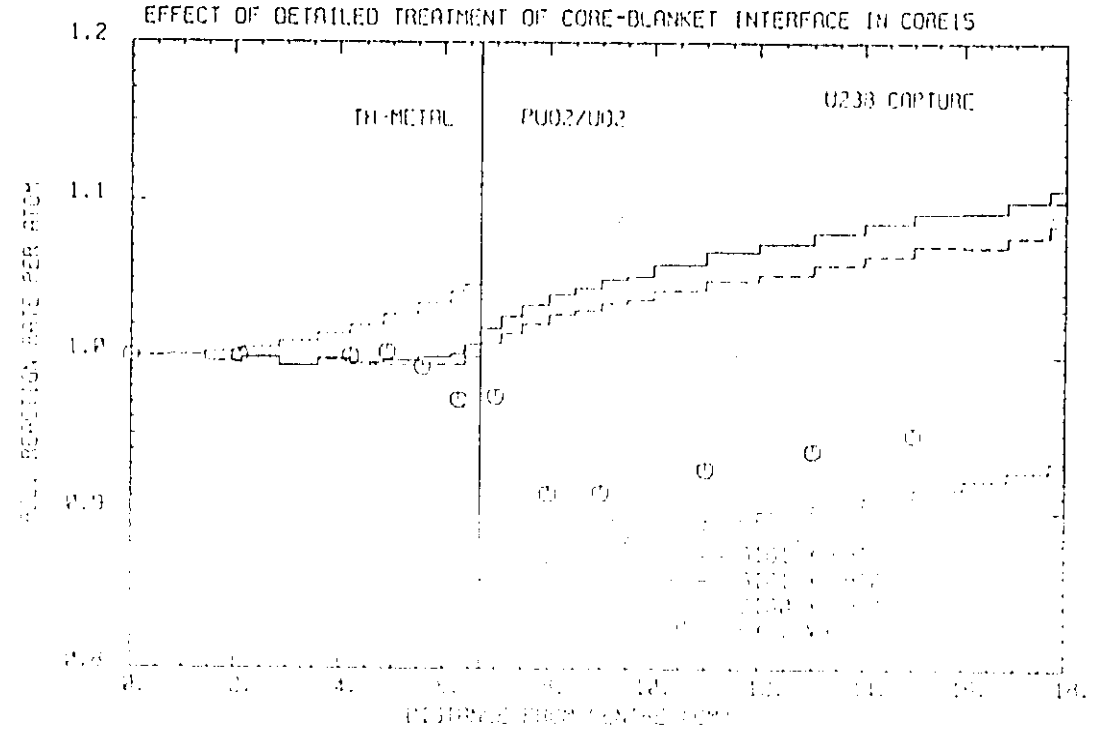

Fig. 24 Radial [illegible] Profiles in Cores 13 and 15

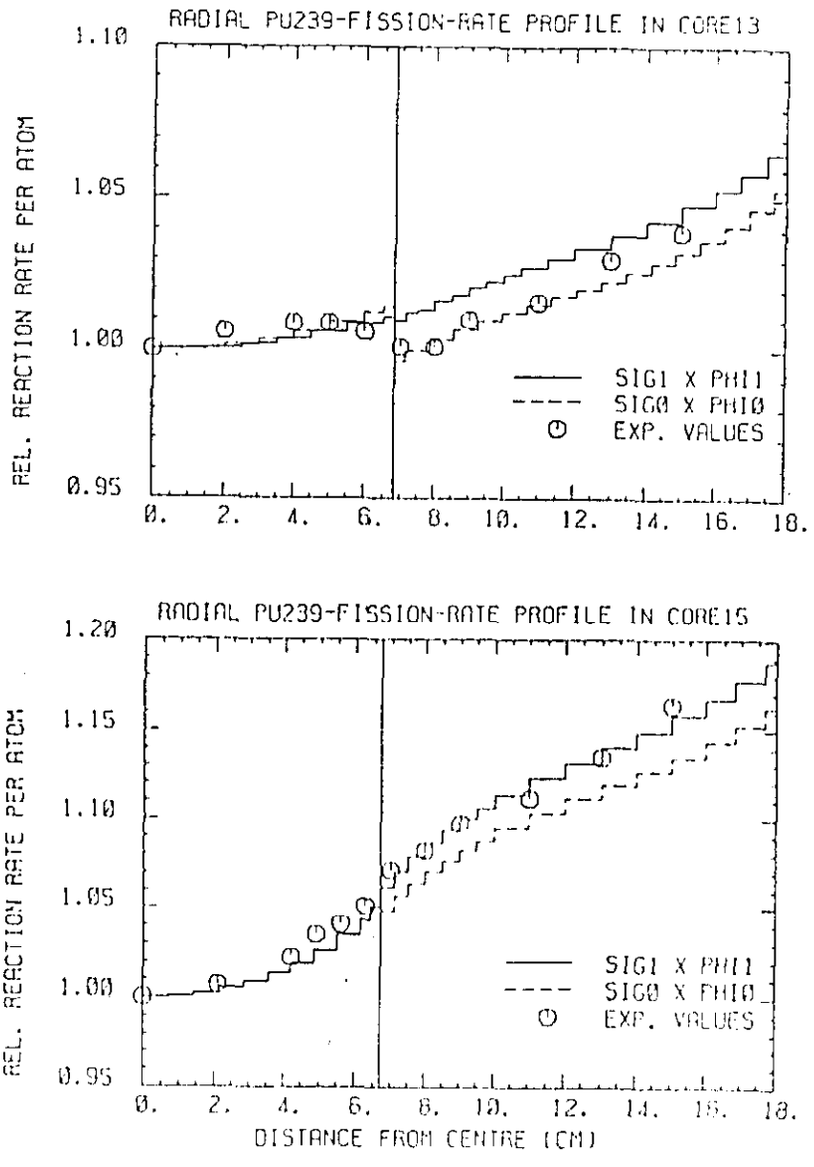

Fig. 25 Radial ^{239}Pu Fission Rate Profiles in Cores 13 and 15

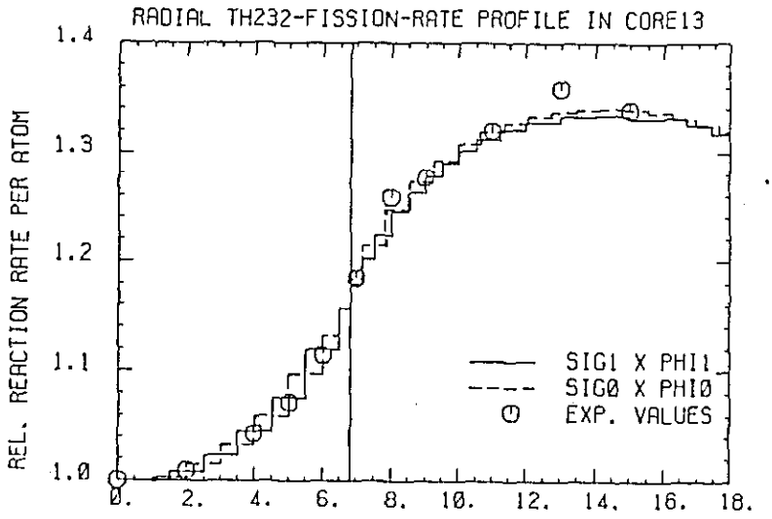

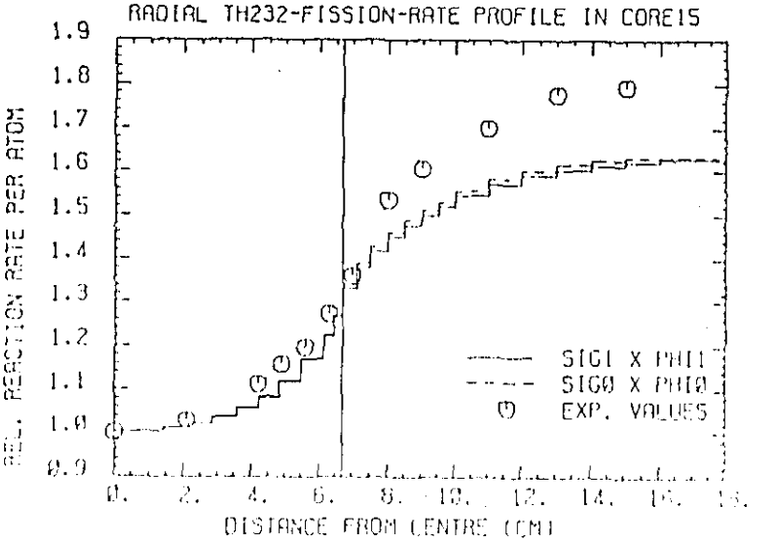

Fig. 2a Radial [illegible]

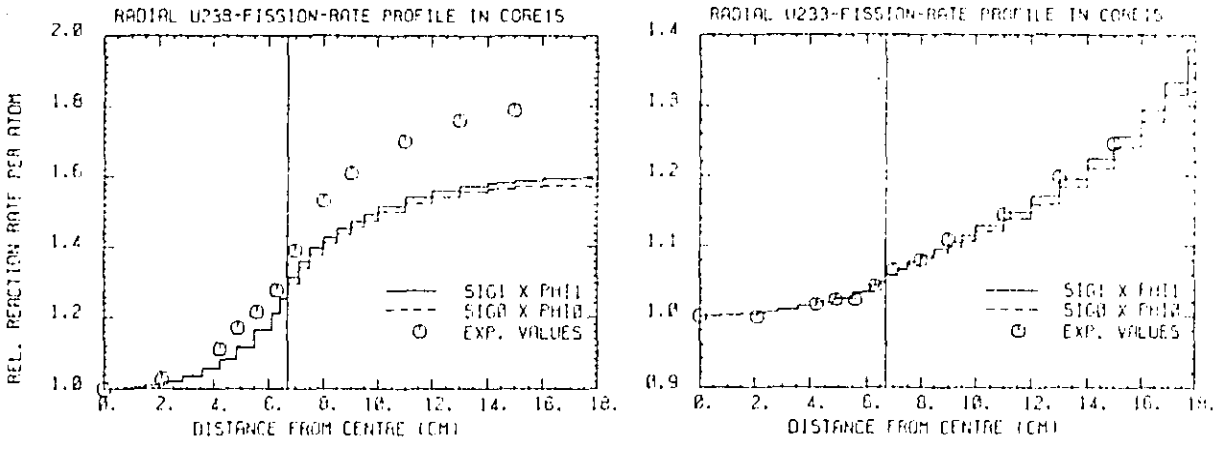

Fig. 27 Radial Profiles for ^{238}U and ^{233}U fission in Core 15

one, and finally, SIG1xPHI1 denotes the full detailed-model results.

Several observations may be made from the comparison of calculation and experiment for the ^{232}Th capture traverses shown in Fig. 23. Within the blanket zones, for example , the detailed model results are seen to be much better than those obtained by the simple model. In the PuO_2/UO_2 zone, on the other hand, neither of the two models appears adequate for reproducing the measured curvature.

Similar comments may be made regarding the ^{238}U capture traverses shown in Fig. 24. The detailed-model results in this case, however, while satisfactory in qualitative terms for Core 13, appear quite erroreous for Core 15. This was mentioned earlier while discussing the C/E values obtained for $\sigma_c(U238)/\sigma_f(Pu239)$ in the centre of the Th-metal zone (Section 5.2.1). While shortcomings in the calculational models currently used are clearly indicated, it should be

noted that ^{238}U capture rate measurements in the thorium blankets are more of academic, rather than practical, interest.

The various fission-rate profiles measured in Cores 13 and 15 (Figs. 25-27 for ^{239}Pu, ^{232}Th and ^{238}U/ ^{233}U, respectively) are all seen to depict relatively smooth variations across the interface of the fertile and fissile zones. With resonance self-shielding effects not being important for these reactions, the calculation of the radial distributions was quite straight-forward. The effects of going from the simple to the detailed model were not significant, there being little need to use spatially dependent broad-group cross-sections as in the case of ^{232}Th and ^{238}U capture.

In Figs. 28 and 29, some of the measured and calculated (detailed model) reaction rate profiles for Cores 13 and 15 are compared with the corresponding ones in the standard lattice (Core 11). The measured and calculated reaction rates for the standard lattice are normalised, in each case, to unity at the centre. In both experiment and calculation, the thermal flux in the PROTEUS C-driver zone was held constant on introduction of the internal-blanket zones. The influence of the blankets on reaction rates in the middle of the standard PuO_2/UO_2 lattice is seen quite clearly in the Fig. 28, 29 representations. Useful observations may also be made from some of the C/E comparisons. Considering the ^{232}Th capture traverses, for example, slight underprediction of the measured "dip" in the reaction rate in the blanket is indicated for both Cores. This is quite consistent with the observation made in Section [illegible] that self-shielding effects for ^{232}Th capture seem to be underestimated [illegible]. A similar under-prediction [illegible] dip [illegible] for [illegible] Th fission traverse in Core 15 (Fig. [illegible]). This, too, is consistent with an earlier observation, viz. that the neutron flux around 1 MeV seems to be overpredicted in the Th-metal zone (Section [illegible]).

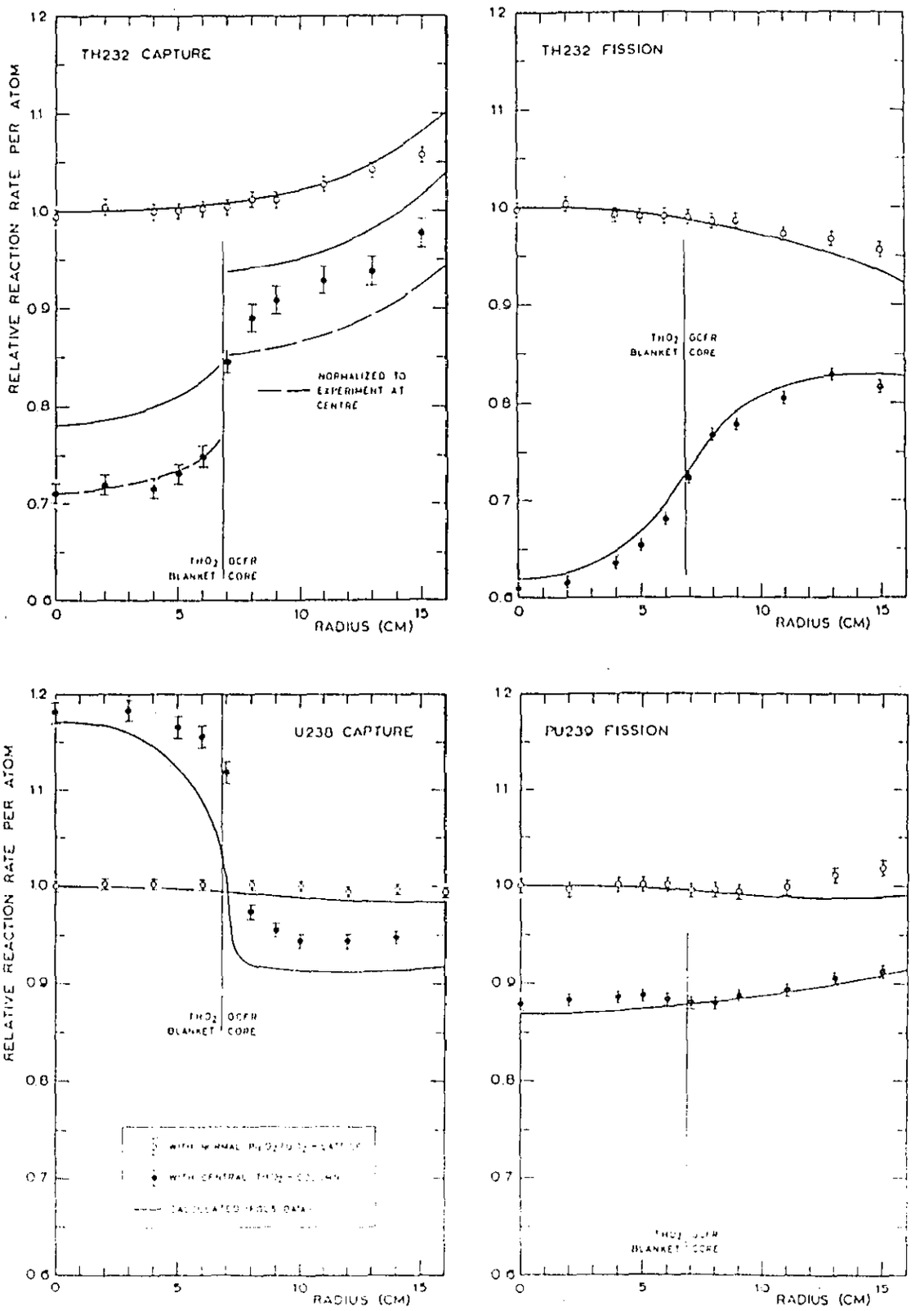

Fig. 28 Comparison of Reaction Rate Profiles in Cores 13 and 11

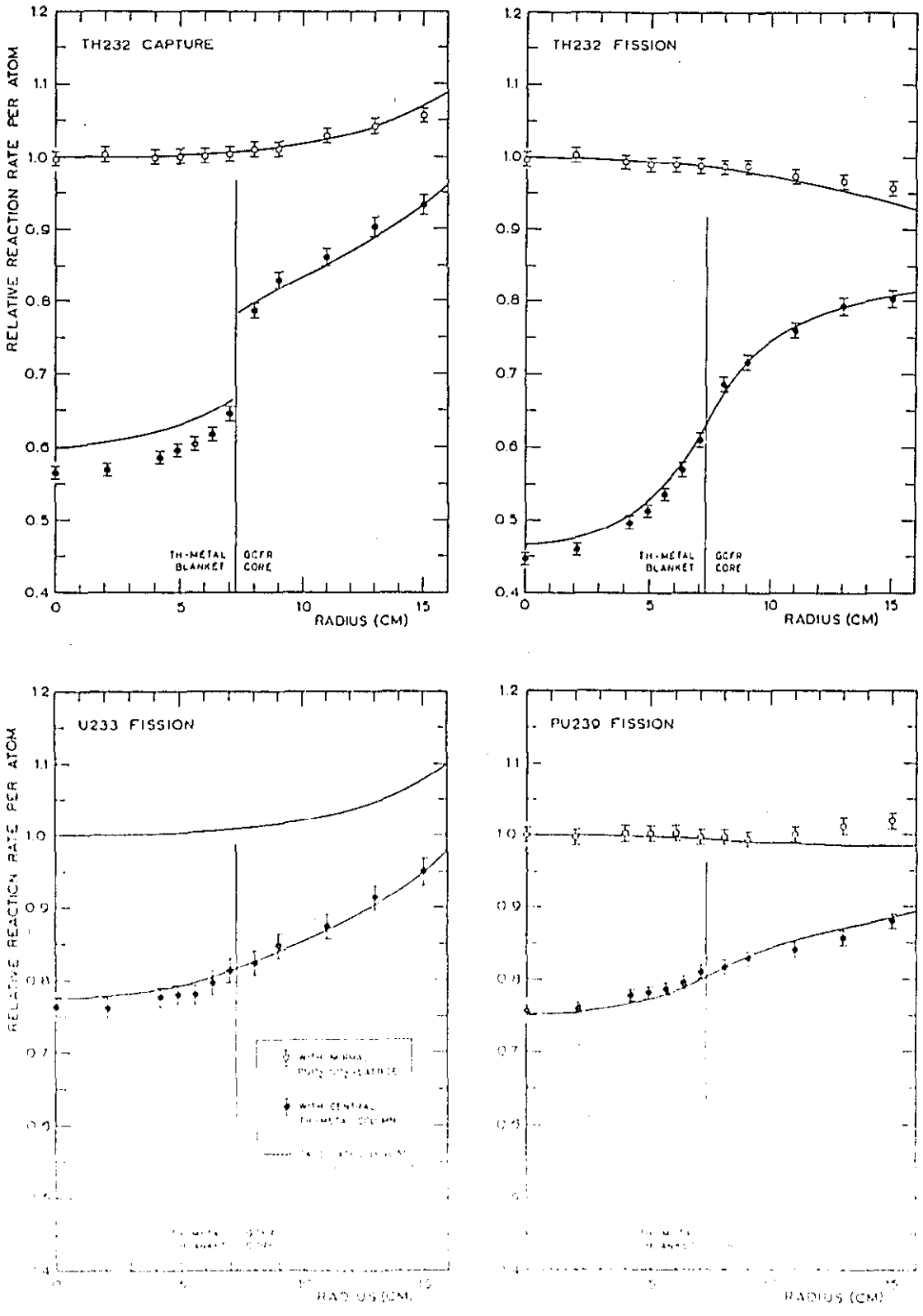

FIG. 29 Comparison of Reaction Rate Profiles in Cases 15 and 11

Although the differences between calculation and experiment for Cores 13 and 15 have been discussed above in considerable detail, it should be pointed out once again that the overall agreement was quite satisfactory in view of the normally ascribed large uncertainties in ^{232}Th cross-sections. In fact, the broad conclusion that one might draw from these "data and methods" benchmarks is that the breeding characteristics of heterogeneous thorium-containing fast reactor cores appear to be predictable to accuracies quite similar to those for ^{238}U-containing systems (38, 43).

5.3. Results for Cores 14 and 16

The configurations of Core 14, with its axial ThO_2 zone, and Core 16, with its Th-metal zone, were external-blanket experiments with larger quantities of thorium in the blanket region than used in Cores 13 and 15 (Section 2.2). The larger size of the fertile zone, together with the fact that core neutrons were incident on it only from one side, rendered analysis for the Core 14 and 16 blankets very much more sensitive to the PROTEUS thermal driver regions than was the case for the internal-blanket experiments. The use of a boron-plastic layer did achieve partial decoupling between the axial-blanket and driver zones (Fig. 6). Nevertheless, it was essential to consider a 2-D whole-reactor model for the analyses.

As already discussed in Section 4.3, two different methods were used for obtaining broad-group cross-sections for the fertile and fissile zones in Cores 14 and 16 - a simple model and a detailed model, analogous to the models used in Cores 13 and 15. The 2-D whole-reactor calculations were currently carried out with the DIFF-2D code, using 10 energy groups and FGL5-based cross-sections. Independent analyses

of the Core 14 and 16 experiments have been carried out at Oak Ridge using the 2-D transport-theory code, DOT-IV, with both ENDF/B-4 and ENDF/B-5 based cross-sections. The results of the ORNL studies are, however, reported separately (24).

5.3.1 Blanket-Centre Reaction Rate Ratios

Table 14 gives the results for measured and calculated (simple model) reaction rate ratios in the centre of the axial blankets of Cores 14 and 16. Corresponding results for the centre of

Table 14 Comparison of Calculated (C) and Experimental (E) Reaction Rate Ratios (per Atom) in the Centre of the Axial ThO_2 and Th-Metal Blankets of Cores 14 and 16

Reaction Rate Ratio	Centre of Normal PuO_2/UO_2-Lattice (CORE 11)		Centre of Axial ThO_2-Blanket (CORE 14)		Centre of Axial Th-Metal Blanket (CORE 16)	
	Expt.Value	C/E	Expt.Value	C/E	Expt.Value	C/E
$\frac{\sigma_c(Th232)}{\sigma_f(Pu239)}$	0.2000±1.3%	0.972	0.112±2.6 %	1.383	0.107±2%	1.235
$\frac{\sigma_f(Th232)}{\sigma_f(Pu239)}$	$8.061.10^{-3}$±2%	0.888	$1.48.10^{-3}$±3%	1.279	$1.28.10^{-3}$±3.8%	1.232
$\frac{\sigma_c(U238)}{\sigma_f(Pu239)}$	0.1327±1.1%	0.984	0.210±3.4%	1.449	0.397±3.2%	0.833
$\frac{\sigma_f(U238)}{\sigma_f(Pu239)}$	$3.111.10^{-2}$±1.3%	1.045	$5.37.10^{-2}$±2.6%	1.580	$4.83.10^{-2}$±3.3%	1.596
$\frac{\sigma_f(U233)}{\sigma_f(Pu239)}$	1.519±1.3%	0.999	1.310±1.7%	1.148	1.71±1.1	1.11
$\frac{\sigma_{2n}(Th232)}{\sigma_f(Pu239)}$	$6.84.10^{-4}$±2.6%	1.019	$1.71.10^{-4}$±4.9	1.122	$2.34.10^{-4}$±4.1	0.996

the reactor (i.e. effectively for the standard PuO_2/UO_2 lattice of Core 11) are also shown for comparison. In both Cores 14 and 16, the blanket-centre values of nearly all the measured reaction rate ratios are seen to be quite unsatisfactory. Table 15 compares calculated results obtained using the detailed model for cross-section preparation with those obtained using the simple model, and it is seen that there is little improvement.

Table 15 Influence of the Different Models for Cross-section Preparation on the Reaction Rate Ratios (C/E Values) in the Centre of the Axial ThO_2 and Th-metal Blankets

Reaction Rate Ratio	Centre of Axial ThO_2-Blanket (CORE 14)			Centre of Axial Th-Metal Blanket (CORE 16)		
	SIG0xPHI0	SIG1xPHI0	SIG1xPHI1	SIG0xPHI0	SIG1xPHI0	SIG1xPHI1
$\frac{\sigma_c(Th232)}{\sigma_f(Pu239)}$	1.383	1.320	1.310	1.235	1.331	1.334
$\frac{\sigma_f(Th232)}{\sigma_f(Pu239)}$	1.279	1.282	1.249	1.232	1.344	1.359
$\frac{\sigma_c(U238)}{\sigma_f(Pu239)}$	1.449	1.460	1.559	0.833	0.562	0.557
$\frac{\sigma_f(U238)}{\sigma_f(Pu239)}$	1.580	1.572	1.532	1.596	1.715	1.734
$\frac{\sigma_f(U233)}{\sigma_f(Pu239)}$	1.148	1.147	1.169	1.116	1.1	1.192
$\frac{\sigma_f(Np237)}{\sigma_f(Pu239)}$	-	-	-	1.343	1.344	1.354
$\frac{\sigma_{2n}(Th232)}{\sigma_c(Th232)}$	0.822	0.889	0.864	0.886	0.8	0.895

An explanation for the poor results for the axial-blanket experiments may be deduced from Fig. 30, which compares certain energy distributions (viz. for neutron flux,

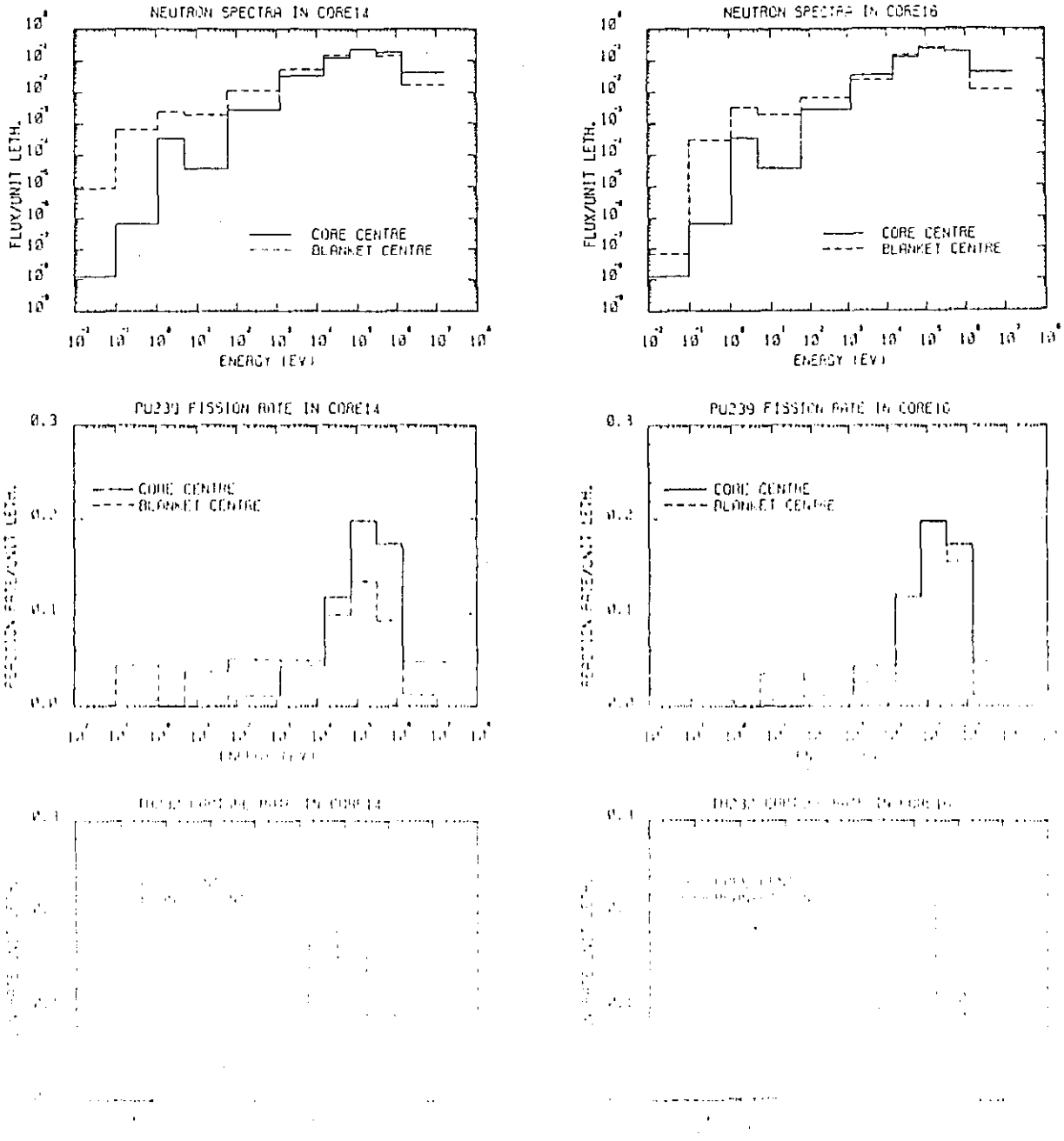

Fig. 30 Energy Distributions for Neutron Flux, ^{239}Pu Fission and ^{232}Th Capture in Cores 14 and 16

^{239}Pu fission and ^{232}Th capture) at the centre of the axial blankets with those in the standard lattice. Considerable contributions from low-energy neutrons are seen to occur at the blanket centre in both Cores 14 and 16. If one assumes that the currently employed whole-reactor calculations are underpredicting the low-energy neutron flux in the blankets, e.g. through underestimation of the thermal-driver influence, it is clear from Fig. 30 that the parameter which would be underestimated most of all would be σ_f(Pu239). Since this parameter features as the denominator in the various reaction rate ratios of Table 14 , such a hypothesis would be consistent with the obtained results, viz. that most of the C/E values are considerably greater than unity. (The case of σ_c(U238)/ σ_f(Pu239) is perhaps different since the cross-section preparation for ^{238}U capture in the thorium-containing zones is particularly difficult).

Subsidiary reaction rate measurements (e.g. at points away from the central axis of the blankets) confirmed that finite contributions were indeed being made by low-energy neutrons from the PROTEUS driver zones (44). The currently used calculational methods seem unable to take adequate account of such contributions, indicating the need for more detailed treatment (i.e. a larger number of groups) at the level of the 2-D whole-reactor calculations.

5.3.2 Axial Reaction Rate Traverses

Figs. 31-34 give the various reaction rate traverses measured through the axial blankets of Cores 14 and 16. Both calculation and experiment have been normalised to unity at the reactor centre. (From the viewpoint of measurement techniques, the ^{237}Np fission traverse perhaps deserves special mention since it could not be measured using activation foils and fission track recorders alone were employed).

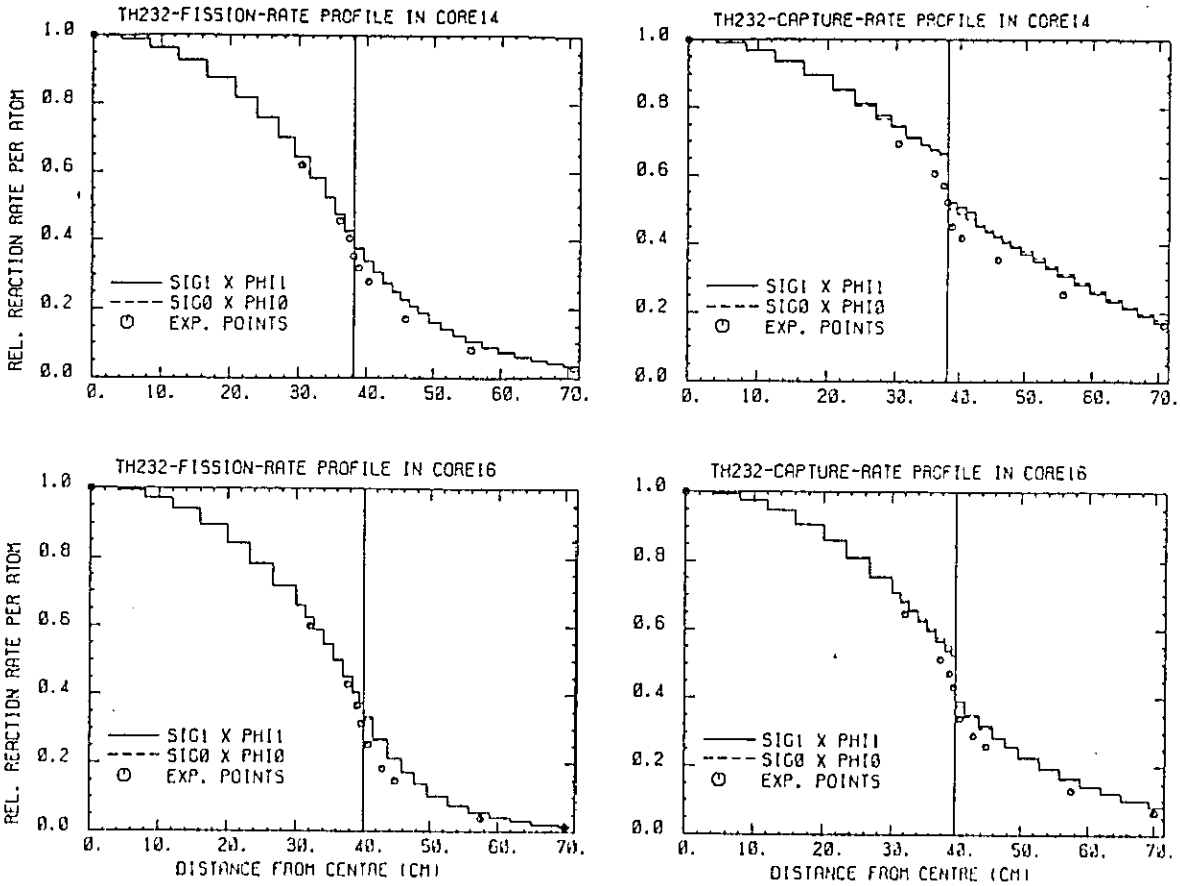

Fig. 31 Axial Traverses for ^{232}Th Capture and Fission in Cores 14 and 16

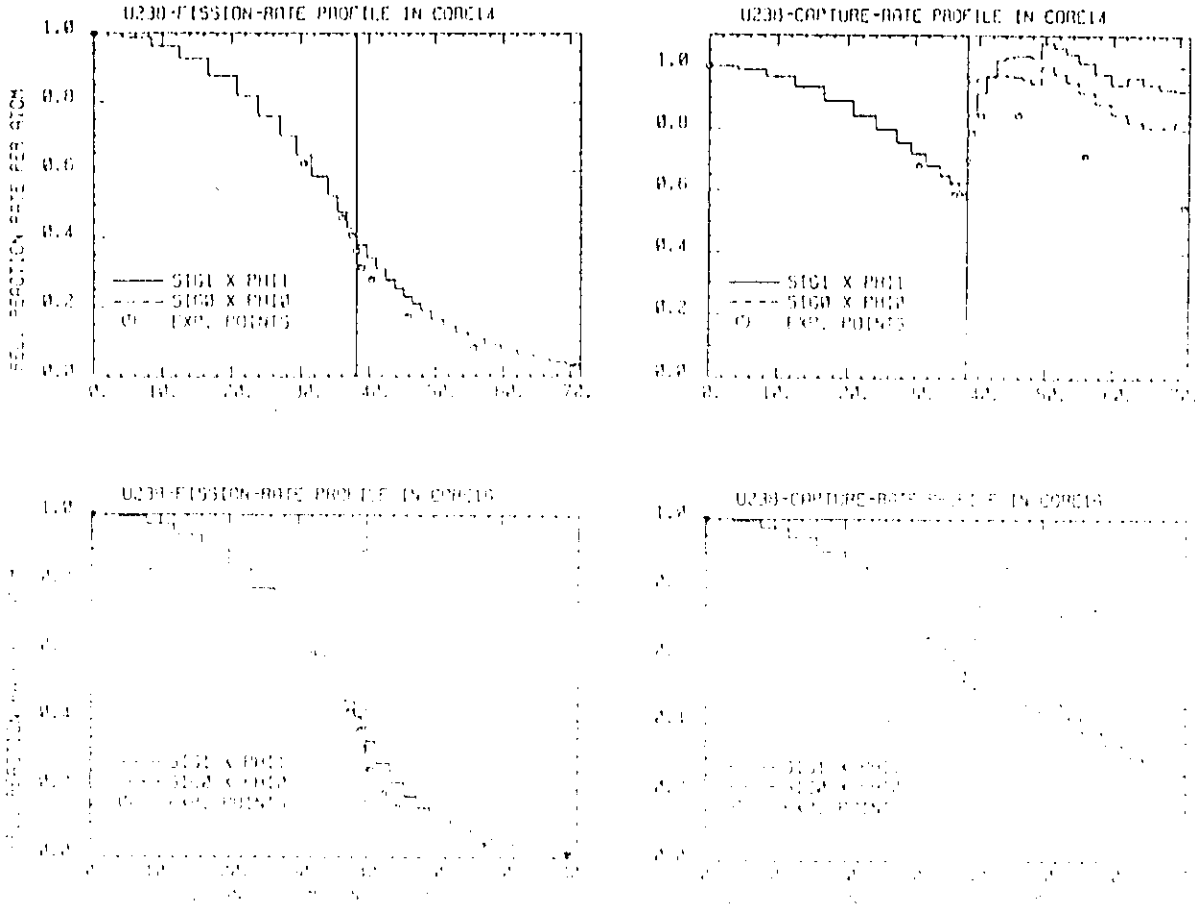

Fig. 32 Axial Traverses for [illegible] Capture and Fission in Cores 14 and 16

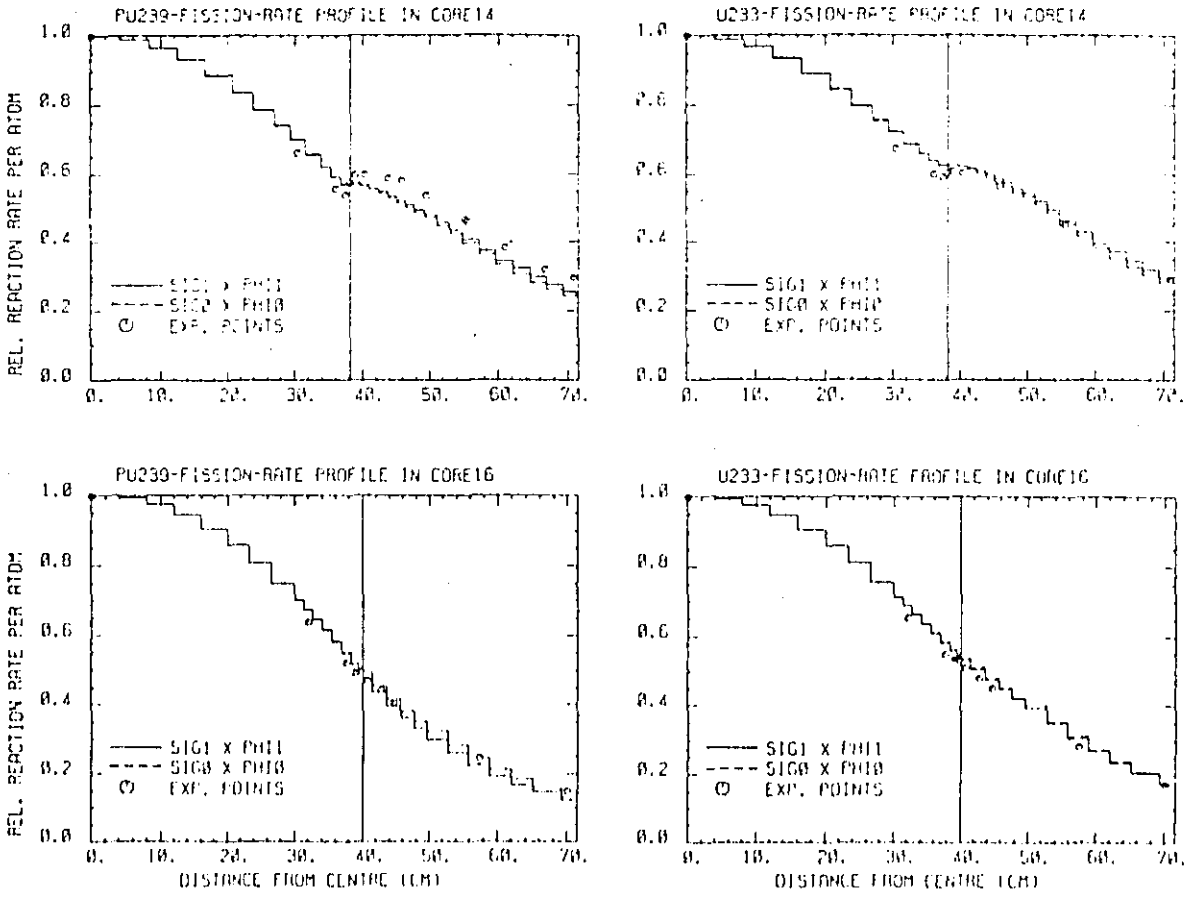

Fig. 33 Axial Traverses for ^{233}U and ^{239}Pu Fission in Cores 14 and 16

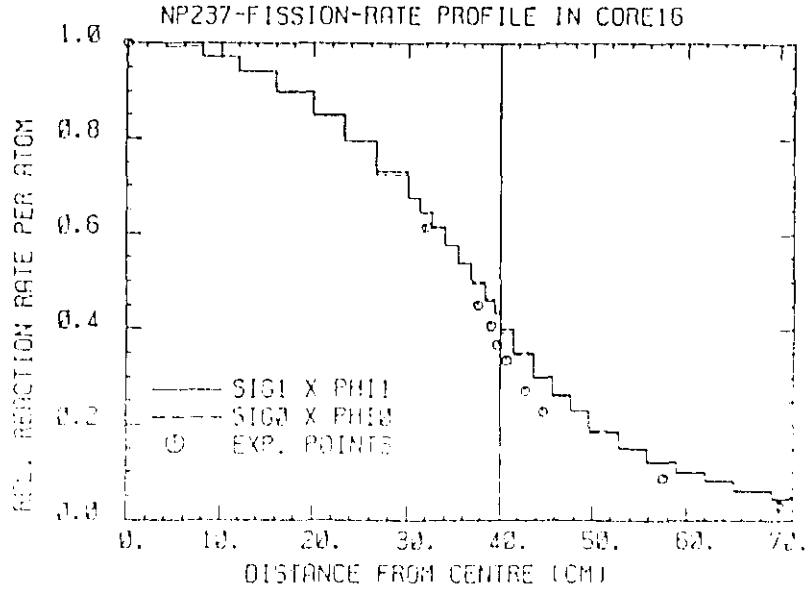

Fig. 34 Axial ^{237}Np Fission Rate Traverse in Core 16

Differences between the simple- and detailed-model results of Figs. 31-34 are seen to be rather insignificant in most cases. For ^{238}U capture, however, the detailed model is clearly erroneous for the Th-metal blanket, as was the case in Core 15 (cf. Figs. 24, 32). On the whole, qualitatively similar conclusions may be drawn from comparison of the calculated and measured traverses as were discussed in Section 5.3.1 in the context of blanket-centre C/E values. While the use of transport theory instead of diffusion theory might be expected to result in some improvement (24), the more important shortcomings in the current calculational results for the reaction rate traverses stem from inadequate detail in treatment of the full reactor.

5.4 Neutron Spectrum Results

5.4.1 For Core 12

Fig. 35 compares the measured (Section 3.2) and MURALB/TOFFEE calculated (Section 4.4.1) neutron spectrum results for Core 12. The experimental and calculated spectra have been normalised to each other over the full measured energy range (covering almost 90 % of the total spectrum).

The overall agreement between the measured and MURALB-based results is seen to be quite satisfactory above 20 keV. Below this energy, however, the calculation underpredicts the measurements by 15-25 %. A similar underprediction in this lower energy range was observed earlier for measurements in the standard [illegible] Core 11.

The measured spectrum [illegible] is up to 10 % below the calculated. This effect, which was also observed earlier, may be related to the observed shift in the position of the [illegible] keV.

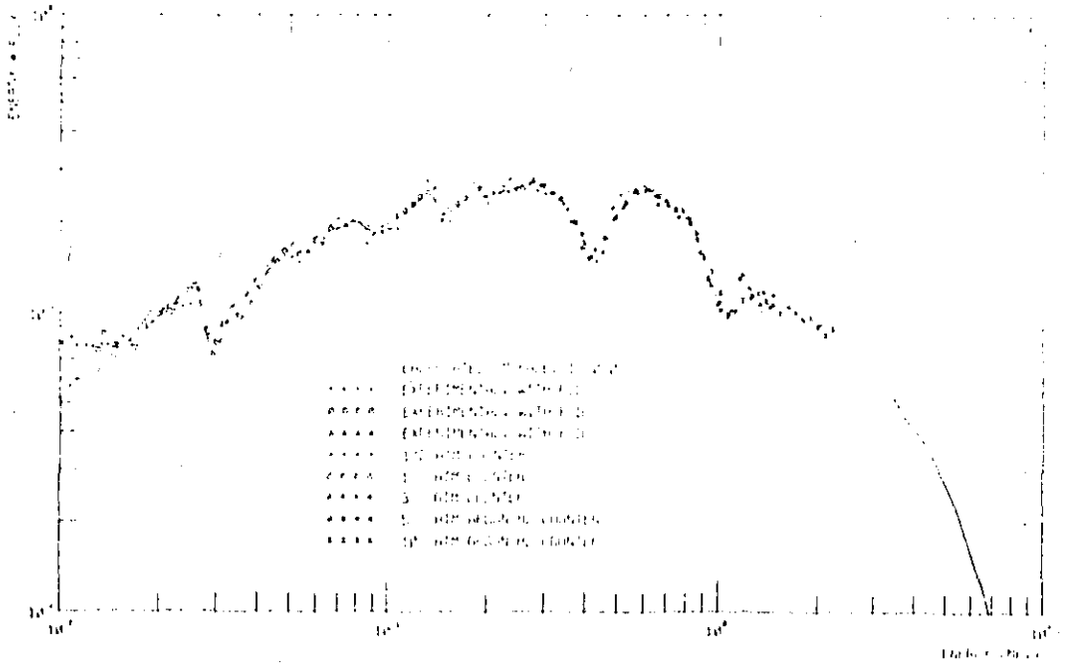

Fig. 35 Comparison of Measured and MURALB-Calculated Neutron Spectra for Core 12

Fig. 36 shows a comparison, in the 99-group GAM-2 structure, between the Core 12 measurements and calculations based on MURALB

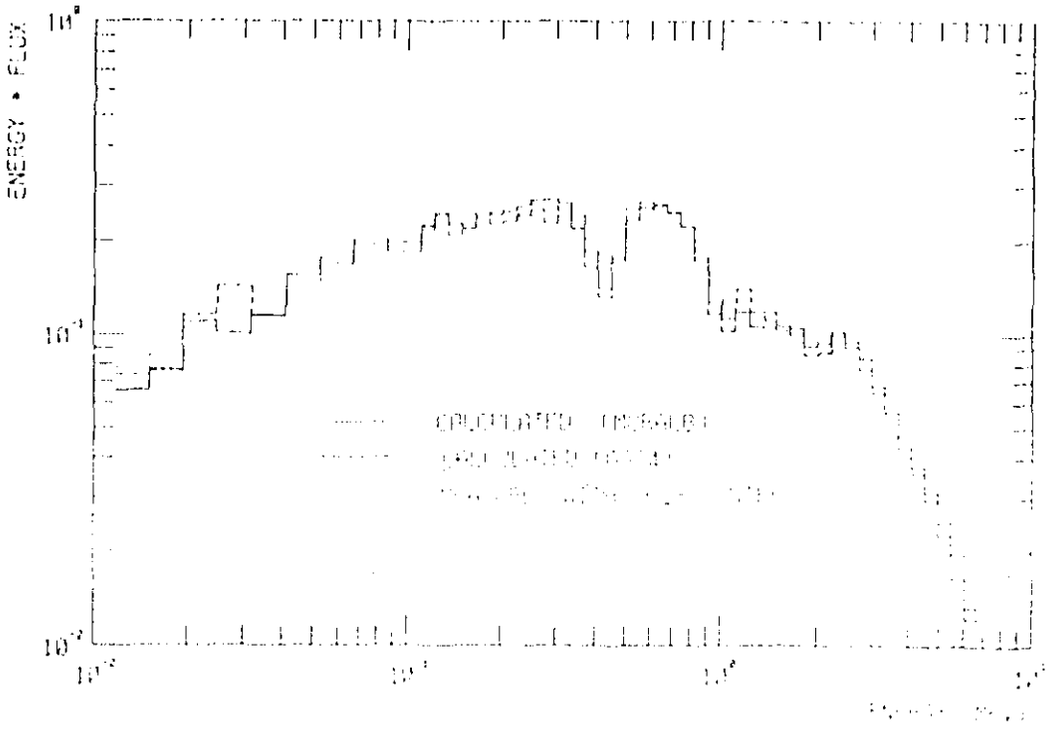

Fig. 36 Comparison of Experimental Results with GGC4- and MURALB-Calculated Spectra for Core 12

(FGL5 data) and GGC-4 (ENDF/B-4 data). The agreement with experimental results is seen to be significantly poorer for the latter calculational route, i.e. ENDF/B-4 data appears to perform much less satisfactorily for the spectrum calculations than does FGL5.

The large discrepancy in the region of the prominent Fe-resonance at ∿ 30 keV may be attributed to the fact that structural materials in the GGC-4 data library, while assumed to occur in their natural isotopic ratios, had resonance parameters defined for the lightest isotope only. Resonance contributions from the other isotopes were considered simply in infinite dilution. Thus, for the iron in the steel tubes used in the lattice, the principal isotope ^{56}Fe (∿ 92 %) was inadequately represented, appropriate data being available only for the lightest isotope ^{54}Fe (occurring to ∿ 6 %).

The GGC-4 calculation is seen to underpredict the measurements between 150-300 keV by 10-15 %. Resonance effects at 290 keV and at 1.2 MeV may be observed in the GGC-4 results for which neither the measurements, nor the MURALB calculation, provide any evidence. In the high-energy region, the MURALB spectrum is seen to lie upto ∿ 20 % above the GGC-4 results.

It is useful to compare the effects of the neutron spectra obtained by the two different calculational routes on the discrepancies between calculation and experiment for the principal reaction rate ratios. For C_8/F_9, for example, the differences between the experimental and FGL5-calculated spectra in Core 12 yielded a C/E value of 0.96. For the ENDF/B-4 based calculation, the corresponding C/E was 1.01. It is thus seen that the spectrum discrepancies for the ENDF/B-4 based calculation had certain compensating effects on C_8/F_9. The differences between the experimental

and MURALB/FGL5 spectra, even though significantly smaller, had a larger net effect on this reaction rate ratio.

5.4.2 For Core 14 (25)

Figure 37 shows a comparison between the experimental neutron spectrum at the centre of the Core 14 ThO_2 axial blanket and the DOT-IV calculation based on ENDF/B-4 cross-section data. As before, the experimental spectrum has been normalized

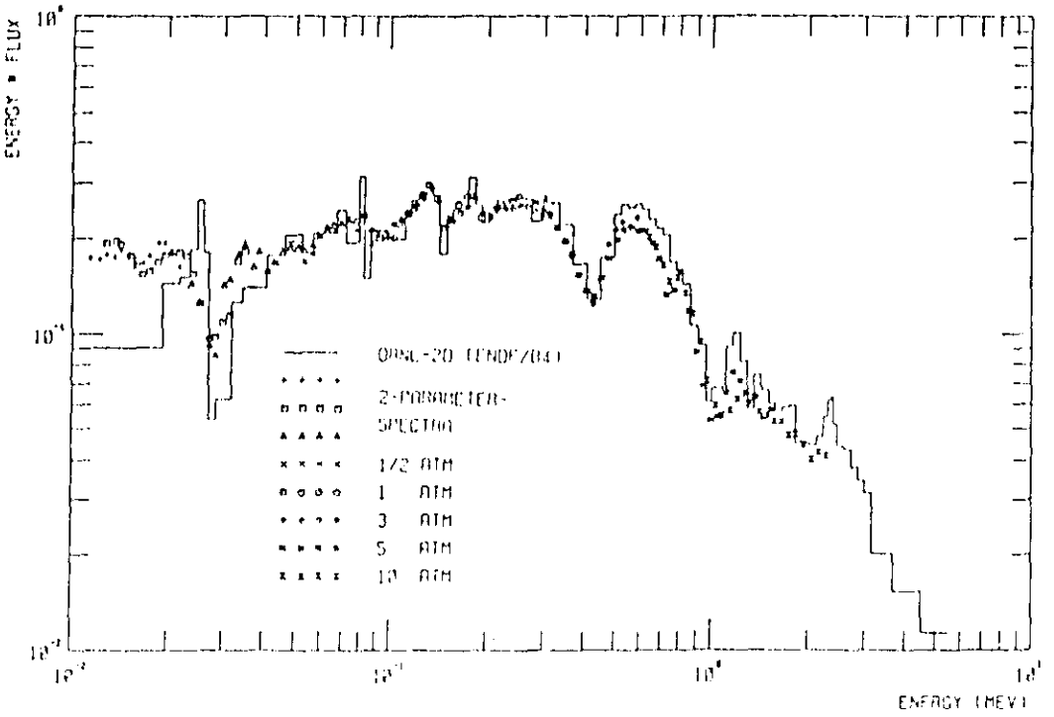

Fig. 37 Comparison of the Measured Spectrum in Core 14 with Calculational Results Based on ENDF/B-4 Data

to the calculated spectrum over the full measured energy range. Agreement between the spectra is generally good, especially between 30 and 500 keV. The fine structure in the

spectrum, which is largely due to oxygen, is represented in both the measured and calculated results. However, the general magnitude of the spectrum appears to be overpredicted above 500 keV and underpredicted below 20-30 keV.

The overprediction of the neutron spectrum above 500 keV has been attributed to the thorium cross-section data and is discussed in Section 5.4.3. The low-energy underprediction, significantly more severe than for the Core 12 results (Section 5.4.1), may be attributed to the truncation of the geometric model which was necessary for the fine-group calculation. Considerable evidence was compiled in the analysis of the reaction rate measurements (24) which concluded that deletion of the thermal driver zones from the analytic model causes significant removal of the lower energy flux in the central test regions, and that this is particularly true for the axial blankets. Such an effect is present in the spectrum calculation, although to a reduced extent because of the implicit inclusion of the thermal drivers in the determination of the distributed fission source (Section 4.4.2).

5.4.3 For Core 16 (25)

Figure 38 gives a comparison between the measured Core 16 Th-metal blanket spectrum and the calculated spectrum based on ENDF/B-4 cross-section data. The results are very similar to the ThO_2 case except that the oxygen structure is not as prominent. The flux depression near 400 keV which is due to the O-resonance is not predicted as well as in the ThO_2 blanket, but this is due to modelling approximations. Whereas the [illegible] allowed [illegible] [illegible] region to the Th-metal blanket, the homogenized core and blanket regions in the analytic model lessened the apparent effects of the oxygen on the blanket spectrum.

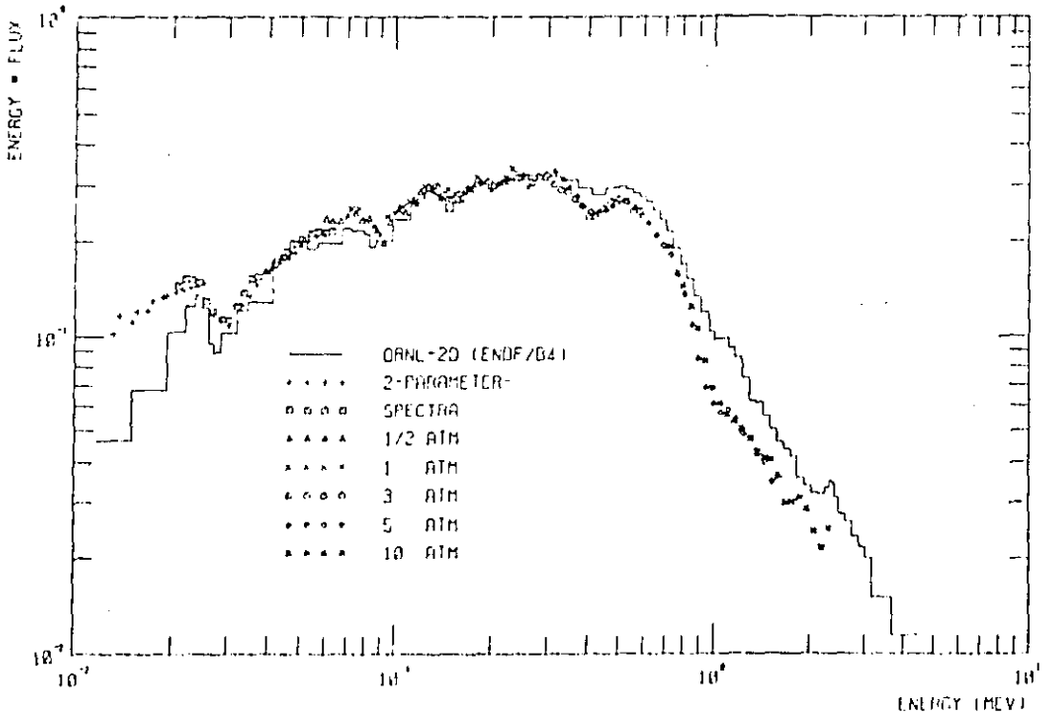

Fig. 38 Comparison of the Measured Spectrum in Core 16 with Calculational Results Based on ENDF/B-4 Data

Core 16 was also calculated using cross-sections for thorium based on ENDF/B-5. The Version-5 Th data was used for both the 10-group full-model calculation which produced the fission source and the 126-group reduced-model calculation (Section 4.4.2). All other materials used Version-4 data. The resulting spectrum in the Th-metal axial blanket is compared in Fig. 39 to the measured neutron spectrum. Agreement between the calculated and measured spectra is significantly better above 500 keV than with ENDF/B-4 thorium. However, below 200 keV, the new data yields substantial discrepancies.

The source of the lower-energy discrepancies observed in Fig. 39 was suggested by an inspection of the basic nuclear

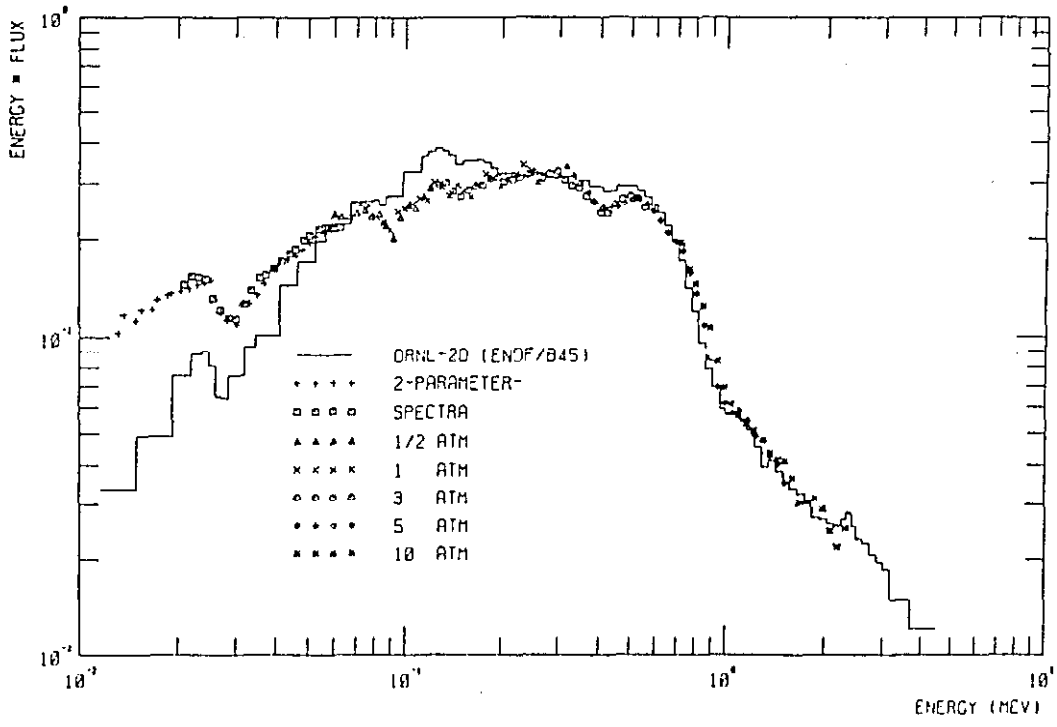

Fig. 39 Comparison of the Measured Spectrum in Core 16 with Calculational Results Obtained Using ENDF/B-5 Data for Thorium

data for thorium, in particular those for the inelastic scattering process (n,n'). Even though the magnitude of the (n,n') cross-section is small compared to the total cross section, the differences between the data in ENDF/B-4 and -5 were found to correlate closely with the differences between the calculated spectra shown in Figs. 38 and 39. In order to verify the correlation, a special hybrid 126-group cross-section set was prepared for thorium which was identical to the ENDF/B-4-based set except that the discrete and continuum inelastic scattering partial cross-sections were replaced with ENDF/B- [illegible] data.

The "hybrid" spectrum, when compared to the ENDF/B-4 and -5 spectra, showed that for the given energy range the shape of

the flux spectrum is largely determined by the (n,n') cross-section. With consideration of the measured spectrum, it appears that the changes in the (n,n') cross-section above 400 keV are appropriate. However, the significant decrease in the cross-section below 200 keV is not supported by the present experimental results. This change apparently causes a reduced flux removal from the corresponding energy groups which causes the flux to increase relative to the ENDF/B-4 case. At lower energies (below 50-60 keV), the flux begins to drop rapidly due to the loss of the downscatter source from the preceding groups.

The effects of the ENDF/B-5 (n,n') data on integral reaction rates were determined by folding various reaction cross-sections with the blanket spectra calculated using: (a) all-ENDF/B-4 thorium data and (b) the hybrid (ENDF/B-4 with ENDF/B-5 (n,n') partials) thorium data. Despite the 20-30 % differences in the two spectra, the hybrid spectrum yielded a thorium capture rate that was only 3 % lower than the capture rate produced by the all-ENDF/B-4 spectrum. One-half of the 3 % decrease was due to spectral differences below 200 keV. On the other hand, the 1.7-MeV-threshold fission rate for thorium was decreased 18 % by the hybrid spectrum relative to the all-ENDF/B-4 case. Therefore, the changes to the thorium (n,n') cross-sections between ENDF/B-4 and -5 could have significant impact on some aspects of alternate fuel cycle studies such as the power distributions within thorium blankets.

It has been seen how the axial-blanket spectrum measurements, being by definition differential in nature with respect to neutron energy, provided a somewhat more comprehensive test of the cross-section data and methods than did the integral reaction rates (cf. Section 5.3). The two types of measurements, however, are clearly complementary. This is

borne out by the manner in which the spectrum results led to useful conclusions regarding ^{232}Th inelastic cross-sections, but provided little evidence regarding the capture and fission data per se. As with the reaction rate measurements, however, a careful analysis is required to understand and eliminate possible effects of model and methods approximations.

Acknowledgements

The authors are grateful to Dr. C. McCombie and Dr. S. Seth for their valuable contributions during the early phases of the thorium programme on PROTEUS. Thanks are also due to Mr. H. Graf for carrying out the fission-track detector measurements and to Mr. P. Bourquin, Mr. A. Klingler, Mr. T. Steiner, Mr. U. Tschanz and Mr. G. Viel, who together with Mr. Graf, operated the reactor so smoothly throughout the experimental period.

The keen interest and active collaboration of Dr. D. Bartine, Dr. D. Ingersoll, Mr. J. White and Mr. M. Williams - all of the Oak Ridge National Laboratory - are also gratefully acknowledged.

Finally, Mrs. V. Bocek deserves a special "thank you" for her patience and efficiency in typing this report.

REFERENCES

1. Report of INFCE Working Group 5: Fast Breeders
IAEA, Vienna, 1980

2. Report to the APS by the Study Group on Nuclear Fuel Cycles and Waste Management, Rev. Mod. Phys., 50, 1978

3. W. Michael Schikarr
"Assessments of the Thorium and Uranium Fuel Cycle in Fast Breeder Reactors and High Temperature Reactors"
IIASA, Laxenburg, Austria,
CP-79-19, 1979

4. D.M. Ligou, R.H. Brogli
"International Symbiosis: The Role of Thorium and the Breeders"
Nucl. Technol., 48, 261, 1980

5. P.R. Kasten et al.
"Assessment of the Thorium Fuel Cycle in Power Reactors",
Report ORNL/TM-5565, 1977

6. R.B. Turski and R.D. McKnight
"Nuclear Data Sensitivity Coefficients for a ^{233}U-^{232}Th Fuelled LMFBR"
Proc. Topical Meeting on Advances in Reactor Physics,
Gatlinburg, Tennessee, 1978

7. R.L. Macklin and J. Halperin,
"$^{232}Th(n,\gamma)$ Cross-sections from 2.6 to 800 keV"
Nucl. Sci. Eng., 64, 849 (1977)

8. J.F. Whalen and A.B. Smith
"Note on the Fast-Neutron Total Cross-section of Thorium"
Nucl. Sci. Eng., 67, 129 (1978)

9. C.L. Beck et al.
"An Evaluation of Fast Integral Data Related to ^{233}U and Thorium"
Proc. Topical Meeting on Advances in Reactor Physics,
Gatlinburg, Tennessee, 1978

10. P. Brandauer et al.
"Measurements of Neutron Spectrum and Reaction Rates in a Gas-Cooled Fast Reactor Lattice"
EIR-Bericht Nr. 239, 1973

References (contd.)

11. D.W. Sweet
"Actinide Fission Rate Measurements in ZEBRA"
Report AEEW-R1090, 1977

12. R. Chawla, K. Gmür and W. Görlich
"Direct Determination of the Ratio of ^{232}Th (n,2n) and (n,γ) Reactions in a Fast Reactor"
Nucl. Instrum. Methods, 174, 179 (1980)

13. R. Chawla and C.B. Besant
"Absolute Measurements of ^{238}U Capture and ^{239}Pu Fission Rates in Fast Reactors"
J. Br. Nucl. Energy Soc., 9, 28 (1970)

14. R. Chawla
"A Method for the Direct Measurement of Relative Capture Rates in ^{232}Th, ^{238}U Containing Lattices"
Ann. Nucl. Energy, 4, 135 (1977)

15. R. Chawla and K. Gmür
"Improved Thorium Reaction Rate Measurements in a GCFR Lattice"
Trans. Am. Nucl. Soc., 31, 264 (1979)

16. P.W. Benjamin, C.D. Kemshall and J. Redfarn
"The Use of a Gas-Filled Spherical Proportional Counter for Neutron Spectrum Measurements in a Zero Energy Fast Reactor"
Report AWRE-NR2/64, 1964

17. P.W. Benjamin, C.D. Kemshall and A. Brickstock
"The Analysis of Recoil Proton Spectra"
Report AWRE-09/68, 1968

18. M. Jermann
"Neutronenspektroskopie mit Rückstossprotonenzählern im Gitter eines gasgekühlten Schnellen Brutreaktors"
EIR-Bericht Nr. 310, 1977

19. U. Schmocker and S. Seth
"Das 2D-Modell der Nullreaktivitätsgitter 6, 7, 8 und 10 des PROTEUS-Reaktors"
EIR Internal Document TM-PH-713, 1976

20. J.D. Macdougall
"MURALB-A Programme for Calculating Neutron Fluxes in Many Groups"
Report AEEW-R962, 1977

References (contd.)

21. J. Adir and M.D. Lathrop
"Theory of Methods Used in the GGC-4 Multigroup Cross-section Code"
Report GA-9021, 1968

22. R.B. Kidman and R.E. MacFarlane
"LIB-IV, A Library of Group Constants for Nuclear Reactor Calculations"
Report LA-6260-MS, 1976

23. N.M. Green et al.
"AMPX: A Modular Code System for Generating Coupled Multigroup Neutron-Gamma Libraries from ENDF/B"
Report ORNL/TM-3706, 1976

24. J.R. White and D.T. Ingersoll
"Analysis of the Thorium Axial Blanket Experiments in the PROTEUS Reactor"
Report ORNL/TM-7471, 1980

25. M. Jermann and D.T. Ingersoll
"Neutron Spectrum Evaluation in the Thorium Axial Blankets of the PROTEUS Reactor"
Proc. ANS Topical Conf. on Advances in Reactor Physics and Shielding, Sun Valley, Idaho, 1980

26. R. Rühle
"RSYST, ein integriertes Modulsystem mit Datenbasis zur automatisierten Berechnung von Kernreaktoren"
Dissertation IKE (Institut für Kernenergetik), Stuttgart, Bericht Nr. 4-12, 1973

27. W.W. Engle, Jr.
"A User's Manual for ANISN, A One-Dimensional Discrete Ordinates Code with Anisotropic Scattering"
Report ORNL/K-1693, 1967

28. J. Stepanek
"The DPN 'Surface Flux' Integral Transport Method with General P_L Polynomial Approximation"
EIR-Bericht Nr. 364, 1977

29. M. [illegible] et al.
"Comparison of Measured and Calculated Values of Neutron Spectra and Reaction Rate Ratios in Gas-Cooled Fast Reactor Benchmark Lattices"
EIR-Bericht Nr. 298, 1976

References (contd.)

30. U. Schmocker
"Die Berechnung von Gittern mit zwei verschiedenen Arten von Brennstoffstäben mit Hilfe des Programms MURALB"
EIR Internal Document TM-PH-645, 1977

31. U. Schmocker
"Berechnung axialer Reaktionsratenprofile im PROTEUS Core 16"
EIR Internal Document TM-PH-821, 1979

32. J.D. Macdougall
"TOFFEE, a Fortran Programme for Calculating Directed Flux Spectra"
Report AEEW-M903, 1969

33. W.A. Rhoades et al.
"The DOT-IV Two-Dimensional, Discrete-Ordinates Transport Code with Space-Dependent Mesh and Quadrature"
Report ORNL/TM-6529, 1978

34. R.W. Roussin et al.
"The CTR Processed Multigroup Cross-section Library for Neutronics Studies"
Report ORNL/RSIC-37, 1978

35. J.R. White et al.
"Analysis of a Swiss Thorium Blanket Integral Experiment"
Proc. Int. Conf. Nuclear Cross-sections for Technology, Knoxville, Tennessee, 1979

36. S. Seth et al.
"GCFR Benchmarks: Experiments and Analysis"
Proc. Conf. Nuclear Cross-sections and Technology, Washington, D.C., 1975

37. R. Richmond et al.
"Testing of Nuclear Data Sets using PROTEUS GCFR Lattice Data" in Advances Reactors: Physics, Design and Economics, ed. J.M. Kallfelz and R.A. Karam, Pergamon Press, 1975

38. M.J. Lineberry et al.
"Physics Studies of a Heterogeneous Liquid-Metal Fast Breeder Reactor"
Nucl. Technol., 44, 21 (1979)

References (contd.)

39. C.L. Beck et al.
"Fast Critical Experiments with Thorium Blankets: Initial Results from ZPPR-8"
Report NEACRP-L-224, 1978

40. R. Chawla and K. Gmür
"Comparison of ^{232}Th (n,2n)/(n,γ) Ratio Measurements in Various PROTEUS Cores"
EIR Internal Document TM-PH-812, 1979

41. U. Schmocker
"Berechnung Radialer Reaktionsratenprofile im PROTEUS Core 13 und die Bestimmung einiger Reaktionsratenverhältnisse im Zentrum der Th_2O Brutzone"
EIR Internal Document TM-PH-802, 1979

42. R. Boehme
"Application of Integral Transport Theory to the Calculation of Reaction Rates in the Vicinity of Boundaries between Fast Reactor Zones"
Proc. IAEA/OECD Specialists' Meeting on Homogenisation Methods in Reactor Physics", Lugano, Switzerland, 1978

43. Y.H. Bouget et al.
"Physics Performances of a Heterogeneous Fast Reactor Core Concept Studied in MASURCA"
Nucl. Technol., 44, 61 (1979)

44. K. Gmür
"PROTEUS Experimental Results for Cores 14 and 16: F_9-Cadmiumverhältnis in Th-Blankets"
EIR Internal Document TM-PH-845, 1979

45. R.L. Macklin and R.R. Winters
"Stable Isotope Capture Cross-sections from the Oak Ridge Electron Linear Accelerator"
Nucl. Sci. Eng., 79, 110 (1981)